A high-resolution study of the early- to late-summer progression in primary production and carbon export potential in the Atlantic Southern Ocean

Amelia Deary

Honours thesis presented for the Degree of Bachelor of Science

In the department of Oceanography

University of Cape Town

January 2021

Supervisor: Dr Sarah Fawcett

Co-supervisor: Raquel Flynn (PhD Candidate)

Plagiarism Declaration

I fully understand the implication of committing the act of plagiarism. I hereby declare that all work contained within this honours thesis is my own, apart from that which I have properly acknowledged and referenced accordingly.

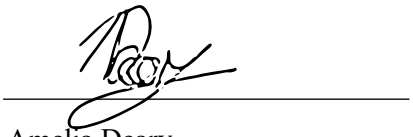

Amelia Deary

22 January 2021

Date

ABSTRACT

Primary productivity in the surface Southern Ocean plays an important role in the global carbon (C) cycle via its contribution to the biological pump, the strength and efficiency of which regulates the oceanic drawdown of atmospheric CO_2. In the framework of the "new production paradigm", phytoplankton growth fueled by nitrate (NO_3^-) mixed up from below ("new production") is proportional to C export, while NPP fueled by recycled ammonium (NH_4^+; "regenerated production") yields no net C export. The relative uptake of new versus recycled nitrogen (N) sources by phytoplankton thus plays an important role in determining whether a region is a sink or source of atmospheric CO_2. While the Southern Ocean appears to be a net sink for CO_2 on an annual basis, it is also widely recognized as a "leak" in the global ocean's biological pump because high concentrations of macronutrients are left unconsumed in its surface waters. A key uncertainty facing our current understanding of the Earth's climate system is thus the role played by biology in the Southern Ocean. Rates (bulk and size-fractionated) of net primary production (NPP) and N uptake (as NO_3^- and NH_4^+) were measured across the Atlantic Southern Ocean in early- (December) and late-summer (March) of the same year to investigate the evolution and drivers of phytoplankton N uptake dynamics and C export potential over the growing season. The highest rates of NPP were observed across the Subantarctic Zone (SAZ) in early-summer (average of 2017.2 ± 13.2 nM C d^{-1}) and Polar Antarctic Zone (PAZ) in late-summer (average of 1692.6 ± 43.4 nM C d^{-1}), with the greatest contribution to C export for the growing season estimated for the PAZ (average of 513.3 ± 213.0 nM C d^{-1} and 220.9 ± 146.4 nM C d^{-1} for early- and late-summer, respectively). Here, late-summer C export was greatest nearest the ice edge (324.4 nM C d^{-1}), highlighting the role of sea ice dynamics (e.g., enhanced iron supply and stratification due to freshening) in increasing C export potential. High rates of NPP across the early-summer SAZ coincided with a low estimate of C export potential (average of 193.5 ± 47.8 nM C d^{-1}). Given the accumulation of C-rich biomass and elevated surface NH_4^+ concentrations across the SAZ, these observations are best explained by high degree of heterotrophic remineralization in the surface layer following an early phytoplankton bloom. A southward shift in biomass accumulation with the seasonal progression occurred concurrent with a tendency towards a smaller cell-dominated phytoplankton assemblage, likely in response to enhanced resource limitation (i.e., iron) as indicated by varying nutrient depletion ratios. At the same time, the Antarctic Zone experienced a clear shift from predominantly new (average f ratio of 0.84 ± 0.09) to predominantly regenerated production (average f ratio of 0.15 ± 0.02) between early- and late-summer. Urea uptake, while not measured directly, appears to have supported a significant amount of NPP in late-summer, providing further evidence for increased surface remineralization across the entire study region at this time, with phytoplankton showing a clear preference for regenerated N (average f ratio of 0.08 ± 0.06 across the transect in late-summer). The seasonal shift to regenerated production led to C export decreasing by 81 ± 16% over the growing season. These findings imply that the higher latitude Atlantic Southern Ocean is a strong sink for atmospheric CO_2 in early-summer, rapidly becoming a weak sink by late-summer.

ACKNOWLEDGEMENTS

First and foremost, I'd like to express my gratitude to my supervisor, Dr Sarah Fawcett, whom afforded me the incredible opportunity to work on this project. Given the unprecedented times we are currently faced with, I am extremely grateful to be able to be starting my journey within the field of biogeochemistry – a sphere of science I have found myself to be greatly passionate about and largely have Sarah to thank for that. Sincerely, thank you Sarah!

The extent to which this project was able to come to life would not have been possible without the help and guidance from my co-supervisor, Raquel Flynn. I cannot thank you enough for the many hours you spent realising this project with me – via ample Zoom calls and hundreds of emails – this wouldn't have been possible without your patient and knowledgeable approach. In addition, for the many hours you spent in the labs processing samples etc. – I am so appreciative.

My thanks go out to all those who were involved in the data collection on the SANAE 58 cruise aboard the SA Agulhas II over the summertime of 2018/2019. I hope to soon be able to return the favour!

To my oceanography partner in crime, Greg Willcocks, for always encouraging me to strive for my best. Thank you, Greg – this has been a real adventure!

To my family, thank you for the support throughout the last four years I've spent at the University of Cape Town, for always being interested to hear about my research and for always allowing me the space to realise my passions and fiercely chase after whatever it may be.

Lastly, I am endlessly grateful to my housemate, Piá Beguinot. This year has been a challenging and unchartered experience to say the least – being confined to our small apartment for many months – staying motivated to continue moving forward with excitement was not always easy. Piá, thank you for the endless support and showing such interest in my work. For always encouraging me and giving me the tough love treatment when necessary – I am so grateful for you!

TABLE OF CONTENTS

1. LITERATURE REVIEW

1.1. The Southern Ocean's role in the global carbon cycle and climate

1.1.1. Ocean productivity and the biological pump

Over timescales of thousands of years, surface ocean chemistry is set by biological productivity, (i.e., primary production by phytoplankton), which in turn regulates the concentration of CO_2 in the atmosphere via a mechanism termed the "biological carbon pump" (Broecker, 1982; Sarmiento & Toggweiler, 1984; Sigman & Boyle, 2000). The biological pump describes the downward flux of organic carbon (C) biomass ("export production") originating from atmospheric CO_2 that is "fixed" by phytoplankton through photosynthesis in sunlit surface waters (typically 50-100m; Sigman & Hain, 2012), and subsequently stored in the ocean's interior (Broecker, 1982; Sarmiento & Toggweiler, 1984; Sigman & Hain, 2012). This process directly controls the concentration of atmospheric CO_2 (Volk and Hoffert 1985).

Phytoplankton productivity (i.e., NPP) in the Southern Ocean plays a crucial role in climate regulation, accounting for ~33% of global ocean CO_2 sequestration annually (Schlitzer, 2002; Takahashi et al., 2002). However, the Southern Ocean is a high-nutrient, low-chlorophyll-a (HNLC) region, which means that its surface waters experience conditions of extreme iron (Fe)-depletion (due to its great distance from land; Jickells & Moore, 2015) and periods of light limitation (Sakshaug et al., 1991; Boyd, 2002), which result in high macronutrient (e.g., nitrate (NO_3^-), phosphate (PO_4^{3-}), and at times, silicate ($Si(OH)_4$)) concentrations. As a consequence of the incomplete consumption of these macronutrients, the strength and efficiency of the Southern Ocean's biological pump is significantly weakened, rendering the region a "leak" in the global ocean's biological pump (Sarmiento & Toggweiler, 1984; Sigman & Hain, 2012).

1.1.2. Quantifying the biological pump in the framework of the "new production paradigm"

In the framework of the "new production paradigm", originally defined by Dugdale & Goering (1967), assuming balanced phytoplankton growth where the rate of NPP is approximated by the rate of total nitrogen (N) uptake multiplied by the Redfield C:N ratio (i.e., 106/16; Redfield et al., 1934 & 1958), the amount of C potentially exported from the surface (i.e., export production) can be equated to the proportion of NPP fueled by NO_3^- (i.e., new production), a "new" N source supplied from outside of the surface system (Eppley & Peterson, 1979). Sources of allochthonous N are supplied to the surface via processes such as deep upwelling and vertical mixing events, N_2-fixation and atmospheric N deposition (Bronk, 2002; Sarmiento, 2004; Cochlan, 2008; Jickells & Moore, 2015), where an increase in new N within the oceanic N reservoir ultimately leads to elevated NPP and thus export production across the global oceans (Eppley & Peterson, 1979; Sigman & Hain, 2012).

New production, however, represents only the small proportion of C potentially exported from the surface to be utilized by higher trophic levels or stored at depth (Eppley & Peterson, 1979; Deppeler & Davidson, 2017), with the majority of organic matter produced by NPP being respired into its inorganic form via heterotrophic consumption and production (i.e., bacterial remineralization within the microbial loop – see further details in section 2.3; Azam et al., 1983) and recycled within the surface layer to sustain NPP (Kirchman, 1994; Azam, 1998; Sigman & Hain, 2012). Termed "regenerated production",

the fraction of NPP fueled by regenerated N sources (e.g., NH_4^+ and urea) consequently has no contribution to C export from the surface (Dugdale & Goering, 1967; Eppley & Peterson, 1979).

The relative contribution of new versus regenerated production is understood using the f-ratio, a parameter characterizing the proportion of new production sustaining the net growth of a phytoplankton community, where an f ratio >0.5 is indicative of a system dominated by NO_3^--fueled NPP, suggesting a strong biological pump and consequently substantial contribution to C export potential. While an f ratio <0.5 is suggestive of a phytoplankton community based predominantly on regenerated production, with the associated export production being nominal (Dugdale & Goering, 1967; Eppley & Peterson, 1979). The f-ratio thus enables the evaluation of C export potential relative to NPP of the upper ocean ecosystem, under the assumptions that: a) the surface layer functions under steady state conditions (i.e., mass balance of surface N inputs/outputs), b) there is no long-term storage of nitrogen in the surface, and c) the effect of surface nitrification on N-supply is nominal (Eppley & Peterson, 1979).

N source preference for NPP is largely controlled by the limitations imposed on the phytoplankton community, depending on the season and hence determining the degree of resource availability (Armstrong, 1999; Cochlan, 2008; Mulholland & Lomas 2008 and references therein). During the winter, significantly deepened mixed layers across the Southern Ocean result in the entrenchment of nutrients from below the euphotic zone (Gordon et al., 1978; Smart et al., 2015). In this regard, wintertime in the Southern Ocean plays a crucial role in the recharge of surface nutrients to be utilized by phytoplankton for NPP during the growing seasons in spring and summer. The onset of summer is marked by the shoaling of the mixed layer (ML), where surface concentrations of micro- (i.e., Fe) and macronutrients are replenished, and light limitation is (mostly) alleviated (see further details in section 2.2.). These conditions experienced within the Southern Ocean surface layer during early-summer hence favor the growth and proliferation of phytoplankton communities (El-Sayed, 1988; Weber & Deutsch, 2012; Deppler & Davidson, 2017), such that efficient C production and export results (Laubscher et al., 1993; Glibert et al. 2016). This balance between wintertime nutrient recharge and summertime nutrient consumption highlights the significant role of the Southern Ocean in the setting levels of atmospheric CO_2 and the surface nutrient distribution across the global oceans (Sarmiento & Toggweiler, 1984; Smart et al., 2015).

Generally, early-summer is characterized by high rates of NPP, where the phytoplankton community is primarily based on new production and export production is consequentially elevated (Laubscher et al., 1993; Sigman & Hain, 2012). As the season progresses, however, intensified resource limitation constrains NPP and the accumulation of phytoplankton biomass at the surface (including detrital biomass) leads to the enhancement of heterotrophic remineralization (Legendre & Gosselin, 1996; Bronk et al., 2002; Deppeler & Davidson, 2017). As a result, the phytoplankton community becomes increasingly reliant on regenerated sources of N in the later summer months, with the potential for a community supported predominantly by regenerated production being greatly enhanced (Smith & Nelson, 1990; Smith, 1991; Joubert et al., 2011; Mdutyana et al., 2020).

1.2. Variability in carbon export potential

1.2.1. Regional hydrography

Surface and subsurface circulation in the Southern Ocean is largely characterized by the strong band of eastward-flowing currents known as the Antarctic Circumpolar Current (ACC), a continuous circulation

belt comprised of numerous dynamic meandering water masses varying in space and time and driven by strong westerly winds prevalent between 40˚- 60˚S (Orsi et al., 1995; Veth et al., 1996; Holliday et al., 1998; Talley, 2011). Traditionally, the ACC is considered to be made up of three distinct oceanic regions separated by frontal boundaries marking distinct changes in variables such as SST, salinity and biogeochemical properties (Lutjeharms et al., 1985; Orsi et al., 1995; Holliday et al., 1998; Marinov et al., 2006; Talley, 2011). The ACC is comprised of the Subantarctic Zone (SAZ), the Polar Frontal Zone (PFZ) and the Open and Polar Antarctic Zones (OAZ and PAZ, respectively), with the region northwards of the ACC defined as the Subtropical Zone (STZ) (Orsi et al. 1995; Chapman et al. 2020).

Punctuating these frontal zones are the associated frontal boundaries, namely the Subtropical Front (STF), Subantarctic Front (SAF), Polar Front (PF) and the Southern ACC Front (SACCF) (Orsi et al., 19945). Frontal boundaries play an important role in surface biological activity, being sites of enhanced exchange between the deep ocean interior and the euphotic zone via vertical mixing processes such as frontal upwelling and mesoscale eddy generation (Allanson et al., 1981; Lutjeharms et al., 1985; Chapman et al., 2020). As a result of this dynamic vertical mixing, frontal boundaries often serve as 'localized' regions supporting elevated rates of NPP and C export potential (Allanson et al., 1981; Lutjeharms et al., 1985; Joubert et al., 2011; Sigman & Hain, 2012; Chapman et al. 2020). Of particular interest is the PF, where elevated rates of NPP have been commonly observed as a result of enhanced frontal upwelling and associated mesoscale mixing events (Tréguer & Jacques, 1992; De Baar et al., 1995; Froneman et al., 2001; Landry et al., 2002).

The characteristic trend of a northward-decreasing meridional nutrient gradient across Southern Ocean surface waters (i.e., to ~300 m; Clowes, 1938; Allanson et al., 1981) is broadly set by the upwelling of Circumpolar Deep Water (CDW) against the Antarctic continental shelf (i.e., the southerly Antarctic Slope Front, ASF), which advances northwards near the surface as Subantarctic Mode Water (SAMW) and below the surface as Upper and Lower Circumpolar Deep Water (UCDW and LCDW, respectively) (Tréguer & Jacques, 1992; Sarmiento, 2004; Marinov et al., 2006; Talley, 2011).

With the Southern Ocean being the site of formation of these major water masses advected northwards (Talley, 2011), surface biological processes occurring within the high latitude Southern Ocean regions play an important role in setting surface nutrient concentrations supplied to low latitude regions and ultimately the rest of the global ocean (Sarmiento, 2004; Marinov et al., 2006). In turn, biological productivity across the Southern Ocean determines the efficiency of the biological pump in drawing down atmospheric CO_2 in low latitude regions and elsewhere across the global oceans (Marinov et al., 2006).

1.2.2. Limitations to primary production across the Southern Ocean

The Southern Ocean is a particularly interesting ocean basin regarding biological activity, based on the unique physical and chemical environment of the waters surrounding the icy continent of Antarctica. Implicating the Southern Ocean as such include the region being the site of deep-water surface ventilation and water mass formation (Talley, 2011). This seasonal overturning circulation recharges surface waters with high concentrations of micro- and macronutrients upwelled from depth (Sarmiento et al., 2004). In theory, the resulting extent of NPP should be high (Sakshaug & Holm-Hansen, 1984), although as a result of the rapid depletion of the micronutrient Fe (Martin & Fitzwater, 1988), the majority of macronutrients remain unconsumed (Allanson et al., 1981; Sarmiento & Toggweiler, 1984).

As a consequence, phytoplankton growth in Antarctic waters is rarely limited by macronutrient concentrations (Levitus et al., 1993; Boyd, 2002). Typically, the dominant controls on phytoplankton primary productivity and the dynamics of N uptake across the Southern Ocean are attributed to light- and Fe-availability, with a considerable role for the availability of $Si(OH)_4$ in regulating community composition (see section 2.3) (Martin & Fitzwater, 1988; Armstrong, 1999; Boyd, 2002; Weber & Deutsch, 2012).

The influence of sea ice dynamics (i.e., ice melt and formation) plays a profound role in generating localized regions of water-column stability, both at the ice edge resulting from the melting of pack-ice (Sakshaug & Holm-Hansen, 1984; Smith & Nelson, 1985; El-Sayed, 1988) and in regions further away from the Antarctic continent resulting from the melting of free-drifting icebergs (Lin et al., 2011). The low salinity of meltwater inputted into the surface waters induces significant vertical stability, with the result being the shoaling of the mixed layer (ML), as first proposed in a study by Marshall (1957) concerning the Arctic waters (El-Sayed, 1988). Enhanced summertime stratification and shallow MLDs across the Southern Ocean result in phytoplankton being retained within the sunlit upper ocean, generating a favorable light environment and thus promoting the blooming of phytoplankton (Smith & Nelson, 1985; El-Sayed, 1988). The blooming of phytoplankton is heavily reliant on the light regime afforded by the surrounding environment, originally outlined by Sverdrup (1953), the Critical-Depth Hypothesis explains that phytoplankton are unable to bloom unless the MLD exceeds that of the critical depth, which is generally around 150-200 m across the Southern Ocean (Gran, 1931; Sverdrup, 1953; El-Sayed, 1988). Typically, the summertime MLD across the Southern Ocean ranges from 60 to 95 m (Jacques & Minas, 1981), however, it is thought that blooms are only able to form where the MLD <40 m, as proposed by Sakshaug & Holm-Hansen (1986), suggesting that much of the Southern Ocean is co-limited by the combined regime of light and Fe during the summertime growing season.

In addition to this, the light-environment of the Southern Ocean, resulting from seasonally varied incident solar radiation, is strongly contrasted between summer and winter, such that the wintertime light regime almost entirely suppresses surface NPP. In spring and summer, however, the intense light regime, where at the height of summer the surface ocean experiences up to 24 hours of direct insolation enabling the blooming of phytoplankton communities, given that additional limiting factors to growth are circumnavigated largely by the dominance of smaller-celled species comprising the phytoplankton communities (see section 2.3) (Neori & Holm-Hansen et al., 1982; El-Sayed, 1988; Deppeler & Davidson, 2017).

The melting of sea ice, in addition to altering the light regime of the upper ocean, is an important micronutrient source to phytoplankton growing within the vicinity of the region implicated by seasonal ice melt, hence affecting both NPP and species composition (El-Sayed, 1988; Armstrong, 1999; Boyd, 2002). Fe-availability plays a crucial role in Southern Ocean NPP, directly limiting phytoplankton growth and N source utilization, as well as having an indirect effect on the cycling of nutrients regulated by surface biological activity (Martin 1991; Takeda, 1998; Armstrong, 1999; Weber & Deutsch, 2012). Phytoplankton growing on NO_3^- require up to 60% more Fe than when growing on NH_4^+ as a consequence of the Fe requirement in reducing NO_3^- to NH_4^+ (i.e. ammonification) before being incorporated into phytoplankton biomass in the form of amino acids (Martin, 1991; Laubscher, 1993; Cochlan, 2008). As a consequence, where low Fe-availability persists, NH_4^+ is preferentially utilized over NO_3^- for NPP and the corresponding implication on the potential for C export being a substantial decrease (Eppley & Peterson, 1979; Sunda, 1989; Cochlan, 2008).

Additionally, under conditions of low Fe-availability, the ratio in which phytoplankton consume nutrients within the surface layer is altered, where generally, less (more) PO_4^{3-} ($Si(OH)_4$) is consumed relative to NO_3^- (Brzezinski et al., 2003; Weber & Deutsch, 2010; Weber & Deutsch, 2012). The effect of this alteration of the consumption of nutrients is most apparent in assemblages of diatoms, where the ratio of Si:N consumption is commonly observed to increase from ~1:1 (Redfield et al., 1934 & 1958) to ~2:1 when Fe is a strong limiting factor to the growth of the community (Takeda, 1998; Brzezinski et al., 2003; Weber & Deutsch, 2012).

The Antarctic Zone (i.e., the AZ, comprising the OAZ and PAZ) has been resolved as largely co-limited by the availability of Fe and light, dependent on the time of year, given the effects of the MLD and meltwater on NPP (Martin & Fitzwater, 1988; Martin, 1990; Armstrong, 1999). The PAZ is generally observed to support higher rates of NPP compared to the OAZ, particularly nearing the end of the growing season (i.e. late-summer) as a result of the mid-season resupply of Fe to the surface ecosystem from melting sea ice (Laubscher et al., 1993; Legendre et al., 1999; Conover et al., 1999; Lin et al., 2011). As a result, the PAZ is generally acknowledged as the AZ region with the greatest potential contribution to C export and hence a strong (although seasonally varying) biological pump, while the OAZ is regarded as having a comparatively weak biological pump, where export production is generally low as a result of perennially deep MLDs and persistent Fe-limitation throughout the growing season (Armstrong, 1999; Landry et al., 2002; Lin et al., 2011; Queguiner, 2013).

Similarly, NPP across the Subantarctic Southern Ocean (i.e., the SAZ and PFZ) is generally low resulting from a combination of perennially deep MLDs, creating conditions of low light availability (Lucas et al., 2007; Deppler & Davidson, 2017) as well as persistently low surface Fe concentrations (Chever et al., 2010). Although these deep MLDs entrain some amount of Fe from depth, NPP remains suppressed due to the low light environment (Lucas et al., 2007; Cochlan, 2008; Joubert et al., 2011; Holmes et al., 2019). The composition of the phytoplankton community and hence the potential for C export across the Subantarctic is largely controlled by Si-limitation, where surface $[Si(OH)_4] \leq 1$ μM has been reported to drive a change from assemblages dominated by larger diatoms to smaller non-siliceous species (Hutchins et al., 2001; Weber & Deutsch, 2012).

In general, the Subantarctic is however regarded as a strong sink to atmospheric CO_2 despite the adverse co-limiting effects of Fe-, light- and $Si(OH)_4$-limitation on the potential for C export (Metzl et al., 1999; Poisson et al., 1993; Boyd et al., 2000; Lourey & Trull, 2001; Lourey, 2003). This alludes to the considerable role of smaller-celled species in contributing to an efficient biological pump (see section 2.3).

The STZ, while technically not considered a region of the Southern Ocean (Orsi et al., 1995), contrasts the frontal zones discussed above (i.e., from south to north, the PAZ, OAZ, PFZ and SAZ) in that it represents a zone characteristic of oligotrophic conditions (Allanson et al., 1981; Sarmiento et al., 2004). Here, the primary controls on NPP are macronutrient limitation (specifically, NO_3^-—limitation) (Sigman & Hain, 2012). The STZ typically experiences a permanently stratified upper water column, where shallow MLDs result in the very slow entrainment of nutrients from below the MLD via vertical mixing events (Sallée et al. 2010). Light-availability is not considered a limiting factor to NPP at any stage of the year across the STZ, with light attenuation reaching depths of ~150 m in some cases (Sallée et al. 2010; Sigman & Hain, 2012).

Similarly, surface Fe concentrations are rarely limiting, with the STZ in close proximity to various landmasses and the resulting flux of Fe-rich dust deposition to the surface ocean being high (Jickells &

Moore, 2015). With sufficient light and Fe, phytoplankton across the STZ rapidly consume the relatively low concentrations of macronutrients in surface waters supplied from the high latitudes, perpetuating the condition of perennial macronutrient limitation (Sarmiento et al., 2004).

1.2.3. Broad phytoplankton community compositions across the frontal zones of the Atlantic Southern Ocean

The dominant species and size-classes comprising the phytoplankton assemblage of a region is a useful means in assessing the various bottom-up, top-down and 'horizontal' (e.g., interspecies competition) processes occurring within the environment (Cullen, 1991; Sunda & Huntsman, 1997; Trull et al., 2015). Cell size is a crucial determinant in the evaluation of export production, with the various phytoplankton size-classes implicated differently with regards to their role in the various marine food chains (i.e., grazing food chain, microbial food chain and pelagic food chain; Pomeroy, 1974; Deppeler & Davidson, 2017).

Generally, smaller-celled phytoplankton species thrive in the cold Antarctic waters of the Southern Ocean, where the strong seasonal variation in the light regime and low Fe-availability afford these small-celled phytoplankton species the competitive advantage over larger species (Sunda & Huntsman, 1997; Smetacek et al., 2004; Poulton et al., 2007). This advantage pertains to the coupled effect of smaller cells having lower cellular nutrient (micro- and macronutrient) requirements and their strong affinity for acquiring nutrients under conditions of low Fe concentrations (Sunda & Huntsman, 1997; Timmermans et al., 2004; Poulton et al., 2007). There does however exist a negative correlation between decreasing cell-size and increasing grazing pressure, such that smaller cells are more efficient assimilators of nutrients but at the cost of experiencing great biomass loss to predation by zooplankton and other heterotrophic organisms (e.g., bacteria) (Cullen, 1991; Sunda & Huntsman, 1997; Timmermans et al., 2004; Poulton et al., 2007).

In addition to this, the varying degrees of limitations imposed on the phytoplankton community largely determine the composition of the assemblage. As outlined in section 2.2, the major controls on NPP across the Southern Ocean have been resolved as a complex interaction of Fe-, light- and $Si(OH)_4$ availability. With regards to evaluating the export production of a region, $Si(OH)_4$ limitation carries a lot of weight in determining the composition of the phytoplankton community (no pun intended!), with diatoms being major role players in surface biomass aggregation and hence the sinking flux of C as a result of their heavy, silicified frustules, with the ability to rapidly sink out of the surface layer (Le Fevre et al., 1998; Trull et al. 2001; de Sallas et al. 2011; Weber & Deutsch, 2012). This direct pathway of C export from the surface has a sizeable effect on the sequestration of C and hence the strength and efficiency of the biological pump (Cullen, 1991; Le Fevre et al., 1998; Weber & Deutsch, 2012).

The autotrophic assemblage across the AZ is generally dominated by smaller, silicifying phytoplankton species (i.e., diatoms) (Bracher et al., 1999; Weber & Deutsch, 2010), and high abundances of nano- and picoflagellates (Mengesha et al., 1998). The competitive adaptations to smaller-celled species facilitates this dominance in the AZ (Smetacek et al., 2004; Poulton et al., 2007), where changes in community compositions are largely driven by persistent Fe- (and at times, light-) limitation rather than macronutrient limitation, as is often the driver in low latitude oceanic regions (Martin, 1990; Sunda & Huntsman, 1997; Fennel et al., 2003; Brzezinski et al., 2003; Sigman & Hain, 2012). The consequence of smaller-celled species dominating the phytoplankton does however have negative implications for C export potential, with the main constituent of organic biomass 'rain' from the surface being larger-

celled species able to rapidly sink out of the surface before being remineralized (Cullen, 1991; Joubert et al., 2011; Sigman & Hain, 2012).

The AZ is also characterized by substantial rates of microzooplankton grazing and effective remineralization of particulate organic matter (POM) at the surface, such that surface nutrient regeneration plays a substantial role and as a consequence the region generally supports a weak biological pump (Froneman et al., 2004; Quéguiner, 2013). Hence, the AZ is observed to oscillate between functioning as a source or sink for atmospheric CO_2, reliant on the source of N utilized for NPP as determined by the phytoplankton community composition and seasonally varying primary limiting factor regulating NPP, in turn determining the strength and efficiency of the biological pump (Cochlan, 2008; Mulholland & Lomas 2008 and references therein).

The PFZ is characterized by sustained high concentrations of NO_3^- and PO_4^{3-}, with a steady decline in surface [$Si(OH)_4$] as a consequence of Si-consumption by diatoms, which dominate phytoplankton assemblages across the region (Odate & Fukuchi, 1995; Lourey, 2003; Sarmiento, 2004; Weber & Deutsch, 2010). The PF is an important region for NPP, being the site of intense seasonal upwelling, resupplying both macronutrients (i.e., alleviating some amount of $Si(OH)_4$-limitation) and Fe to the surface (Kanda & Fukuchi, 1979; Lutjeharms et al., 1985; Tréguer & Jacques, 1992; De Baar et al., 1995; Froneman et al., 2001). As a result, blooms of larger, heavily silicified diatom species are common in the region directly surrounding the PF (Laubscher et al., 1993), having significant positive implications for C export potential (El-Sayed, 1988; Froneman et al., 1995; Tremblay et al., 2001).

The SAZ is characterized by sufficiently greater seasonal surface nutrient depletion, with surface concentrations of NO_3^- and PO_4^{3-} rapidly decreasing northwards of the SAF (~50˚S). Perennially low surface [$Si(OH)_4$] appears to be the major limitation on the success of large diatoms species across the region (Boyd et al., 2002; Sarmiento, 2004). Conditions of seasonal Si-depletion and surface waters rich in [NO_3^-] and [PO_4^{3-}] favor the growth and dominance of smaller celled, non-siliceous phytoplankton species, where as a consequence, the potential for C export is expected to be low (Sarmiento, 2004; Queguiner, 2013; Deppeler & Davidson, 2017). As a result of the high seasonality in resource availability and NPP (Sakshaug & Holm-Hansen, 1984; El-Sayed, 1988), the SAZ characteristically experiences great seasonal variation in the phytoplankton assemblage, dependent on the primary limiting factor constraining the growth of the community (Armstrong, 1999; Henley et al., 2020).

Phytoplankton assemblages across the SAZ are generally dominated by cyanobacteria, autotrophic flagellates and coccolithophores, with small, lightly-silicified diatom species existing in very low abundances (Odate & Fukuchi, 1995; Lourey, 2003; Sarmiento, 2004). Despite the dominance of smaller-celled species comprising the phytoplankton assemblage in the SAZ, a strong biological pump is characteristic for the region (Lourey & Trull, 2001; Boyd et al., 2000; Lourey, 2003), suggesting the significant role of smaller species in contributing to export production (Trull et al., 2001; Deppeler & Davidson, 2017).

The distinctive oligotrophic conditions which characterize the STZ region (Sarmiento et al., 2004), where macronutrient limitation prevails, is reflected by the persistent dominance of picophytoplankton, with smaller-celled species leveraged over larger-celled species under conditions of nutrient limitation (Brzezinski et al., 2003; Poulton et al., 2007; Weber & Deutsch, 2012; Deppeler & Davidson, 2017). As a consequence, the STZ supports a high degree of surface nutrient regeneration and considerably

low export production, such that the STZ is regarded as a year-round source to atmospheric CO_2 (Laubscher et al., 1993; Le Fevre et al., 1998; Joubert et al., 2011).

2. INTRODUCTION : SCOPE OF RESEARCH

The global carbon (i.e., C) cycle is greatly influenced by the flux of C between the upper ocean and lower atmosphere across the Southern Ocean, where the strong seasonality in atmospheric CO_2 drawdown is governed by a combination of physico-chemical processes and bottom-up and top-down controls on biological productivity (i.e., NPP) (Broecker, 1982; Volk and Hoffert 1985; Sarmiento & Toggweiler, 1984; Sigman & Boyle, 2000). The functioning of the biological pump across the Southern Ocean, the largest HNLC region in the global ocean, is crucial to its capacity to remove C from the atmosphere. Indeed, the Southern Ocean currently constitutes a "leak" in the global ocean's biological pump because the high concentrations of macronutrients that remain unconsumed in its surface waters represent a missed opportunity for CO_2 removal (Sarmiento & Toggweiler, 1984; Sigman & Hain, 2012). The biotic and abiotic factors regulating surface NPP are highly variable across spatial and temporal scales, with changes in surface nutrient cycling (particularly nitrogen (i.e., N) cycling) providing an indication of the strength of the Southern Ocean's biological sink for atmospheric CO_2 (Dugdale & Goering, 1967; Eppley & Peterson, 1979).

The framework of the new production paradigm allows for the evaluation of the potential export production of a region (Dugdale & Goering, 1967; Eppley & Peterson, 1979). Given the generally tight coupling between phytoplankton C and N cycling (i.e., in a ratio of 106:16; Redfield et al., 1934 & 1958), measurements of the N cycle (e.g., the relative importance of the various N sources to phytoplankton growth) can be used to directly estimate C export potential (Dugdale & Goering, 1967; Eppley & Peterson, 1979), although recognizing that such an approach yields only a snapshot of ecosystem functioning in time and space. As a consequence of the paucity of seasonally-resolved NPP and N uptake data for the Southern Ocean, however, many dynamics of biological C and N cycling are difficult to disentangle. Sampling at the beginning and end of a single growing season thus makes this study unique, with previous similar studies commonly reporting measurements averaged over an entire season (e.g., Bracher et al., 1999; Froneman et al., 2001 & 2004; Joubert et al., 2011; Gandhi et al., 2012; Mdutyana et al., 2020).

The primary goal of the study is to test the hypothesis of an early- to late-summer shift in the dominant N source utilized by the phytoplankton community across the Atlantic sector of the Southern Ocean. High-resolution observations of upper ocean N source dependence by phytoplankton are used to estimate C export potential in both early- and late-summer, with varying surface nutrient depletion ratios used to infer the possible composition of the phytoplankton community. More specifically, the addition of ^{15}N-labelled nutrient sources to simulated *in situ* experiments and subsequent calculations of the f-ratio are used to resolve the relative importance of nitrate (i.e., a "new" nutrient source) versus ammonium (i.e., a "regenerated" nutrient source) for fueling surface NPP in order to quantify the potential for C export from the euphotic zone (Dugdale & Goering, 1967; Eppley & Peterson, 1979), with the implication being that a switch from nitrate- to ammonium-fuelled production defines the moment at which the upper ocean ecosystem stops sequestering atmospheric CO_2. Size-fractionated C and N uptake rates allow for an investigation of the seasonal evolution of the dominant phytoplankton size-class(es), as well as being useful for assessing the potential for surface nutrient regeneration and higher trophic level processes that may alter the C drawdown capacity of the region.

This study thus aims to gain a more complete understanding of the hypothesized seasonal shift from new to regenerated production by the upper ocean ecosystem across the Atlantic Southern Ocean, with consideration of the interactions among the changing environmental and ecological conditions of the various frontal zones. High-resolution studies of the N cycle in the upper Southern Ocean, given the implications for C production and export, provide a tool for understanding the strength and seasonality of the Southern Ocean as a biological sink for atmospheric CO_2, with far-reaching implications for global C cycling and climate.

3. METHODS

3.1. Study site

Sampling was conducted during the 58th South African National Antarctic Expedition (SANAE 58) summertime cruise aboard the R/V *SA Agulhas II.* The cruise took place from December 2018 (early-summer; Fig. 1a) to March 2019 (late-summer; Fig. 1b) along the GoodHope (GH) line (NOAA AX25) between Cape Town (~34˚S) and Antarctica (~70˚S). Seawater samples were collected from the ship's underway system (~7 m intake) every 2-4 hours for nutrients, and rate experiments were conducted twice a day totaling 13 stations in early-summer (S1-S13) and 18 stations in late-summer (S14-S31). The northward leg of the cruise (i.e., late-summer leg) diverted off the GH line between 60˚S and 54˚S, travelling longitudinally from 0-39˚S, reaching South Georgia Island (SG), and back to 0˚S before continuing northwards along the GH line.

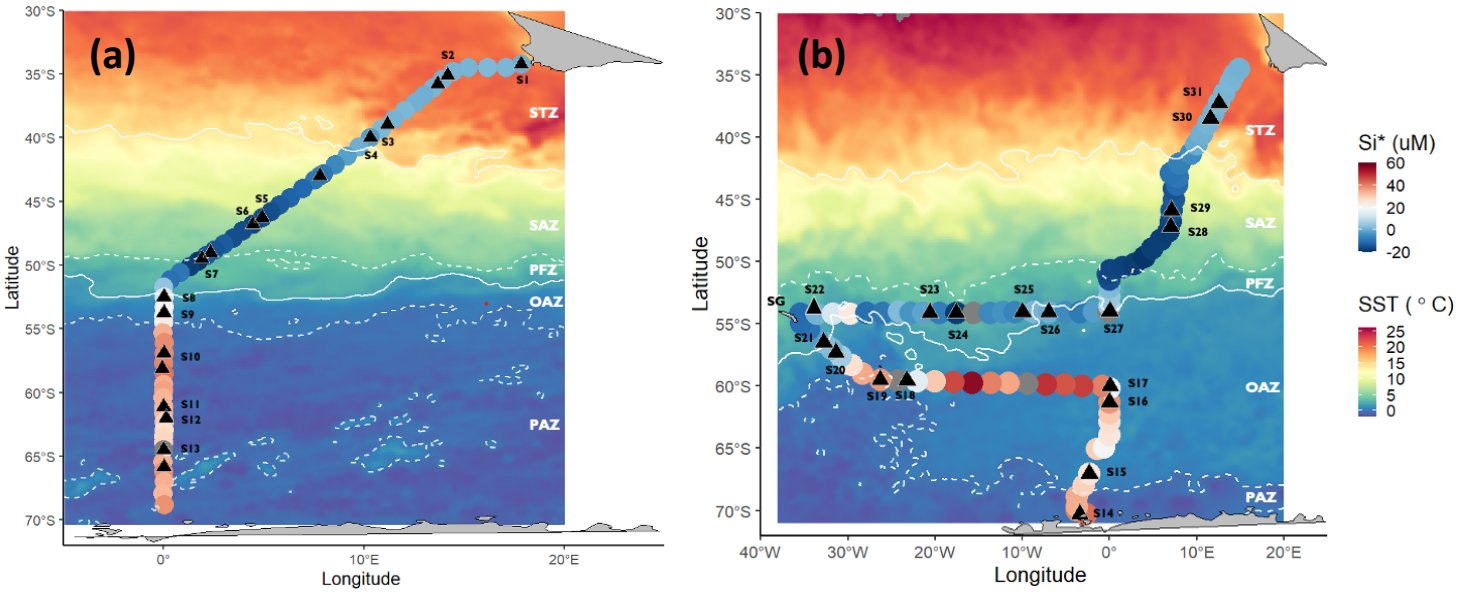

Figure 1: Map of the Atlantic sector of the Southern Ocean showing the stations sampled between Cape Town and Antarctica along the GoodHope line during (a) the early-summer and (b) the late-summer legs of the cruise overlaid on monthly satellite SST. The mean frontal positions, as defined by Orsi et al. (1995), are indicated by white temperature contours and the major Southern Ocean frontal zones are labelled (STZ: Subtropical Zone, SAZ: Subantarctic Zone; PFZ: Polar Frontal Zone, OAZ: Open Antarctic Zone, PAZ: Polar Antarctic Zone). The cruise track is overlain with Si* values, which were used in addition to SST to define the frontal positions. The location of South Georgia Island is indicated on panel b, where SG: South Georgia.

3.2. Regional hydrography

High resolution sea surface temperature (SST) and surface salinity data used to identify surface hydrological features (i.e., frontal positions) were collected every 10 minutes via the underway ferrybox. Frontal positions were identified based on SST and salinity criteria as outlined by Orsi et al. (1995) and Holliday et al. (1998). Defining the positions of the fronts in late-summer proved complicated as a result of the enhanced meandering nature of the various ACC fronts (Veth et al., 1997). In this case, Si* was used in addition to SST and surface salinity criteria to define the frontal positions,

particularly the Polar Front (PF) and the Southern Antarctic Circumpolar Current Front (SACCF) (Sarmiento et al., 2004). Si* is calculated as follows:

$$Si^* = [Si(OH)_4] - [NO_3^-] \quad (1.1)$$

Si* is a useful tracer of water mass evolution, as well as an indication of diatom nutrient status. Characteristic Si* values of various water masses aid in defining the frontal zones as well as determine the extent of Si-depletion relative to NO_3^- (Sarmiento et al., 2004).

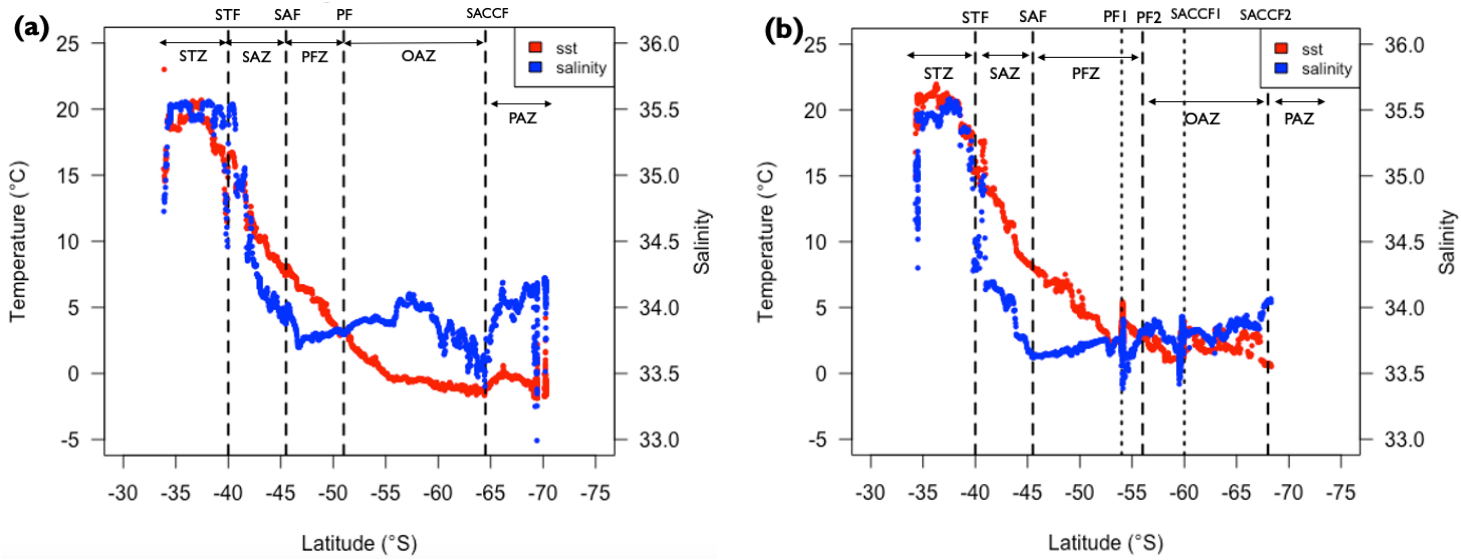

Figure 2: Surface temperature (red) and surface salinity (blue) with latitude along the GoodHope cruise track measured by the underway ferrybox for (a) the early-summer and (b) the late-summer transects. Frontal positions at the time of sampling are indicated by vertical dashed black lines and labelled (STF: Subtropical Front, SAF: Subantarctic Front, PF: Polar Front; SACCF: Southern Antarctic Circumpolar Current Front) and frontal zone extent is indicated by horizontal black arrows and zone labels (STZ: Subtropical Zone, SAZ: Subantarctic Zone; PFZ: Polar Frontal Zone, OAZ: Open Antarctic Zone, PAZ: Polar Antarctic Zone).

3.3. Nutrient concentrations

Seawater samples for surface ammonium (NH_4^+) concentrations were collected at 2-hour intervals from the underway system. Duplicate samples were collected in high-density polyethylene (HDPE) bottles "aged" with NH_4^+ working reagent in order to minimize contamination. Once collected, the samples were stored at -20˚C until analysis shipboard, which typically occurred within 2 days. Samples for nitrate (NO_3^-), nitrite (NO_2^-), phosphate (PO_4^{3-}), silicate ($Si(OH)_4$), and urea concentrations were collected at 4-hour intervals. Samples were collected in rinsed 50 mL centrifuge tubes and frozen at -20˚C until analysis. The concentrations of NO_2^- and PO_4^{3-} were measured onboard, while NO_3^-, $Si(OH)_4$ and urea concentrations were measured onshore following the cruise.

Concentrations of nitrate+nitrite ($[NO_3^- + NO_2^-]$) were measured using a Lachat QuikChem® Flow Injection Analysis platform in a configuration with a detection limit of 0.1 µM, with a standard deviation of ≤0.5 µM for duplicate samples. During each autoanalyzer run, aliquots of certified reference material (JAMSTEC; Lot CG; $[NO_3^-]$ = 24.3 µM) were analysed to ensure measurement accuracy. NO_2^- concentrations were determined manually via the colorimetric method of Grasshoff et al. (1983), with a detection limit of 0.05 µM and standard error of ≤0.05 µM for duplicate samples. The $[NO_3^-]$ of each sample was determined by subtraction of $[NO_2^-]$ from $[NO_3^- + NO_2^-]$.

Concentrations of ammonium ($[NH_4^+]$) were analysed fluorometrically using a Turner Designs Trilogy Laboratory fluorometer equipped with a UV module according to the method of Holmes et al. (1999). The detection limit was 0.05 µM and standard error was ≤0.05 µM for duplicate samples. The matrix effect (ME) that results from the calibration of seawater samples with Milli-Q water standards was calculated using the standard addition method (Saxberg and Kowalski 1979). All samples were corrected for the ME, which was always <10% and typically ≤5%.

Concentrations of silicic acid ($[Si(OH)_4]$) were measured using a Lachat QuikChem® Flow Injection Analysis platform in a configuration with a detection limit of 0.1 µM and standard deviation of ≤0.5 µM for duplicate samples, with lower error for lower concentration samples. During each autoanalyzer run, aliquots of certified reference material (JAMSTEC; Lot CG; $[Si(OH)_4]$ = 57.9 µM) were analysed to ensure measurement accuracy.

Concentrations of phosphate ($[PO_4^{3-}]$) were determined manually via the colorimetric method of Grasshoff et al. (1983) using a Thermo Scientific Genesis 30 Visible spectrophotometer. The detection limit of the method was 0.05 µM and standard error was 0.1 µM for duplicate samples.

Urea concentrations were measured following the colourimetric method of Revilla et al. (2015) using a Thermo Scientific Genesis 30 Visible spectrophotometer. The detection limit was 0.05 µM and the standard deviation for duplicate samples was ≤0.05 µM.

The surface concentration of dissolved inorganic N (DIN), was defined as the combined concentrations of NO_3^-, NO_2^- and NH_4^+ measured at the surface, where $[DIN] = [NO_3^-] + [NO_2^-] + [NH_4^+]$. Surface [DIN] represents the bioavailable forms of N for utilization by phytoplankton, and in some cases for heterotrophic consumption (Bronk, 2002). The ratio of surface $[DIN]:[PO_4^{3-}]$ was then computed to address the relative change in uptake of N:P when all inorganic N sources available for uptake are included. Given that NO_2^- exists in very low concentrations at the surface, the relative uptake of NH_4^+ to PO_4^{3-} can be assessed, with the ratio calculated as follows:

$$\frac{[DIN]_{measured}}{[PO_4^{3-}]_{measured}} \quad (1.2)$$

3.4. Nutrient consumption

To calculate the concentration of nutrients consumed between winter (i.e., the period of nutrient supply) and early-summer and winter and late-summer, the measured surface nutrient concentrations (see section 1.3.) were subtracted from the source water nutrient concentrations:

$$[NO_3^-]_{source} - [NO_3^-]_{measured} = [NO_3^-]_{consumed} \quad (1.3)$$

$$[Si(OH)_4]_{source} - [Si(OH)_4]_{measured} = [Si(OH)_4]_{consumed} \quad (1.4)$$

$$[PO_4^{3-}]_{source} - [PO_4^{3-}]_{measured} = [PO_4^{3-}]_{consumed} \quad (1.5)$$

The source water nutrient concentrations supplied to the surface during winter mixing were calculated using the computed MLDs, where depth-averaged nutrient concentrations were calculated between the base of the ML and depth of the isopycnal line defining the subsurface water mass characteristic of each frontal zone (Talley, 2013*)*. In the STZ, depth-averaged nutrient concentrations were calculated between the MLD and the depth of the 26.6 kg m^{-3} isopycnic line. In the SAZ, depth-averaged nutrient concentrations were calculated between the MLD and the depth of the 27 kg m^{-3} isopycnic line. South of the PF (i.e., across the PFZ, OAZ and PAZ), depth-averaged source nutrient concentrations were computed between the MLD and the depth of the temperature minimum layer (T_{min}). After the event of deep winter mixing and the shoaling of the ML marked by the onset of summer, the T_{min} layer refers to what would have been the base of the winter ML (Gordon et al., 1977). The T_{min} layer is thus utilized as a summertime record of wintertime conditions (Altabet & François, 2001; Smart et al., 2015).

The fraction (or, ratio) of nutrients consumed at the surface was then calculated as:

$$\frac{[Si(OH)_4]_{consumed}}{[NO_3^-]_{consumed}} \quad (1.6)$$

$$\frac{[NO_3^-]_{consumed}}{[PO_4^{3-}]_{consumed}} \quad (1.7)$$

3.5. Determination of Chl-a concentrations

Seawater samples used for chlorophyll-a determination were collected at 4-hour intervals from the underway system. 2 L of sample was collected in a dark HDPE bottle. Prior to filtration, the bottles were gently and repeatedly inverted to homogenize the sample. 1 L of seawater from each sample was filtered through a 20 µm nylon mesh filter, 500 mL through a 2.7 µm GF/F and the remaining 500 mL was filtered through a 0.3 µm GF-75 filter. Filters were immediately transferred to 20 mL glass

scintillation vials to which 8 mL of 90% acetone was added before the vials were left in the -20°C freezer for 24 hours to extract.

The updated method for chlorophyll-a determination outlined by Rathbun (1997) was used to measure the chlorophyll-a concentrations on board the ship. Samples and standards were measured using a Turner Designs fluorometer with a chl-a non-acidified module.

3.6. Rates of NPP and N uptake and concentrations of particulate organic matter (POM)

Simulated *in situ* experiments were conducted at 31 stations to determine surface water size-fractionated rates of NPP, NO_3^- uptake (ρNO_3^-) and NH_4^+ uptake (ρNH_4^+). At each station, seawater from the underway system was prescreened through a 200 µm nylon filter to remove large grazers and transferred into four 1 L polycarbonate (PC) bottles and four 2 L PC bottles. Two 1 L and two 2 L PC bottles were amended with $NaH^{13}CO_3$ and $^{15}NH_4Cl$ tracers at 5-10% of the ambient concentrations, yielding final tracer concentrations of 100 µmol L^{-1} and 0.05 µM, respectively. The remaining PC bottles were amended with $K^{15}NO_3$ at 5-10% of the ambient concentration, yielding a final tracer concentration of 0.5 µM for the stations in the STZ and 1 µM for the stations south of the STF. At every station, duplicate experiments were conducted for each size-class and each tracer.

Samples were incubated on deck in a custom-built incubator screened to mimic surface PAR (~55% light level) for 3-6 hours. A continuous surface water supply to the incubators ensured constant near-in situ temperature throughout the experiments. The experiments were terminated by filtration of samples onto pre-combusted (450ºC for 5 hours) 0.3 µm GF-75 and 2.7 µm GF/Fs, and Milli-Q-washed 20 µm nylon mesh filters. For each sample, 0.5 L was filtered through the 0.3 µm and 2.7 µm filters, and 2 L through the 20 µm nylon mesh. Particles captured on the 20 µm nylon mesh were resuspended in ~50 mL of 0.2 µm filtered seawater, then filtered onto a pre-combusted 2.7 µm GF/F. The filters were oven-dried shipboard for 24 hours at 45˚C, then pelletized into tin cups and stored in a desiccator until analysis in the Stable Light Isotope Laboratory in the Archaeology Department at the University of Cape Town.

The concentration and isotopic composition of particulate organic carbon and nitrogen (POC and PON) were analysed using a Thermo Delta V Plus isotope ratio mass spectrometer combined with a Flash 2000 elemental analyser (EA-IRMS), with a detection limit of 2 µg C and 1 µg N. Using the measured POC and PON concentrations (µM) and atom% of ^{13}C and ^{15}N, rates (nM hr^{-1}) of NPP, ρNO_3^- and ρNH_4^+ were calculated according to the equations of Dugdale and Wilkerson (1986) for each filtered fraction. For three phytoplankton size-classes, picophytoplankton (0.3 – 2.7 µm), nanophytoplankton (2.7 – 20 µm) and microphytoplankton (20 – 200 µm), biomass concentrations and uptake rates were then calculated as follows:

$$[PM]_{total} = [PM]_{(>0.3\ \mu m)} \quad ; \quad \rho M_{total} = \rho M_{(>0.3\ \mu m)} \tag{1.8}$$

$$[PM]_{Pico} = [PM]_{(>0.3\ \mu m)} - [PM]_{(>2.7\ \mu m)} \quad ; \quad \rho M_{Pico} = \rho M_{(>0.3\ \mu m)} - [PM]_{(>2.7\ \mu m)} \tag{1.9}$$

$$[PM]_{Nano} = [PM]_{(>2.7\ \mu m)} - [PM]_{(>20\ \mu m)} \quad ; \quad \rho M_{Nano} = \rho M_{(>2.7\ \mu m)} - [PM]_{(>20\ \mu m)} \tag{1.10}$$

$$[PM]_{Micro} = [PM]_{(>20\ \mu m)} \quad ; \quad \rho M_{Micro} = \rho M_{(>20\ \mu m)} \tag{1.11}$$

Where 'M' denotes the chemical species (C, NO_3^- or NH_4^+), [PM] is the concentration of POC or PON (μM), and ρM is the transport rate of the species (nM hr^{-1}).

The absolute uptake rates (nM hr^{-1}) were converted to daily rates (nM d^{-1}) by multiplying the hourly rates by the number of daylight hours incident at each station at the time of sampling (Cornwall et al., 2021).

Assuming balanced phytoplankton growth, the rate of NPP should be approximated by the total rate of N uptake multiplied by the Redfield C:N ratio (i.e., 106:16; Redfield et al., 1934 & 1958). Since only ρNO_3^- and ρNH_4^+ were measured during this study, the relationship of NPP to $\rho NO_3^- + \rho NH_4^+$ (hereafter, ρN_X) is leveraged to determine the reliance of the phytoplankton community on an N source additional to NO_3^- and NH_4^+ (e.g., forms of recycled dissolved organic N such as urea) (Peng et al. 2017) as follows:

$$\rho\text{Urea} = \rho\text{C} - \rho N_x \times 6.63 \qquad \text{(Fig. 14)} \qquad (1.12)$$

Where data points on figure 14 fall above the 1:1 slope, the rate of C fixation was not matched by the rate of $NO_3^- + NH_4^+$ uptake, suggesting an unaccounted-for N source supported some fraction of surface NPP at those stations. This "missing" N source is assumed to be urea, a labile form of dissolved organic N (DON) produced at the surface via organic matter decomposition and organismal excretion (Bronk, 2002). The assumption of the unaccounted-for N source to be urea was made on the basis that: a) conditions are unfavorable for N_2-fixation over the summertime in the Southern Ocean, where temperatures and Fe-availability are low and/or [NO_3^-] is high (Staal et al., 2003; Cochlan, 2008), and b) the Southern Ocean experiences very low rates of dust deposition/flux as a result of it being a great distance from any major landmass (Jickells & Moore, 2015).

3.7. Specific rates of NPP, nitrate, ammonium and urea uptake

The specific rates (hr^{-1}) of NPP (V_C), NO_3^- (V_{NO3^-}), NH_4^+ (V_{NH4+}) and urea uptake (V_{urea}) were determined by normalizing the transport rates (ρM) to the corresponding measured [POC] or [PON].

$$V_C = \frac{\rho\text{C}}{POC} \qquad (1.13)$$

$$V_N = \frac{\rho\text{N}}{PON} \qquad (1.14)$$

Where ρC is the absolute carbon fixation rate (NPP) and ρN corresponds to ρNO_3^-, ρNH_4^+ or ρUrea, depending on the specific uptake rate being calculated (i.e., V_{NO3^-}, V_{NH4+} or V_{urea}, respectively). In the case of V_{urea}, [PON] is taken to be the average [PON] collected from both experimental bottles for the nitrate and ammonium uptake experiments at each station.

The above calculations (1.13 and 1.14) were performed for each size-class as well as the total (bulk) phytoplankton community.

3.8. F ratio calculations

The specific uptake rates of NO_3^- and NH_4^+ were used to calculate the f-ratio at each station, according to Eppley and Peterson (1979), as follows:

$$f\ ratio = \frac{V_{\mathrm{N}O_3^-}}{V_{\mathrm{N}O_3^-} + V_{\mathrm{N}H_4^+}} \tag{1.15}$$

At the stations where urea appeared to support a significant fraction of NPP, the f-ratio calculation was adjusted to include V_{urea}, as follows:

$$f\ ratio_{urea} = \frac{V_{\mathrm{N}O_3^-}}{V_{\mathrm{N}O_3^-} + V_{\mathrm{N}H_4^+} + V_{urea}} \tag{1.16}$$

The above calculations (1.15 and 1.16) were performed for each size-class as well as the total (bulk) phytoplankton community.

3.9. Computation of absolute carbon export estimates, derived from new production

The amount of C that was potentially exported from the surface (i.e, absolute rate of C export) was estimated by multiplying the daily rate of NPP (nM d^{-1}) by the corresponding f-ratio$_{urea}$ calculated for the bulk community at each station, as follows:

$$Abs\ C\ export = NPP\ \times\ f\ ratio_{urea} \tag{1.17}$$

4. RESULTS

4.1. Regional hydrography and nutrient distributions

4.1.1. Frontal zone identification

The GoodHope (GH) transect crossed all hydrographic fronts and frontal zones of the Southern Ocean along both the southward (Fig. 1a, early-summer) and northward (Fig. 1b, late-summer) legs of the cruise. The region north of the Subtropical Front (STF, 41-41.5˚S) was defined as the Subtropical Zone (STZ), with SST >14˚C and surface salinity >35 (Fig. 1; Fig. 2). The region between the STF and the Subantarctic Front (SAF; 50-51.5˚S) was defined as the Subantarctic Zone (SAZ), where SST ranged from 5-14˚C and salinity from 34-35. In addition, the SAZ was defined based on its characteristically negative Si* (average of -13.4 ± 3.6 µM in early-summer and -14.9 ± 3.6 µM in late-summer) (Sarmiento et al., 2004; Fig. 4). The region located between the SAZ and the Polar Front (PF) was defined as the Polar Frontal Zone (PFZ), where SST ranged between 2-5˚C, salinity was >34 and Si* averaged -0.3 ±11.3 µM in early-summer and -2.8 ± 9.7 µM in late-summer (Fig 1 and Fig. 3-4). Along the southward leg, the PF was located at roughly 51.7˚S, shifting further south to 54˚S by late-summer. The meandering nature of the PF (Veth et al., 1997) resulted in the cruise track crossing the PF twice along the northward leg during the westward transect to South Georgia (PF1 at 54˚S and PF2 at ~56˚S) (Fig. 1b). The Southern ACC Front (SACCF) was located at ~54.5˚S along the southward leg (Fig. 1a), shifting further south in late-summer to be crossed by the northward cruise track at two points (SACCF1 at 59˚S and SACCF2 at ~68˚S) (Fig. 1b). The region falling between the PF and the SACCF was defined as the Open Antarctic Zone (OAZ), where SST ranged from 0-2˚C and salinity ~34 (Fig. 1; Fig. 2). South of the SACCF was defined as the Polar Antarctic Zone (PAZ), defined by SST <0˚C and salinity <34.

4.1.2. Surface nutrient concentrations

The frontal zones sampled during the cruise were characterized by a broad range of biogeochemical conditions, which is to be expected given that with the observed surface nutrient concentrations are set by large scale oceanic circulation, localized upwelling and mixing events and biological processes occurring across the five oceanic regions. Generally, the surface NO_3^-, PO_4^{3-} and $Si(OH)_4$ concentrations decreased from high to low latitude across the GH transect, while NH_4^+ and urea were highly variable across all zones in both early- and late-summer (Fig. 3).

In the STZ, surface nutrient concentrations typical of an oligotrophic region were observed, albeit slightly elevated during late-summer (Fig. 3; Table 1a and 1b). Surface [NO_3^-] remained low over the sampling period (average of 0.6 ± 1.2 µM in early-summer and 1.6 ± 1.5 µM in late-summer), while surface [PO_4^{3-}] (average of 0.2 ± 0.1 µM in early-summer and 0.4 ± 0.1 µM in late-summer) and [$Si(OH)_4$] (average of 1.4 ± 0.5 µM in early-summer and 2.1 ± 0.7 µM in late-summer) increased. Surface [NH_4^+] remained deplete over the entire sampling period (average of 0.0 ± 0.0 µM in early-summer and 0.1 ± 0.0 µM in late-summer) (Table 1b). Similarly, surface [urea] remained deplete over the entire sampling season (average of 0.1 ± 0.1 µM in early-summer and 0.1 ± 0.1 µM in late-summer).

In the SAZ, moderate surface [NO_3^-] was sustained over the sampling period (average of 14.9 ± 4 µM in early-summer and 18.1 ± 5.1 µM in late-summer), with the highest concentration occurring at the SAF in late-summer (average of 24.6 ± 1.3 µM; Fig 2a, 2b; Table 1a and 1b). Surface [PO_4^{3-}] was low

in early- and late-summer (average of 1.0 ± 0.3 µM and 1.3 ± 0.4 µM, respectively), while surface [$Si(OH)_4$] increased substantially near the SAF (average of 7.7 ± 0.0 µM and 18.0 ± 13.9 µM at the SAF in early- and late-summer, respectively, assuming that the position of the SAF, determined largely from hydrographic data, is correct. If the SAF were located very slightly further north in late-summer, surface [$Si(OH)_4$] would be indistinguishable from that measured at the SAF in early-summer). Surface [NH_4^+] increased between sampling periods (average of 0.1 ± 0.1 µM in early-summer and 0.5 ± 0.3 µM in late-summer), while [urea] remained deplete (average of 0.1 ± 0.1 µM in early-summer and 0.0 ± 0.1 µM in late-summer).

In the PFZ, elevated surface [NO_3^-] was sustained between sampling periods (average of 22.3 ± 0.9 µM in early-summer and 22.1 ± 2.1 µM in late-summer; Fig. 3; Table 1a and 1b). Surface [PO_4^{3-}] increased gradually over the season (average of 1.6 ± 0.1 µM in early-summer and 2.0 ± 0.1 µM in late-summer). A substantial increase in surface [$Si(OH)_4$] was observed between the SAZ and PFZ, with high surface [$Si(OH)_4$] sustained over the sampling period (average of 22.6 ± 12.7 µM in early-summer and 20.3 ± 10.8 µM in late-summer). The highest [$Si(OH)_4$] in the PFZ was measured at S22 (38.8 ± 0.2 µM; Table 1b), within the oceanic region susceptible to the IME due to its close proximity to SG (Fig. 1b; Table 1b). Similarly, the highest measured surface [NO_3^-] and [PO_4^{3-}] in the late-summer PFZ occurred at S22 (25.9 ± 0.2 µM for NO_3^- and 2.1 ± 0.1 µM for PO_4^{3-}, respectively). Surface [NH_4^+] (average of 0.1 ± 0.1 µM in early-summer and 0.8 ± 0.7 µM in late-summer) and [urea] (average of 0.1 ± 0.1 µM in early-summer and 0.3 ± 0.2 µM in late-summer) increased slightly over the sampling period, with particularly elevated [NH_4^+] observed in the vicinity of SG in late-summer (average of 1.4 ± 0.7 µM; between S20-S22) (Fig. 3; Table 1a and 1b).

In the OAZ, high surface [NO_3^-] was sustained across the sampling period (average of 24.7 ± 0.1 µM in early-summer and 23.1 ± 2.4 µM in late-summer), with S26 located just south of the PF showing the highest surface [NO_3^-] of all stations (29.8 ± nd µM; Fig. 3; Table 1a and 1b). Surface [PO_4^{3-}] increased gradually over the season (average of 1.7 ± 0.1 µM in early-summer and 2.0 ± 0.2 µM in late-summer). Surface [$Si(OH)_4$] was high throughout the sampling period (average of 45.6 ± 1.4 µM in early-summer and 49.6 ± 17.6 µM in late-summer; Table 1a and 1b), with markedly high concentrations at the SACCF1 in late-summer (54.5 ± 12.8 µM) as well as at S16 and S17 (61.3 ± 0.2 µM at S16 and 64.4 ± 0.4 µM at S17) (Table 1b). Between the SAF and the SACCF, the gradient in surface [$Si(OH)_4$] was far steeper than that of [NO_3^-] and [PO_4^{3-}]. Surface [NH_4^+] increased three-fold over the season (average of 0.3 ± 0.1 µM in early-summer and 0.9 ± 1.0 µM in late-summer), primarily due to the inclusion of stations near SG in late-summer, while low surface [urea] was sustained (average of 0.1 ± 0.1 µM in early-summer and 0.1 ± 0.0 µM in late-summer; Fig. 3; Table 1a and 1b).

In the PAZ, surface [NO_3^-] decreased slightly over the sampling period (average of 26.3 ± 1.7 µM in early-summer and 23.4 ± 2.4 µM in late-summer), while [PO_4^{3-}] increased slightly (average of 1.7 ± 0.1 µM in early-summer and 2.1 ± 0.1 µM in late-summer) and [$Si(OH)_4$] remained consistently high (average of 60.9 ± 3.6 µM in early-summer and 59.3 ± 4.6 µM in late-summer; Fig. 3; Table 1a and 1b). Low surface [NH_4^+] was sustained over the season (average of 0.1 ± 0.1 µM in early-summer and 0.4 ± 0.4 µM in late-summer), with the highest concentration observed at S14 in late-summer (0.6 ± nd; Table 1b). Low surface [urea] was sustained across the seasonal progression (average of 0.1 ± 0.1 µM in early-summer and 0.1 ± 0.1 µM in late-summer).

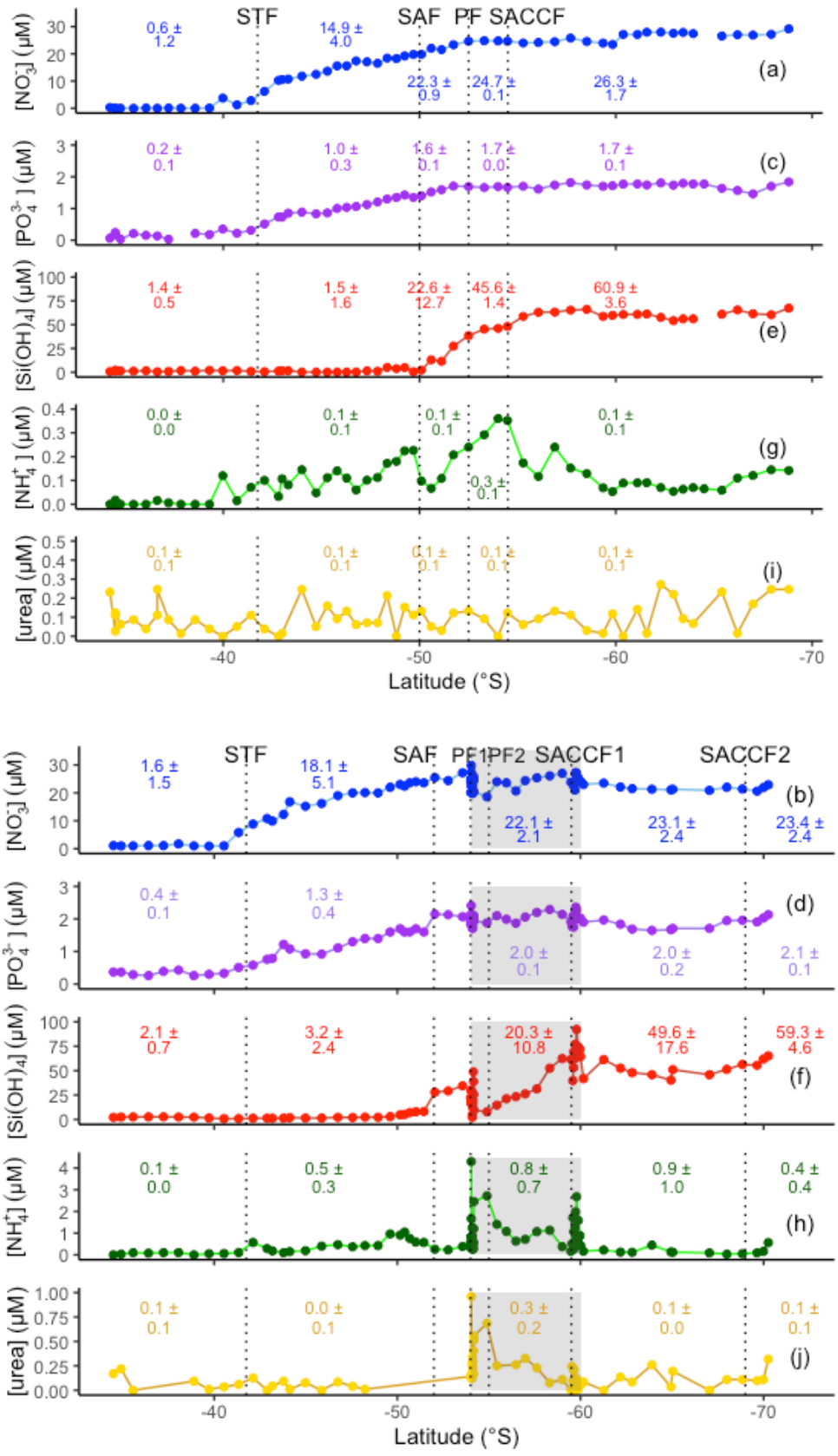

Figure 3: Surface nutrient concentrations of (a, b) Nitrate [NO_3^- ; μM], (c, d) Phosphate [PO_4^{3-} ; μM], (e, f) silicate [$Si(OH)_4$; μM], (g, h) Ammonium [NH_4^+ ; μM], and (i, j) Urea [μM] for (a, c, e, g, i) the early-summer and (b, d, f, h, j) the late-summer transects. The mean frontal positions are denoted by dashed black vertical lines, with abbreviations as in Fig. 2. The average nutrient concentrations for each zone are labelled on the panel, reported with one standard deviation (± 1 S.D.). In panel b, the region downstream

of SG that appears to be influenced by the IME is indicated by the opaque shaded area. Note the differences in the y-axes between panels.

4.1.3. Surface nutrient dynamics

Surface Si* generally decreased from high to low latitudes, although it was higher in the STZ than in the SAZ (Fig. 4). The lowest Si* values were observed across the SAZ (average of -13.4 ± 3.6 µM in early-summer and -14.9 ± 3.6 µM in late-summer), characteristic of $Si(OH)_4$-deplete waters associated with the region northwards of SAMW and AAIW formation and subduction, occurring in the PFZ (-10 to -15 µM; Sarmiento et al., 2004). The greatest variability in Si* both seasonally and inter-zonally was observed across the PFZ (average of -0.3 ± 11.3 µM in early-summer and -2.8 ± 9.7 µM in late-summer). Si* variability across the late-summer OAZ was notably high, potentially attributed to the IME (Doty & Oguri, 1956), with S20 and S18 falling within the region downstream of SG (average of 27.3 ± 19.4 µM).

In early-summer, across all zones southwards of the STF, surface [DIN]: $[PO_4^{3-}]$ was slightly lower than the Redfield ratio of 16:1 (Redfield et al., 1934 & 1958) (average ratio of 14.8 ± 0.6; Fig. 5a). In late-summer, across all zones southwards of the SAF, surface [DIN]:$[PO_4^{3-}]$ declined, with ratios ranging from 11.5 to 12.3 (average ratio of 11.9 ± 0.4; Fig. 5b). Surface [DIN]:$[PO_4^{3-}]$ across the SAZ was invariant over the sampling period (14.6 ± 1.2 in early-summer and 14.8 ± 1.8 in late-summer), while surface [DIN]:$[PO_4^{3-}]$ across the STZ was very low (3.7 ± 4.0 in early-summer and 4.2 ± 2.6 in late-summer; Fig. 5), which is to be expected given that this region is primarily N (rather than PO_4^{3-}) limited (Sarmiento et al., 2004; Sigman & Hain, 2012).

Surface consumption of $[Si(OH)_4]$:$[NO_3^-]$ decreased across all zones over the sampling period from an average molar ratio of 2.8 ± 2.3 in early-summer to 1.6 ± 1.7 in late-summer, with the largest decrease observed across the PAZ (average of 5.9 ± 0.5 in early-summer and 3.8 ± 0.5 in late-summer) (Fig. 6). South of the SAF where $[Si(OH)_4]$ begins to rise (Fig. 3), the average surface consumption of $[Si(OH)_4]$:$[NO_3^-]$ decreased from 4.3 ± 1.5 to 2.8 ± 0.9 between early- and late-summer (Fig. 6). The greatest variability in $[Si(OH)_4]$:$[NO_3^-]$ consumption was observed across the PAZ in early-summer and across the PFZ in late-summer, the latter due to the zonal transect between the GH line and SG island. Elevated surface consumption of $[Si(OH)_4]$ relative to $[NO_3^-]$ was observed in the regions of the PF1 (average of 9.3 ± 3.9), while in the region of the SACCF1 surface $[Si(OH)_4]$:$[NO_3^-]$ consumption decreased (average of 5.0 ± 1.3) in late-summer (Fig. 6b).

Surface consumption of $[NO_3^-]$:$[PO_4^{3-}]$ increased substantially across all zones with the seasonal progression, with the exception of in the SAZ where $[NO_3^-]$:$[PO_4^{3-}]$ remained roughly the same (average of 14.7 ± 2.8 in early-summer and 13.4 ± 5.6 in late-summer) (Fig. 7). South of the SAF, $[NO_3^-]$:$[PO_4^{3-}]$ consumption ranged between 13.1 ± 0.6 in early-summer to 35.5 ± 8.4 in late-summer, an observed increase of two to three-fold. Particularly elevated consumption of $[NO_3^-]$:$[PO_4^{3-}]$ was observed in the region downstream of SG in late-summer (average of 42.4 ± 19.6), indicating the very low consumption of PO_4^{3-} relative to NO_3^-.

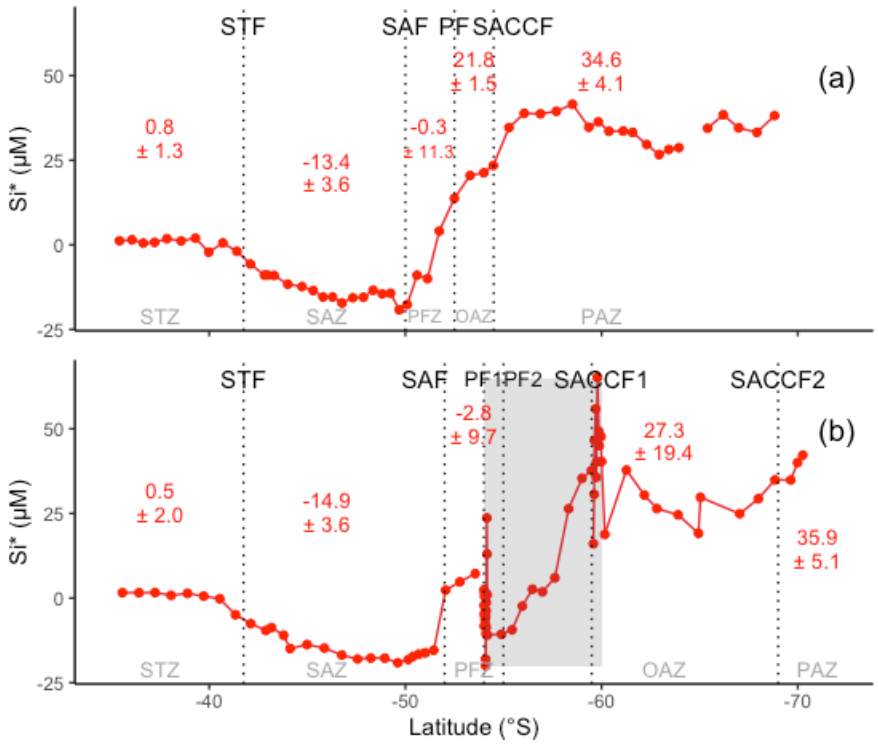

Figure 4: Surface Si* concentrations [μM] with latitude for (a) the early-summer and (b) the late-summer transects. The mean frontal positions are denoted by dashed black vertical lines, with abbreviations as in Fig. 2. Si* concentrations were calculated using equation 1.1, with the average Si*concentration for each zone labelled on the panel (± 1 S.D.). In panel b, the region downstream of SG that appears to be influenced by the IME is indicated by the opaque shaded area.

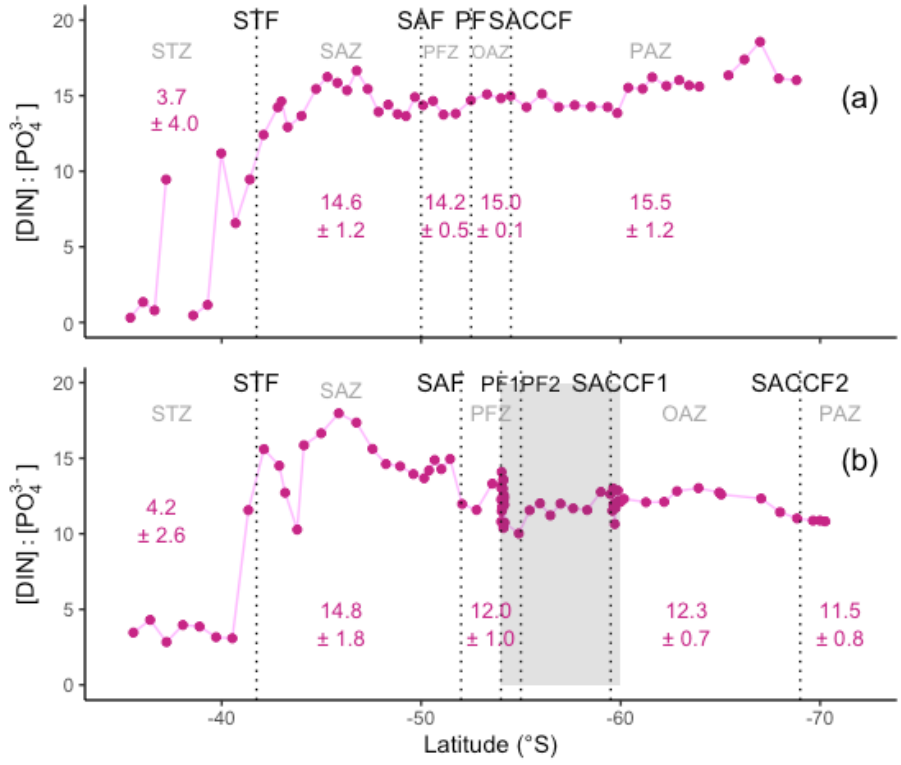

Figure 5: Surface dissolved inorganic nitrogen (DIN) to Phosphate concentration ratios with latitude for (a) the early-summer and (b) the late-summer transects. The mean frontal positions are denoted by dashed black vertical lines, with abbreviations as in Fig. 2. The ratio of DIN to phosphate was calculated from equation 1.2, with the average DIN to Phosphate concentration ratio for each zone labelled on the panel (± 1 S.D.). In panel b, the region downstream of SG that appears to be influenced by the IME is indicated by the opaque shaded area.

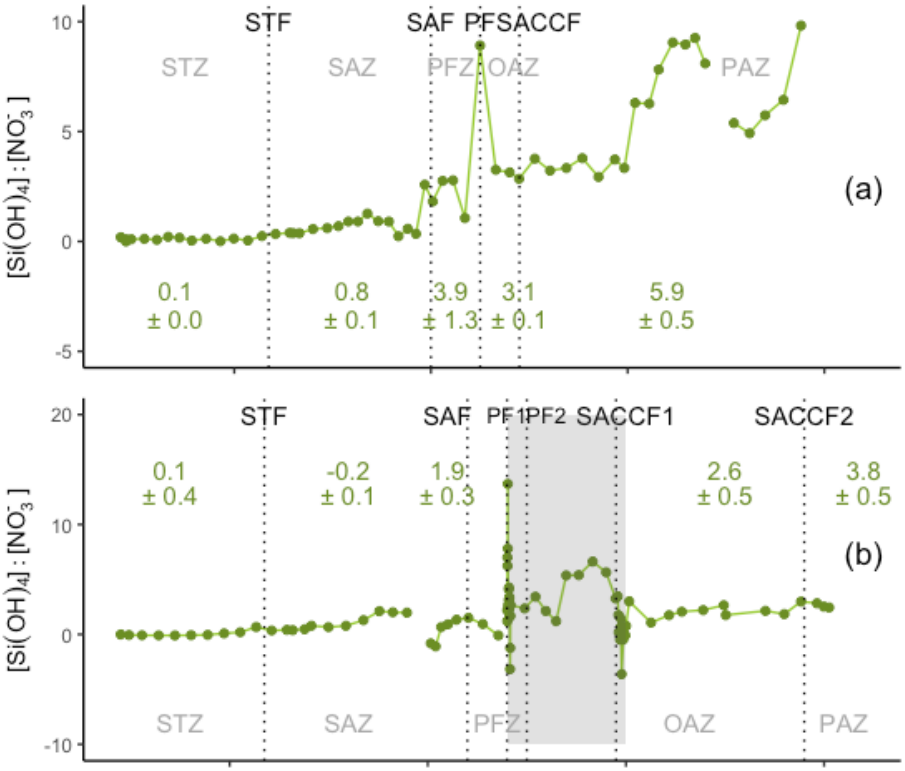

Figure 6: Surface consumption ratios of $Si(OH)_4$:NO_3^- consumption for (a) the early-summer and (b) the late-summer transects. The mean frontal positions are denoted by dashed black vertical lines, with abbreviations as in Fig. 2. The concentrations of nutrients consumed were calculated from equations 1.4 and 1.3 for $Si(OH)_4$ and NO_3^-, respectively. The ratio of consumed surface $Si(OH)_4$:NO_3^- was calculated from equation 1.6, with the average nutrient consumption ratios for each zone labelled on the panel (± 1 S.D.). In panel b, the region downstream of SG that appears to be influenced by the IME is indicated by the opaque shaded area. Note the differences in the y-axes between panels.

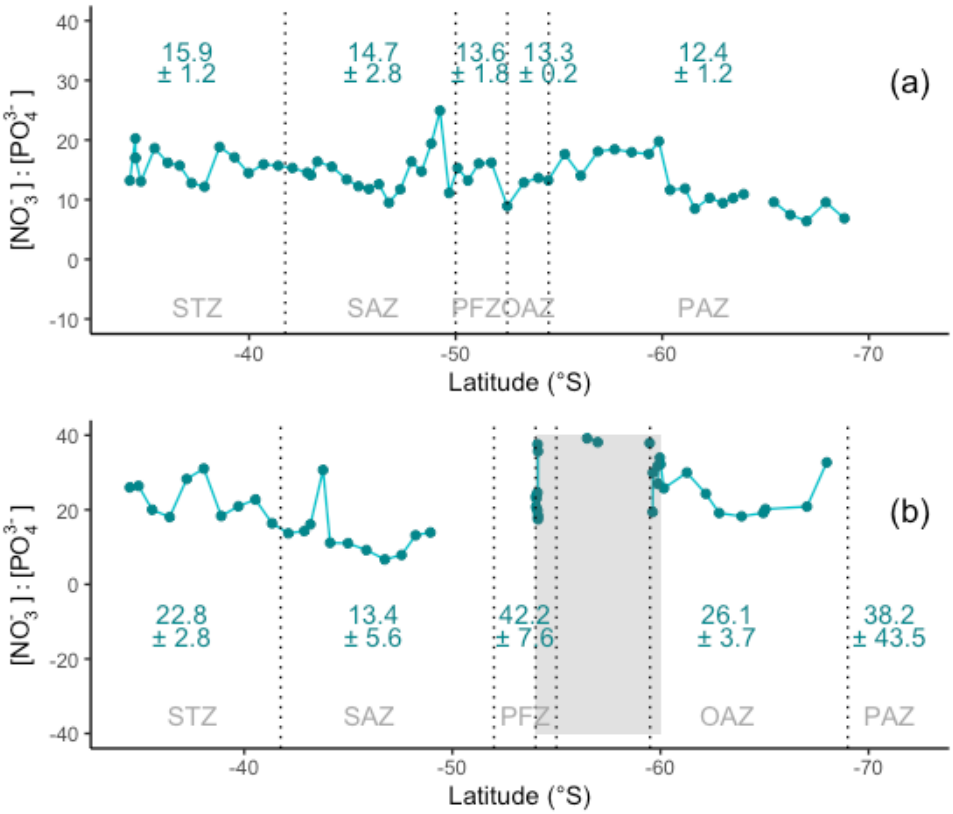

Figure 7: Surface consumption ratios of NO_3^-:PO_4^{3-} consumption for (a) the early-summer and (b) the late-summer transects. The mean frontal positions are denoted by dashed black vertical lines, with abbreviations as in Fig. 2. The concentrations of source nutrients consumed are calculated from equations 1.3 and 1.5 for NO_3^- and PO_4^{3-}, respectively. The ratio of consumed surface NO_3^-:PO_4^{3-} was calculated from equation 1.7, with the average nutrient consumption ratios for each zone are labelled on the panel (± 1 S.D.). In panel b, the region downstream of SG that appears to be influenced by the IME is indicated by the opaque shaded area. Note the differences in the y-axes between panels.

	Latitude	Si* (µM)	$[NO_3^-]$ (µM)	$[PO_4^{3-}]$ (µM)	$[Si(OH)_4]$ (µM)	$[NH_4^+]$ (µM)	[Urea] (µM)
STZ mean		**0.8 (1.3)**	**0.6 (1.2)**	**0.2 (0.1)**	**1.4 (0.5)**	**0.02 (0.03)**	**0.1 (0.1)**
STF	41°41.15'S	-3.8	4.5 (0.2)	0.4 (0.0)	0.8 (0.1)	0.1 (nd)	
S1	34°13.6'S	0.4	0.3 (0.2)	0.1 (0.0)	0.7 (0.3)	0.0 (nd)	0.2 (0.1)
S2	35°06.134'S	1.2	0.0 (0.0)	0.2 (0.0)	1.2 (0.4)	0.0 (nd)	0.1 (0.0)
S3	38°56.464'S	1.2	0.0 (0.0)	0.2 (0.0)	1.2 (0.1)	0.0 (nd)	0.1 (0.0)
S4	39°58.562'S	-2.2	3.7 (0.0)	0.4 (0.0)	1.6 (0.2)	0.1 (nd)	0.0 (0.1)
SAZ mean		**-13.4 (3.6)**	**14.9 (4.9)**	**1.0 (0.3)**	**1.5 (1.6)**	**0.1 (0.1)**	**0.1 (0.1)**
SAF	50°09.39'S	-13.3	20.9 (0.5)	1.5 (0.0)	7.7 (0.0)	0.1 (nd)	
S5	46°17.175'S	-15.4	15.6 (0.3)	1.0 (0.1)	0.2 (0.2)	0.1 (nd)	0.1 (0.0)
S6	46°46.152'S	-17.2	17.4 (0.4)	1.1 (0.0)	0.2 (0.0)	0.1 (nd)	0.1 (0.1)
S7	49°02.003'S	-14.5	18.3 (0.5)	1.4 (0.0)	3.8 (0.4)	0.2 (nd)	0.0 (0.0)
PFZ mean		**-0.3 (11.3)**	**22.3 (0.9)**	**1.6 (0.1)**	**22.6 (12.7)**	**0.1 (0.1)**	**0.1 (0.1)**
PF	51°72.87'S	17.1	24.0 (0.3)	1.7 (0.0)	41.9 (0.1)	0.2 (nd)	
S8	52°29.857'S	13.7	24.7 (0.6)	1.7 (0.0)	38.4 (0.1)	0.2 (nd)	0.11 (0.0)
OAZ mean		**21.8 (1.5)**	**24.7 (0.1)**	**1.7 (0.0)**	**46.5 (1.4)**	**0.3 (0.1)**	**0.1 (0.1)**
SACCF	54°48.09'S	29.0	24.3 (0.5)	1.7 (0.1)	53.4 (0.2)	0.3 (nd)	
S9	53°44.284'S	21.3	24.8 (0.4)	1.7 (0.0)	46.1 (0.1)	0.4 (nd)	0.0 (0.0)
PAZ mean		**34.6 (4.1)**	**26.3 (1.7)**	**1.7 (0.1)**	**60.9 (3.6)**	**0.1 (0.1)**	**0.1 (0.1)**
S10	56°53.195'S	38.7	24.5 (0.6)	1.7 (0.1)	63.2 (0.3)	0.2 (nd)	0.1 (0.0)
S11	61°05.928'S	33.6	27.1 (0.2)	1.8 (0.1)	60.8 (0.4)	0.1 (nd)	0.1 (0.1)
S12	61°58.890'S	29.7	28.0 (0.4)	1.8 (0.0)	57.6 (0.1)	0.1 (nd)	0.3 (0.0)
S13	64°29.838'S	28.7	27.4 (0.3)	1.8 (0.0)	56.1 (0.1)	0.1 (nd)	0.1 (0.1)

Table 1a: Surface nutrient concentrations [µM] and the derived parameter Si* [µM] for the early-summer transect. The mean zone and station values are reported with one standard deviation (± 1 S.D.), where available (nd = no data, where standard deviation data was unavailable).

	Latitude	Si* (µM)	$[NO_3^-]$ (µM)	$[PO_4^{3-}]$ (µM)	$[Si(OH)_4]$ (µM)	$[NH_4^+]$ (µM)	[Urea] (µM)
STZ mean		**0.5 (1.2)**	**1.6 (1.5)**	**0.4 (0.1)**	**2.1 (0.7)**	**0.1 (0.0)**	**0.1 (0.1)**
STF	41°33.71'S	-6.2	7.3 (2.1)	0.6 (0.1)	1.1 (0.2)	0.3 (0.3)	0.1 (0.0)
S31	37°14.119'S	1.6	1.1 (0.3)	0.4 (0.2)	2.7 (0.1)	0.10 (nd)	0.0 (0.1)
S30	38°28.859'S	1.4	1.0 (0.3)	0.3 (0.0)	2.4 (0.1)	0.00 (nd)	0.1 (0.1)
SAZ mean		**-14.9 (3.6)**	**18.1 (5.1)**	**1.3 (0.4)**	**3.2 (2.4)**	**0.5 (0.3)**	**0.0 (0.0)**
SAF	51°44.93'S	-6.5	24.6 (1.3)	1.9 (0.4)	18.0 (13.9)	0.4 (0.2)	0.1 (0.1)
S29	45°52.110'S	-14.8	16.2 (0.1)	0.9 (0.1)	1.4 (0.2)	0.4 (nd)	0.0 (0.0)
S28	47°11.759'S	-18.0	20.0 (0.1)	1.3 (0.0)	2.0 (0.1)	0.4 (nd)	0.0 (0.0)
PFZ mean		**-2.8 (9.7)**	**22.1 (2.1)**	**2.0 (0.1)**	**20.3 (10.8)**	**0.8 (0.7)**	**0.1 (0.1)**
PF1	54°00.96'S	-5.3	24.9 (1.8)	2.1 (0.2)	21.1 (5.9)	0.8 (0.6)	0.3 (0.0)
PF2	56°28.321'S	-2.2	22.6 (2.6)	2.0 (0.1)	24.8 (2.1)	0.7 (0.1)	0.3 (0.0)
S27	53°59.275'S	-2.2	24.1 (0.1)	2.0 (0.1)	21.9 (0.3)	0.3 (nd)	0.1 (0.0)
S25	54°03.170'S	-6.5	23.1 (0.4)	2.0 (0.0)	16.6 (0.2)	0.5 (nd)	0.2 (0.0)
S24	54°05.350'S	-18.0	22.4 (0.5)	1.9 (0.0)	4.4 (0.2)	1.2 (nd)	0.1 (0.0)
S23	54°05.379'S	-1.3	19.8 (0.1)	1.9 (0.0)	18.5 (0.1)	0.5 (nd)	0.3 (0.0)
S22	54°09.363'S	13.0	25.9 (0.2)	2.1 (0.1)	38.9 (nd)	0.6 (nd)	0.4 (0.1)
S21	56°28.321'S	2.6	20.7 (0.0)	1.9 (0.0)	23.3 (0.1)	0.6 (nd)	0.3 (0.0)
OAZ mean		**27.3 (19.4)**	**23.1 (2.4)**	**2.0 (0.2)**	**49.6 (17.6)**	**0.9 (1.0)**	**0.1 (0.1)**
SACCF1	59°00.28'S	36.5	24.8 (1.9)	1.8 (0.1)	54.5 (12.8)	0.7 (0.7)	0.1 (0.0)
S26	54°02.881'S	0.5	29.8 (0.0)	2.2 (0.0)	30.3 (0.2)	4.3 (nd)	1.0 (0.0)
S20	57°16.961'S	6.0	25.4 (0.5)	2.2 (0.1)	31.4 (0.1)	1.1 (nd)	0.2 (0.0)
S18	59°33.601'S	16.1	23.7 (0.0)	2.1 (0.0)	39.8 (0.0)	1.7 (nd)	0.1 (0.0)
S17	59°58.420'S	40.3	24.1 (0.2)	2.0 (0.1)	64.4 (0.4)	0.4 (nd)	0.1 (0.2)
S16	61°16.027'S	37.8	23.5 (0.5)	2.0 (0.1)	61.3 (0.2)	0.2 (nd)	0.0 (0.0)
S15	67°02.462'S	24.9	20.9 (0.3)	1.7 (0.1)	45.8 (0.3)	0.1 (nd)	0.0 (0.0)
PAZ mean		**35.9 (5.1)**	**23.4 (2.4)**	**2.1 (0.1)**	**59.3 (4.6)**	**0.4 (0.4)**	**0.1 (0.1)**
SACCF2	67°99.06'S	32.1	21.7 (0.4)	2.0 (0.0)	53.8 (3.5)	0.0 (0.0)	0.1 (0.0)
S19	59°28.431'S	37.7	23.8 (0.2)	1.9 (0.1)	61.5 (0.5)	0.2 (nd)	0.0 (0.0)
S14	70°17.060'S	42.2	22.9 (0.6)	2.1 (0.0)	65.1 (0.3)	0.6 (nd)	0.3 (0.0)

Table 1b: Surface nutrient concentrations [µM] and the derived parameter Si* [µM] for the late-summer transect. The mean zone and station values are reported with one standard deviation (± 1 S.D.), where available (nd = no data, where standard deviation data was unavailable).

4.2. Biomass distribution

4.2.1. Surface [PON] and relative size-class biomass contribution

In early-summer, surface particulate organic nitrogen (PON) concentrations were similar across the STZ, PFZ and OAZ, with zonal averages of 0.8 ± 0.1 µM, 0.8 ± 0.0 µM and 0.6 ± 0.0 µM, respectively (Fig. 8a). The highest surface [PON] were observed in the SAZ and PAZ (average of 1.5 ± 0.1 µM and 1.3 ± 0.1 µM, respectively), with the SAZ being the zone of highest observed surface [PON] (Fig. 8a green bars). The relative contribution of the different phytoplankton size-classes to surface biomass (i.e., [PON]) was similar across all zones, with the greatest contribution from nanophytoplankton (ranging from 52-74% of total surface [PON]; Table 4a). Relative contributions to total surface [PON] from microphytoplankton and picophytoplankton were more variable across all zones, although their respective contributions were typically similar, except in the SAZ where microphytoplankton dominated surface [PON] (39%) compared to picophytoplankton (9%; Table 4a).

An increase in surface [PON] was observed across all zones during late-summer, with the exception of the SAZ where surface [PON] decreased between early- and late-summer (~33% decrease; Fig. 8b, Table 4b). The largest increase in surface [PON] was observed south of the SAF across the PFZ, OAZ and PAZ (averages of 1.8 ± 0.4 µM, 1.7 ± 0.3 µM and 2.5 ± 0.1 µM for the PFZ, OAZ and PAZ, respectively). The AZ was characterized by the highest total surface [PON] in late-summer, with maximum values observed across the PAZ (average of 2.5 ± 0.1 µM; Fig. 8b). Relative phytoplankton size-class contributions to surface [PON] were consistent across the STZ and SAZ, with a slight decrease in nanophytoplankton contribution, albeit still retaining the dominance in surface [PON] contribution (59% and 50% of total PON for the STZ and SAZ, respectively). The contribution from microphytoplankton to surface [PON] across the STZ decreased from 10% to 5%, while the contribution from picophytoplankton was observed to increase from 22% to 36% over the season (Table 4a and 4b). Similarly, a marked decrease in microphytoplankton contribution to surface [PON], from 39% to 0%, was observed across the SAZ over the sampling period, with a concurrent increase in picophytoplankton contribution, from 9% to 50%. Nanophytoplankton contribution to surface [PON] across the PFZ was relatively consistent over the season, while a substantially decreased contribution from microphytoplankton from 11% to 0.2% and an increased contribution from picophytoplankton from 15% to 22% was observed. Relative contributions in surface [PON] were consistent across the AZ in late-summer, with the greatest contribution from nanophytoplankton (average of 68 ± 4.2%) and contributions from micro- and picophytoplankton consistent across the season, where the contribution from picophytoplankton was slightly higher than microphytoplankton.

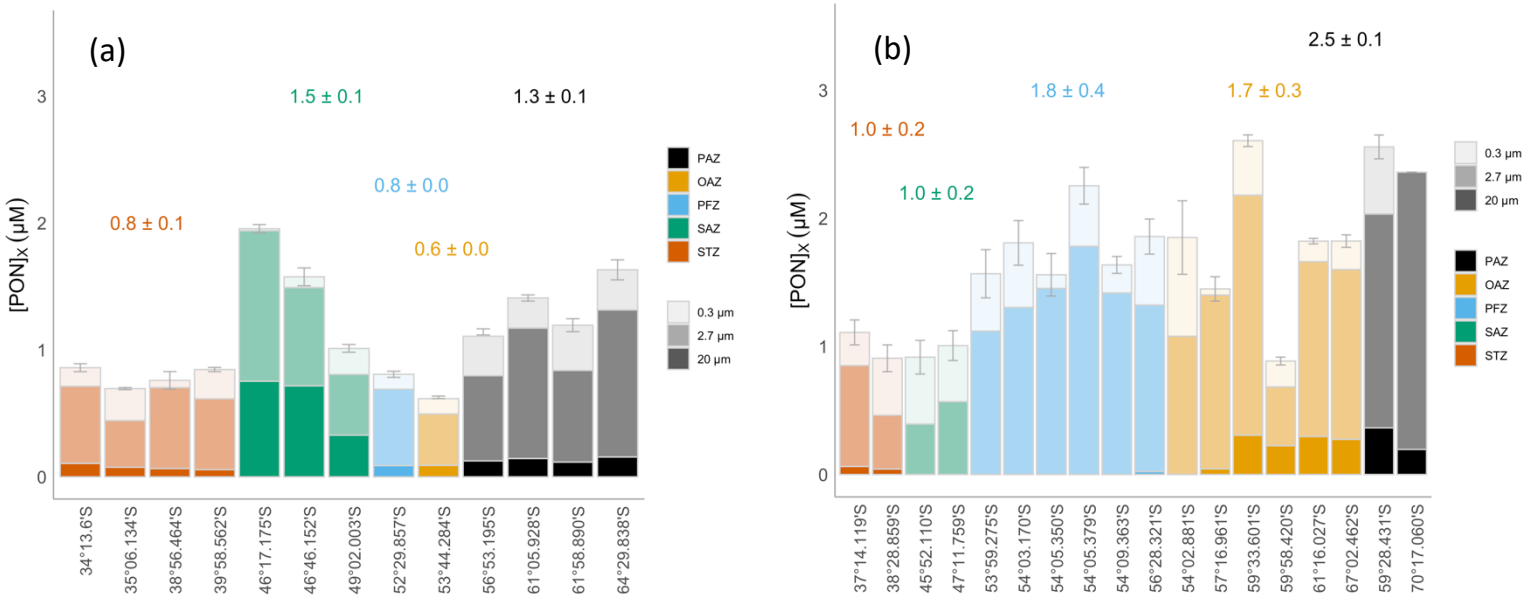

Figure 8. Total surface particulate organic nitrogen (PON) [µM] concentration measured at each station for a) the early-summer and b) the late-summer transects. Shaded segments on the bars represent the different phytoplankton size-fractions (0.3-2.7 µm, 2.7-20 µm and 20-200 µm) and colours indicate the frontal zones, from north to south - STZ (orange), SAZ (green), PFZ (blue), OAZ (yellow) and PAZ (black). The concentration and isotopic composition of PON was determined according to equations 1.8 – 1.11, with the average surface PON concentration (± 1 S.D.) for each zone labelled on the panel. The error bars represent ± 1 S.D. of 4 measurements of each sample. Where applicable, the error has been propagated according to standard statistical practices.

4.2.2. Size-fractionated POC:PON concentration

In early-summer, the biomass C:N ratio (i.e., [POC]/[PON]) across all zones generally conformed to the expected C:N ratio of 6.63:1 that is typical for bulk marine biomass (Redfield et al., 1934 & 1958), with an average ratio of 6.9 ± 1.1 (Fig. 9a). The highest C:N ratio was observed across the PAZ (average of 8.3 ± 1.9) as was the highest variability in C:N among the size-classes, while the lowest biomass C:N ratio was observed across the OAZ (average of 5.6 ± 0.1).

In late-summer, an increase in the C:N ratio across all zones was observed (Fig. 9b). The average ratio across the transect was 9.3 ± 1.9, although it decreased with increasing latitude The highest C:N ratio was observed across the STZ (average of 12.6 ± 2.1), while the lowest ratio was apparent across the PAZ (average of 8.0 ± 3.0), similar to that measured in early-summer (Fig. 9a). The highest degree of size-class variability in C:N was observed across the STZ, with picophytoplankton being the size-class most frequently observed to have a C:N ratio >6.63 in all the other zones (Fig. 9b).

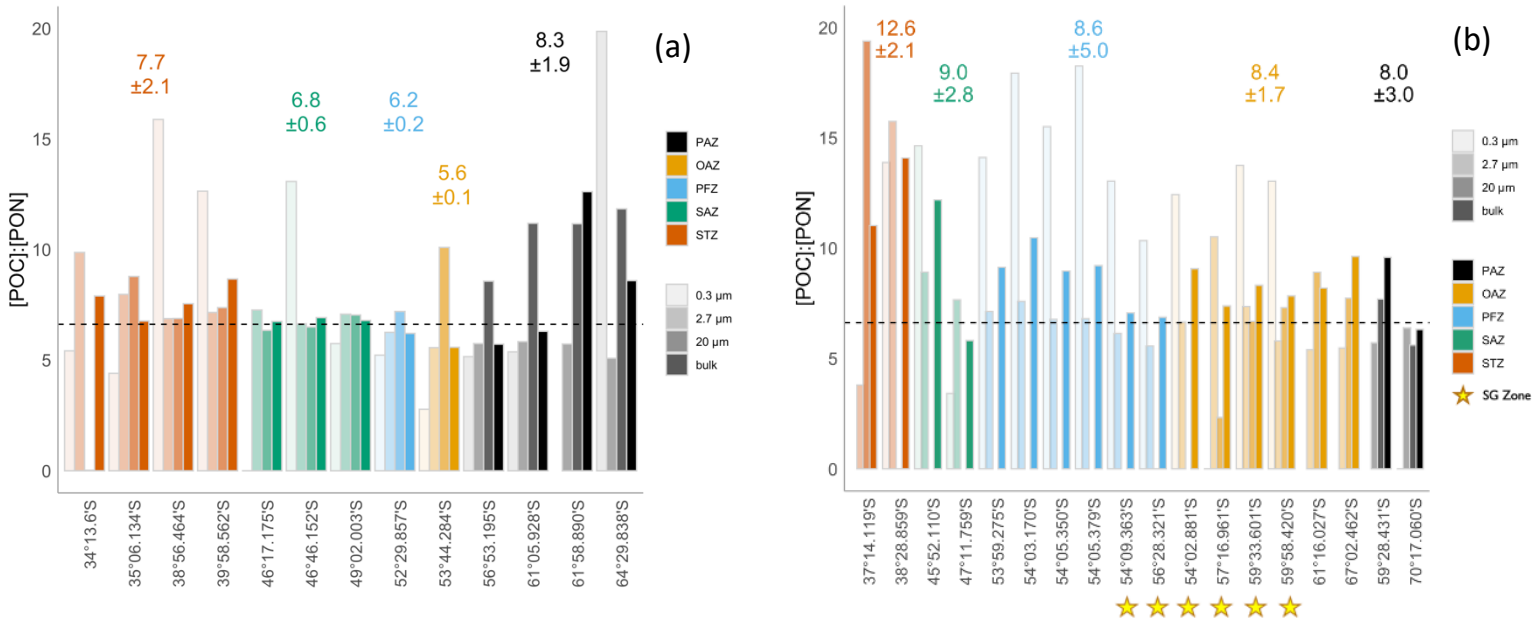

Figure 9: Surface particulate organic carbon (POC) to PON ratios at each station for a) the early-summer and b) the late-summer transects. The colour and shading of the bars are representative of the size-class and frontal zones as defined in Figure 8. The Redfield ratio of 106:16 (Redfield et al., 1934 & 1958) is denoted by the dashed black horizontal line. The concentration and isotopic composition of POC and PON were determined according to equations 1.8 – 1.11, with the average surface POC to PON concentration ratio (± 1 S.D.) for each zone labelled on the panel. In panel b, the region downstream of SG that appears to be influenced by the IME is indicated by the opaque shaded area.

4.2.3. Latitudinal distribution of surface Chl-a

In early-summer, Chl-a concentrations associated with the bulk phytoplankton community were consistently low across the STZ, PFZ and OAZ (averages of 0.5 ± 0.2 µg L^{-1}, 0.5 ± 0.1 µg L^{-1} and 0.5 ± 0.1 µg L^{-1}, respectively; Fig. 10a). Higher Chl-a concentrations were observed across the SAZ and

PAZ (averages of 1.9 ± 0.9 µg L^{-1} and 0.9 ± 0.3 µg L^{-1}, respectively), with the SAZ supporting the highest Chl-a concentrations. This result is coincident with the SAZ being the region of highest [PON] compared to all other zones in early-summer (Fig. 8a; Table 3a).

Late-summer was characterized by a southward shift in the regions of highest measured Chl-a concentrations, with an increase observed across the PAZ, OAZ and PFZ (average of 1.7 ± 1.2 µg L^{-1}, 0.7 ± 0.7 µg L^{-1} and 1.11 ± 0.7 µg L^{-1}, respectively), albeit with a significant degree of variability (Fig. 10b). This result is consistent with the PAZ being the region of highest [PON] in late-summer (Fig. 8b; Table 3b). Chl-a concentrations across the STZ and SAZ decreased over the sampling period (average of 0.3 ± 0.2 µg L^{-1} and 0.4 ± 0.1 µg L^{-1}, respectively, in late-summer), with the largest decrease observed across the SAZ (average of 1.9 ± 0.9 µg L^{-1} in early-summer and 0.4 ± 0.1 µg L^{-1} in late-summer; Fig. 10).

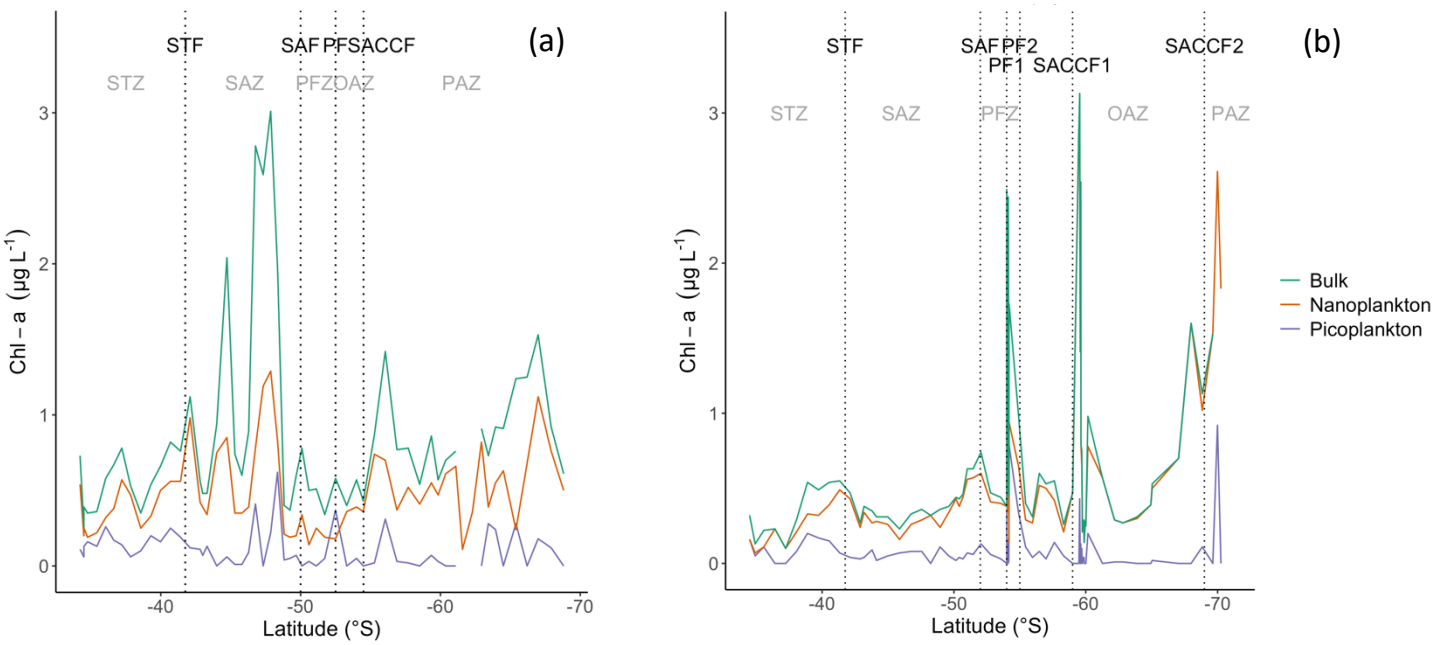

Figure 10: Surface chlorophyll-a (chl-a) concentration [µg L^{-1}] with latitude for a) the early-summer and b) the late-summer transects. The mean frontal positions are denoted by dashed black vertical lines, with abbreviations as in Fig. 2. Size-fractionated chl-a concentrations are indicated by the colour (plot) lines – picophytoplankton (0.3-2.7 µm; purple), nanophytoplankton (2.7-20 µm; orange) and the bulk community chl-a concentration (0.3-200 µm; green).

4.3. Rates of net primary production, nitrate and ammonium uptake

4.3.1. Absolute uptake rates and relative size-class contributions to NPP and N-uptake

The absolute uptake rates of C and N (ρC and ρN, respectively) were averaged across the various frontal zones crossed along the GH transect for early- and late-summer to yield uptake rates comparable across the frontal zones (i.e., zonally) as well as between early- and late-summer (i.e., seasonally).

The highest surface rates of NPP averaged across the respective frontal zones were observed across the SAZ in early-summer (average of 2017.2 ± 13.2 nM C d^{-1}) and the PAZ in late-summer (average of 1692.6 ± 43.4 nM C d^{-1}). A southward shift in the frontal zone supporting the highest rates of NPP was observed with the seasonal progression (Fig. 11; Table 3a and 3b). The STZ (average of 1124.8 ± 9.6 nM C d^{-1} in early-summer and 255.1 ± 11.7 nM C d^{-1} in late-summer) and SAZ (average of 2017.2 ± 13.2 nM C d^{-1} in early-summer and 326.1 ± 5.6 nM C d^{-1} in late-summer) showed substantial decreases in rates of NPP with the seasonal progression (Fig. 11; Table 3a and 3b). Conversely, rates of NPP in the OAZ (average of 271.2 ± 4.3 nM C d^{-1} in early-summer and 589.5 ± 9.4 nM C d^{-1} in late-summer) and PAZ (average of 659.5 ± 9.6 nM C d^{-1} in early-summer and 1692.6 ± 43.4 nM C d^{-1} in late-summer) increased with the seasonal progression, with NPP in the PAZ rising by more than a factor of two. Similarly, rates of NPP across the PFZ (average of 711.3 ± 25.5 nM C d^{-1} in early-summer and 1004.8 ± 8.0 nM C d^{-1} in late-summer) increased over the sampling season, with notably high rates of NPP observed at S23 (2433.9 ± 59.7 nM C d^{-1}), which is located within the region potentially influenced by SG Island.

In early-summer, the nanophytoplankton contributed the most to total rates of NPP across all zones south of the STF, with an average contribution of 76.8-98% (Fig. 11a; Table 4a), while the microphytoplankton contribution was low (average ranging from 2-17.4%) and that of the picophytoplankton was negligible (average ranging from 0-5.8%). The contribution to NPP by picophytoplankton was substantially higher across the STZ in early-summer compared to all other zones (average of 41.4%), while the contribution from microphytoplankton was negligible (average of 1.1%).

In late-summer, the nanophytoplankton again contributed most to NPP across all zones south of the SAF, with an average contribution ranging from 87.1-95.3%, while contributions from both micro- and picophytoplankton were negligible (average range of 0-7.8% for micro- and 0-5.1% for picophytoplankton; Fig. 11b, Table 4b). North of the SAF, nanophytoplankton also contributed most to NPP (average of 62.4% and 75% in the STZ and SAZ, respectively), with the contribution from picophytoplankton being comparably higher than in the PFZ and AZ (average of 36.2% and 25.0% for the STZ and SAZ, respectively) and the contribution from microphytoplankton being negligible (average of 1.4% and 0% for the STZ and SAZ, respectively).

The highest rates of nitrate uptake (ρNO_3^-) were observed across the PAZ in both early- (average of 119.8 ± 4 nM N d^{-1}) and late-summer (average of 162.2 ± 9.1 nM N d^{-1}) (Fig. 12; Table 3a and 3b; note that the OAZ in early-summer, where the rate of nitrate uptake was extremely high (264.7 ± 41.2 nM d^{-1}), is not considered here as only one station was sampled). ρNO_3^- decreased substantially across all zones with the seasonal progression, with the exception of in the PAZ where it increased by ~42 nM N d^{-1}. The STZ sustained low ρNO_3^- over the sampling period, hosting the lowest measured ρNO_3^- in early-summer (average of 51.7 ± 4.1 nM N d^{-1} in early-summer and 2.6 ± 0.5 nM N d^{-1} in late-summer) (Fig. 12; Table 3a and 3b; note that the PFZ in early-summer, where nitrate uptake was markedly low (35.1 ± 1.3 nM N d^{-1}), is not considered here as only one station was sampled).

The highest ammonium uptake rate (ρNH_4^+) was observed in the SAZ during early-summer (average of 85 ± 3.8 nM N d^{-1}) and in the OAZ and PAZ during late-summer (average of 71.4 ± 2.6 nM N d^{-1} and 85.6 ± 1 nM N d^{-1}, respectively) (Fig. 13; Table 3a and 3b). The general trend of ρNH_4^+ was generally similar to that of ρNO_3^-, although a marked increase in ρNH_4^+ was observed across the OAZ over the sampling period (average of 28.4 ± 0.1 nM N d^{-1} in early-summer and 71.4 ± 2.6 nM N d^{-1} in late-summer), coincident with elevated surface [NH_4^+] across the OAZ region due, at least in part, to

the proximity of the stations to SG Island (OAZ average surface [NH_4^+] of 0.3 ± 0.04 µM in early-summer and 0.9 ± 0.6 µM in late-summer). Removing the stations potentially influenced by SG Island yields an average ρNH_4^+ of 57.5 ± 7.6 nM N d^{-1} for the late-summer OAZ. A notable increase in ρNH_4^+ was also observed across the PAZ over the sampling period (average of 34.5 ± 2.4 nM N d^{-1} in early-summer and 85.6 ± 1 nM N d^{-1} in late-summer).

In early-summer, across all zones south of the STF, nanophytoplankton contributed most to ρNO_3^- and ρNH_4^+ (average range of 70.8-91.6% for ρNO_3^- and 70.3-87.8% for ρNH_4^+), with much smaller and similar contributions from microphytoplankton (average range of 0-17.3% for ρNO_3^- and 7.6-10.8% for ρNH_4^+) and picophytoplankton (average range of 3.5-20.6% for ρNO_3^- and 1.5-22.1% for ρNH_4^+). In general, the trends in size-class contribution to ρNO_3^- and ρNH_4^+ across the early-summer zones were similar to those observed for NPP (Table 4a). In the STZ, the nanophytoplankton also dominated ρNO_3^- and ρNH_4^+ (average of 71.2% for ρNO_3^- and 77.7% for ρNH_4^+), while the contributions from microphytoplankton were considerably greater compared to all zones south of the STF (average of 28.1% for ρNO_3^- and 21.6% for ρNH_4^+) and the contribution of the picophytoplankton was negligible (average of 0.7% for ρNO_3^- and 0.7% for ρNH_4^+).

In late-summer, south of the SAF, nanophytoplankton contributed most to ρNO_3^- and ρNH_4^+ (average range of 84.1-93.9% for ρNO_3^- and 83.4-91.8% for ρNH_4^+), with fairly minor contributions from microphytoplankton (average range of 1.4-6% for ρNO_3^- and 5.2-8.2% for ρNH_4^+) and picophytoplankton (average range of 0.1-10.8% for ρNO_3^- and 0-11.4% for ρNH_4^+) (Table 4b). North of the SAF, nanophytoplankton again made the greatest contribution to ρNO_3^- and ρNH_4^+ (average range of 76.2-77.7% for ρNO_3^- and 62.2-69% for ρNH_4^+), while the contribution from microphytoplankton was comparably larger than for all of the AZ (average range of 18.9-22.3% for ρNO_3^- and 25.2-37.8% for ρNH_4^+) and contributions from picophytoplankton were low (average range of 0-4.9% for ρNO_3^- and 0-5.8% for ρNH_4^+).

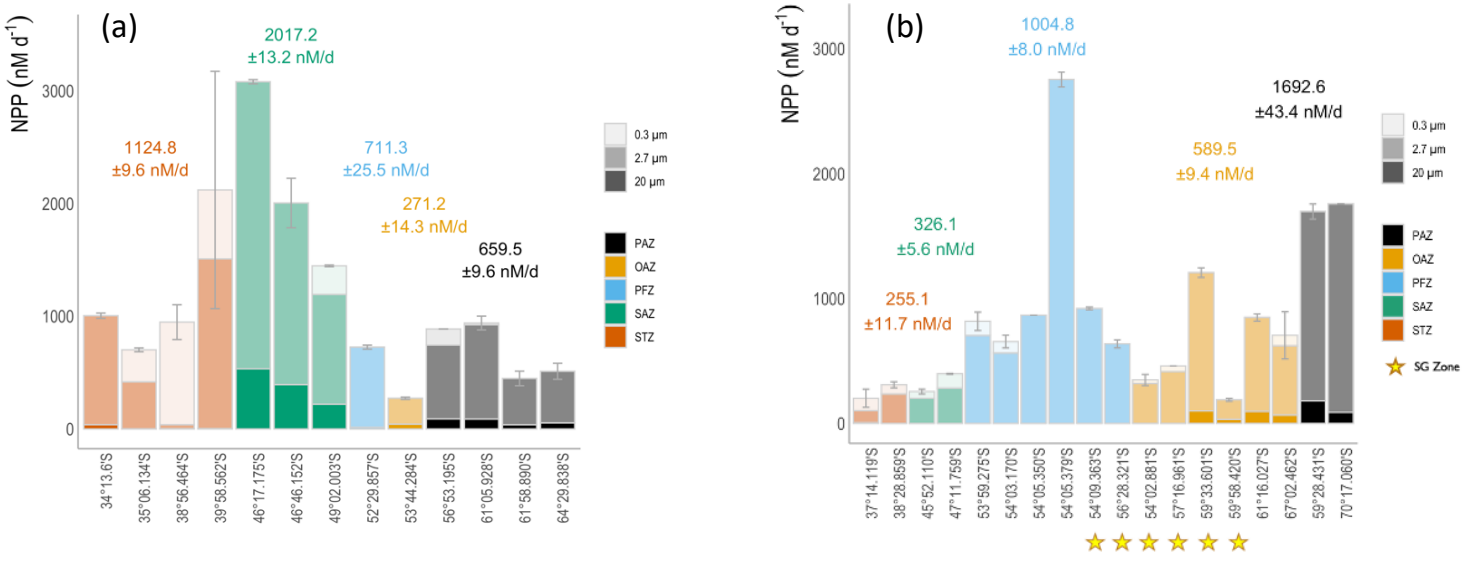

Figure 11: Surface rates of daily NPP (ρC) [nM d^{-1}] at each station for a) the early-summer and b) the late-summer transects. The colour and shading of the bars are representative of the size-class and frontal zones as defined in Figure 8. The size-fractionated daily rates were calculated from equations 1.8 – 1.11, with the average surface rate of daily NPP (± 1 S.D.) for each zone labelled on the panel. The error bars represent of 4 measurements of each sample. Where applicable, the error has been propagated according to standard statistical practices. In panel b, the region downstream of SG that appears to be influenced by the IME is denoted by the yellow star symbols along the x-axis.

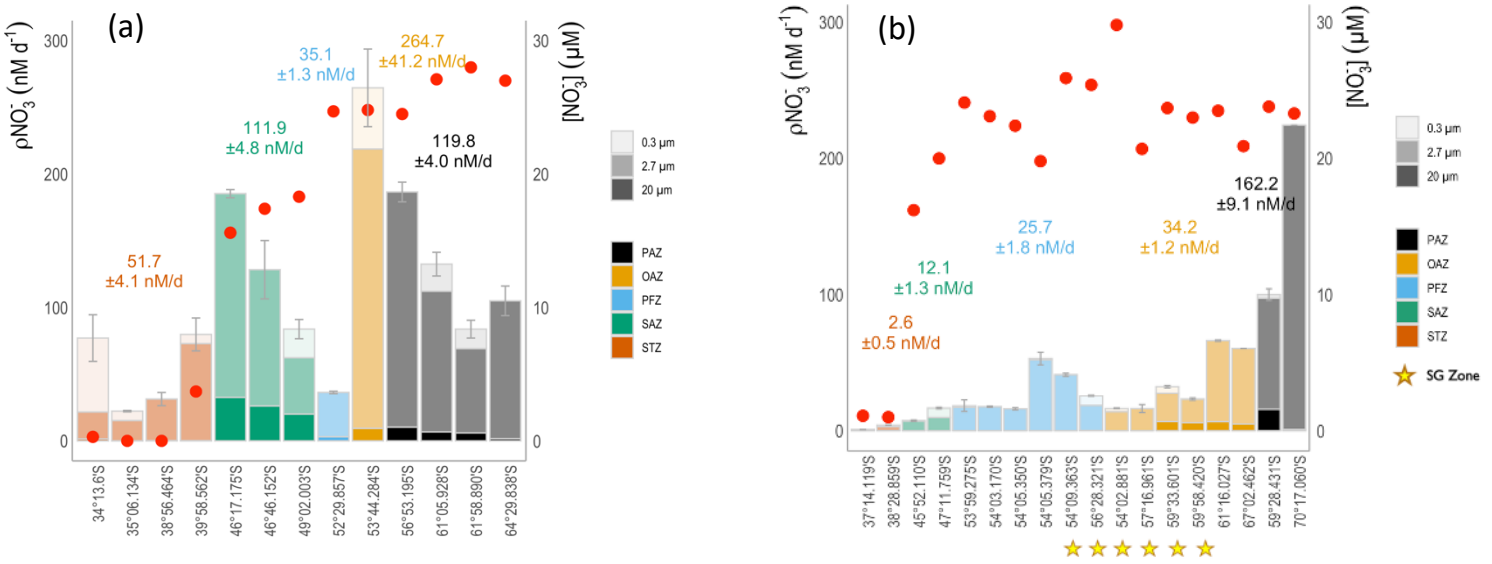

Figure 12: Surface rates of daily NO_3^- uptake (ρNO_3^-) [nM d^{-1}] and surface NO_3^- concentrations [µM] at each station for a) the early-summer and b) the late-summer transects. The colour and shading of the bars are representative of the size-class and frontal zones as defined in Figure 8. The size-fractionated daily rates were calculated from equations 1.8 – 1.11, with the average surface rate of daily NO_3^- uptake for each zone labelled on the panel. The error bars represent ± 1 S.D. of 4 measurements of each sample. Where applicable, the error has been propagated according to standard statistical practices. In panel b, the region downstream of SG that appears to be influenced by the IME is denoted by the yellow star symbols along the x-axis.

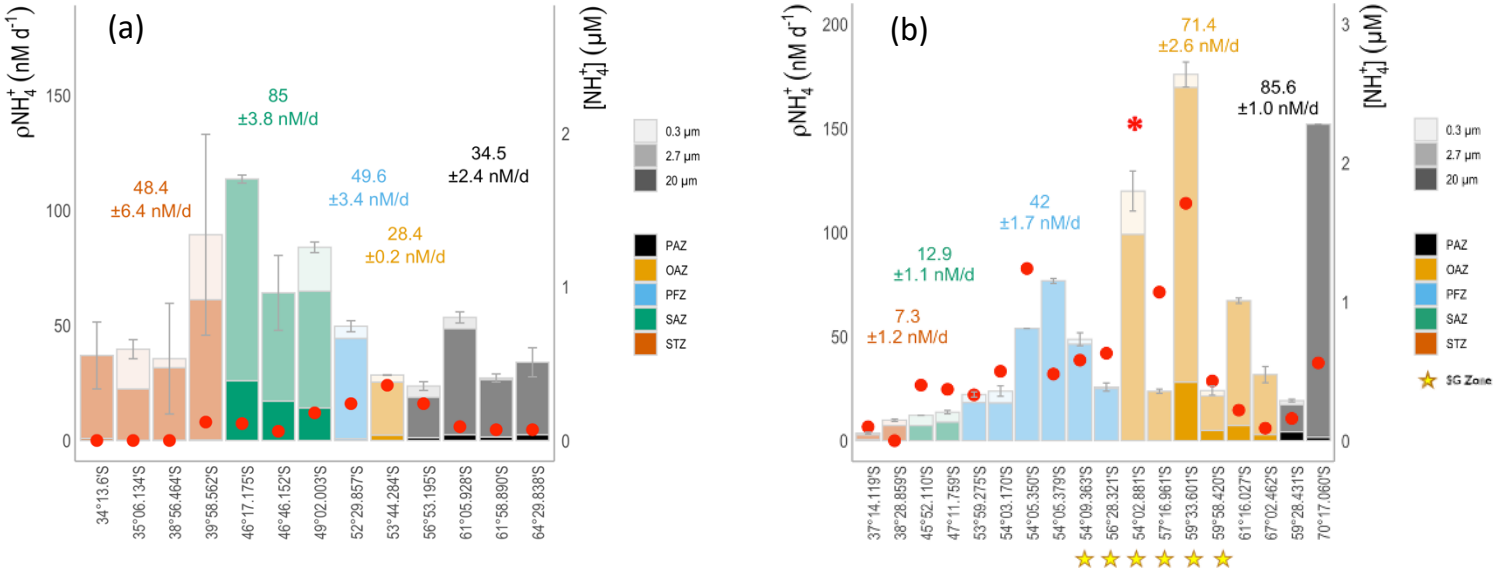

Figure 13: Surface rates of daily NH_4^+ uptake (ρNH_4^+) [nM d^{-1}] and surface NH_4^+ concentrations [µM] at each station for a) the early-summer and b) the late-summer transects. The colour and shading of the bars are representative of the size-class and frontal zones as defined in Figure 8. The size-fractionated daily rates were calculated from equations 1.8 – 1.11, with the average surface rate of daily NH_4^+ uptake for each zone labelled on the panel. The error bars represent ± 1 S.D. of 4 measurements of each sample. Where applicable, the error has been propagated according to standard statistical practices. In panel b, the region downstream of SG that appears to be influenced by the IME is denoted by the yellow star symbols along the x-axis.

	Latitude	Size class (μm)	NPP (nM d^{-1})	ρNO_3^- (nM d^{-1})	ρNH_4^+ (nM d^{-1})	V_C (hr^{-1})	V_{NO3-} (hr^{-1})	V_{NH4+} (hr^{-1})
STZ mean		***Bulk***	**1124.8 (9.6)**	**51.7 (4.1)**	**48.4 (6.4)**			
STF	41°41.15'S							
S1	34°13.6'S	*Bulk*	730.9 (23.4)	77.0 (17.5)	29.1 (14.5)	0.007 (0.0001)	0.007 (0.002)	0.003 (0.0004)
		Pico	0.0 (nd)	55.5 (18.1)	0.0 (15.5)	0	0.04	0
		Nano	966.8 (138.6)	20.2 (4.9)	36.1 (5.4)	0.01	0.002	0.004
		Micro	37.5 (12.9)	1.4 (0.3)	0.8 (0.2)	1	0.001	0.0005
S2	35°06.134'S	*Bulk*	701.6 (17.1)	22.3 (0.5)	39.6 (4.1)	0.01 (0.0007)	0.002 ($1x10^{-5}$)	0.004 (0.0005)
		Pico	284.7 (53.7)	7.1 (2.5)	17.3 (4.2)	0.02	0.002	0.006
		Nano	415.9 (50.9)	15.1 (2.5)	22.3 (0.7)	0.01	0.003	0.004
		Micro	1.1 (1.0)	0.1 (0.0)	0.1 (0.0)	0.0001	$5x10^{-5}$	$6x10^{-5}$
S3	38°56.464'S	*Bulk*	947.5 (154.3)	27.7 (4.9)	35.6 (24)	0.008 (0.008)	0.003 (0.0001)	0.003 (0.002)
		Pico	910.3 (387.9)	0 (4.9)	4.0 (24.3)	0	0	0.003
		Nano	35.4 (355.9)	31.1 (0.2)	31.5 (3.2)	0.0005	0.004	0.003
		Micro	1.6 (0.7)	0.2 (0.1)	0.1 (0.0)	0.0002	0.0002	0.0001
S4	39°58.562'S	*Bulk*	2119 (nd)	79.8 (12.3)	89.3 (43.6)	0.01 (0.01)	0.006 (0.0008)	0.007 (0.004)
		Pico	611.1 (6.5)	6.9 (13)	28.2 (43.8)	0	0.002	0.009
		Nano	1505 (6.5)	72.8 (4)	60.9 (4)	0.03	0.009	0.007
		Micro	3.4 (0.7)	0.1 (0.1)	0.2 (0.0)	0.0005	0.0002	0.0002
SAZ mean		***Bulk***	**2017 (13.2)**	**111.9 (4.8)**	**85 (3.8)**			
SAF	50°09.39'S							
S5	46°17.175'S	*Bulk*	2652.1 (18.5)	134.8 (3.0)	110.4 (1.7)	0.01 (0.0003)	0.004 (0.0002)	0.004 ($6x10^{-5}$)
		Pico	0.0 (30.8)	0.0 (19.9)	0.0 (12.0)	0.14	0	0
		Nano	2545.7 (24.6)	152.7	87.6 (11.9)	0.02	0.008	0.005
		Micro	533.5 (22.4)	(19.7)	25.9 (2.4)	0.007	0.003	0.002
				32.6 (8.4)				
S6	46°46.152'S	*Bulk*	1953.3 (219.5)	117.1	60.8 (16.3)	0.01 (0.0005)	0.005 (0.0005)	0.002 (0.0005)
		Pico	0.0 (430.7)	(21.9)	0.0 (19.5)	0	0	0
		Nano	1610.9 (370.6)	0.0 (22.5)	47.0 (10.7)	0.02	0.008	0.004
		Micro	392.9 (14.2)	102.2 (5.3)	17.1 (1.4)	0.005	0.002	0.002
				26.1 (1.5)				
S7	49°02.003'S	*Bulk*	1446.3 (7.6)	83.8 (7.2)	83.9 (2.3)	0.01 (0.0001)	0.005 (0.0005)	0.005 ($1x10^{-5}$)
		Pico	253.6 (152.3)	21.5 (15.1)	19.1 (8.6)	0.01	0.006	0.005
		Nano	973.2 (152.1)	42.2 (13.3)	50.8 (8.3)	0.02	0.006	0.005
		Micro	219.4 (5.4)	20.1 (5.1)	14.1 (0.5)	0.006	0.004	0.002
PFZ mean		***Bulk***	**711.3 (25.5)**	**35.1 (1.3)**	**49.6 (3.4)**			
PF	51°72.87'S							
S8	52°29.857'S	*Bulk*	711.3 (18.0)	35.1 (0.9)	49.6 (2.4)	0.008 ($6x10^{-5}$)	0.003 ($9x10^{-5}$)	0.003 (0.0001)
		Pico	0.0 (41.9)	0.0 (2.1)	5.3 (3.4)	0	0	0.002
		Nano	711.2 (37.9)	33.2 (1.9)	43.6 (2.4)	0.01	0.003	0.004
		Micro	14.4 (13.8)	3.1 (1.6)	0.7 (0.4)	0.001	0.002	0.0005
OAZ mean		***Bulk***	**271.2 (14.3)**	**264.7 (41.2)**	**28.4 (0.2)**			

SACCF	54°48.09'S							
S9	53°44.284'S	*Bulk*	271.2 (10.1)	264.7	28.4 (0.1)	0.005 (0.0002)	0.02 (0.002)	0.003 ($4x10^{-5}$)
		Pico	0.0 (27.4)	(29.1)	3.1 (1.0)	0	0.02	0.002
		Nano	230.1 (25.5)	45.9 (30.7)	24.2 (0.9)	0.006	0.03	0.003
		Micro	42.1 (18.1)	209.4 (9.9)	1.2 (0.9)	0.003	0.007	0.0008
				9.4 (3.0)				
PAZ mean		***Bulk***	**659.5 (9.6)**	**119.8 (4)**	**34.5 (2.4)**			
S10	56°53.195'S	*Bulk*	886.5 (nd)	162.4 (7.4)	23.6 (1.9)	0.008 ($4x10^{-5}$)	0.008 (0.0005)	0.001 (0.0001)
		Pico	142.9 (nd)	0.0 (9.7)	4.9 (2.1)	0	0	0.0009
		Nano	654.6 (nd)	176.3 (6.4)	17.5 (1.0)	0	0.02	0.001
		Micro	89.0 (nd)	10.3 (2)	1.2 (0.0)	0	0.004	0.0006
S11	61°05.928'S							
		Bulk	939.4 (61.3)	132.5 (8.9)	53.5 (2.4)	0.005 ($5x10^{-5}$)	0.005 (0.0002)	0.002 ($3x10^{-5}$)
		Pico	16.0 (69.8)	20.3 (9.5)	4.9 (2.5)	0.0006	0.004	0.001
		Nano	835.9 (33.4)	105.4 (3.4)	46.1 (0.5)	0.007	0.005	0.002
		Micro	87.6 (31.7)	6.7 (0.1)	2.5 (0.5)	0.003	0.003	0.0007
S12	61°58.890'S							
		Bulk	355.1 (64.9)	83.8 (6.7)	27.1 (1.8)	0.001 (0.0004)	0.004 (0.0001)	0.001 ($4x10^{-5}$)
		Pico	0.0 (72.8)	14.6 (7.0)	0.8 (5.4)	0	0.003	$9 x10^{-5}$
		Nano	411.1 (33.2)	63.2 (2.2)	24.9 (5.1)	0.005	0.004	0.002
		Micro	36.8 (3.4)	6.0 (0.8)	1.5 (0.3)	0.001	0.003	0.0007
S13	64°29.838'S							
		Bulk	457 (70.9)	100.7	33.7 (6.3)	0.002 ($9x10^{-6}$)	0.003 (0.0003)	0.001 ($8x10^{-5}$)
		Pico	0.0 (73.3)	(11.1)	0.0 (6.3)	0	0	0
		Nano	458.2 (18.8)	0.0 (42.2)	31.5 (0.7)	0.004	0.004	0.001
		Micro	53.4 (14.2)	103.4 (40.7)	2.5 (0.6)	0.001	0.0009	0.0005
				1.6 (0.2)				

Table 3a: Surface daily rates of NPP and N uptake [nM d^{-1}] and specific rates of C and N uptake [hr^{-1}] for the early-summer transect. The mean zone values are reported with one standard deviation (± 1 S.D.) and size-fractionated values are reported with standard error, calculated according to standard statistical practices.

	Latitude	Filter size (µm)	NPP (nM d^{-1})	ρNO_3^- (nM d^{-1})	ρNH_4^+ (nM d^{-1})	V_C (hr^{-1})	V_{NO3-} (hr^{-1})	V_{NH4+} (hr^{-1})
STZ mean		***Bulk***	**255.1 (11.7)**	**2.6 (0.5)**	**7.3 (1.2)**			
STF	41°33.71'S							
S31	37°14.119'S	*Bulk*	201.2 (72.8)	0.9 (0.1)	3.6 (0.4)	0.001 (0.0005)	$8x10^{-5}$ ($2x10^{-6}$)	0.0002 ($4x10^{-5}$)
		Pico	98.0 (74.6)	0.1 (0.1)	0.9 (0.7)	0.001	$3x10^{-5}$	0.0002
		Nano	98.0 (16.3)	0.8 (0.1)	2.3 (0.5)	0.003	$9x10^{-5}$	0.0002
		Micro	5.5 (0.0)	0.1 (0.1)	0.4 (0.1)	0.0004	0.0001	0.0004
S30	38°28.859'S							
		Bulk	308.9 (24.3)	4.3 (0.1)	11 (0.6)	0.002 (0.003)	0.0005 ($4x10^{-6}$)	0.0008 ($6x10^{-6}$)
		Pico	73.5 (24.3)	1.4 (0.1)	2.6 (0.8)	0.001	0.0003	0.0004
		Nano	235.4 (0.6)	2.8 (0.1)	7.2 (0.5)	0.003	0.0007	0.001
		Micro	0.0 (0.0)	0.1 (0.0)	0.0 (0.0)	0	$1x10^{-4}$	0
SAZ mean		***Bulk***	**326.2 (5.6)**	**12.1 (1.3)**	**12.9 (1.1)**			
SAF	51°44.93'S							
S29	45°52.110'S	*Bulk*	255.2 (19.1)	7.4 (0.5)	12.2 (0.1)	0.002 (0.0003)	0.0008 ($8x10^{-5}$)	0.0008 ($5x10^{-5}$)
		Pico	54.2 (25.4)	0.2 (0.5)	4.9 (0.6)	0.0006		0.0005
		Nano	201.0 (16.8)	7.2 (0.1)	7.2 (0.6)	0.005	$6x10^{-5}$	0.001
		Micro	0.0 (0.0)	0.0 (0.0)	0.0 (0.0)	0	0.001	0
							0	
S28	47°11.759'S	*Bulk*	397.2 (3.1)	16.7 (0.7)	13.7 (0.8)	0.005 ($9x10^{-6}$)	0.001 ($7x10^{-5}$)	0.001 ($7x10^{-5}$)
		Pico	114.4 (16.8)	6.9 (0.8)	4.8 (1.1)	0.006	0.0008	0.002
		Nano	283.0 (16.5)	9.7 (0.3)	8.9 (0.7)	0.005	0.001	0.001
		Micro	0.0 (0.0)	0.0 (0.0)	0.0 (0.0)	0	0	0
PFZ mean		***Bulk***	**1004.8 (8)**	**25.7 (1.8)**	**42 (1.7)**			
PF1	54°00.96'S							
PF2	54°05.53'S							
S27	53°59.275'S	*Bulk*	817.4 (73.7)	18.4 (4.3)	22.2 (1.2)	0.004 ($3x10^{-5}$)	0.001 ($2x10^{-5}$)	0.0009 ($3x10^{-5}$)
		Pico	114.7 (135.1)	1.1 (5.2)	4 (2.9)	0.001	0.0003	0.0005
		Nano	702.7 (113.3)	17.3 (3.0)	18.3 (2.6)	0.007	0.001	0.001
		Micro	0.0 (0.0)	0.0 (0.0)	0.0 (0.0)	0	0	0
S25								
	54°03.170'S	*Bulk*	654.4 (50.8)	15.9 (0.4)	23.8 (2.5)	0.003 ($9 x10^{-5}$)	0.0009 ($1x10^{-5}$)	0.0008 ($4x10^{-5}$)
		Pico	91.0 (65.5)	0.0 (1.0)	5.7 (2.6)	0.0008	0	0.0005
		Nano	563.6 (41.3)	17.7 (0.9)	18.1 (0.5)	0.004	0.001	0.001
		Micro	0.0 (0.0)	0.0 (0.0)	0.0 (0.0)	0	0	0
S24								
	54°05.350'S	*Bulk*	746.4 (nd)	15.2 (0.8)	55.4 (nd)	0.002 (0.001)	0.0007 ($2x10^{-5}$)	0.002 (0.0009)
		Pico	0.0 (57.4)	0.0 (0.9)	0.0 (1.4)	0	0	0.005
		Nano	867.6 (57.4)	16 (0.0)	53.9 (1.4)	0.007	0.0009	0.003
		Micro	0.0 (0.0)	0.0 (0.0)	0.0 (0.0)	0	0	0
S23								
	54°05.379'S	*Bulk*	2433.9 (59.7)	53.1 (4.6)	74.9 (1.2)	0.009 (0.0005)	0.002 ($6x10^{-5}$)	0.002 ($1x10^{-5}$)
		Pico	0.0 (155.2)	1.2 (4.7)	0.0 (1.6)	0	0.0003	0
		Nano	2752.7 (143.3)	51.9 (0.6)	76.7 (1.0)	0.02	0.002	0.002
		Micro	0.0 (0.0)	0.0 (0.0)	0.0 (0.0)	0	0	0
S22								
	54°09.363'S	*Bulk*	846.0 (10.5)	39.1 (1.1)	48.7 (3.1)	0.006 (0.0008)	0.002 ($1x10^{-5}$)	0.002 (0.0003)
		Pico	0.0 (16.8)	0.0 (1.2)	2.4 (3.6)	0	0	0.0002
		Nano	920.2 (13.1)	41.2 (0.5)	46.3 (1.7)	0.008	0.002	0.001
		Micro	0.0 (0.0)	0.0 (0.0)	0.0 (0.0)	0	0	0
S21								
	56°28.321'S	*Bulk*	530.6 (32.2)	12.6 (0.4)	25.7 (2.0)	0.003 (0.0001)	0.0009 ($3x10^{-5}$)	0.001 ($1x10^{-6}$)
		Pico	0.0 (33.9)	7.0 (0.6)	0.7 (2.0)	0	0.0009	0.0001
		Nano	636.4 (10.6)	18.4 (0.4)	25 (0.0)	0.007	0.001	0.002
		Micro	0.0 (0.0)	0.2 (0.3)	0.0 (0.0)	0	0.0004	0

OAZ mean		***Bulk***	**589.5 (9.4)**	**34.2 (1.2)**	**71.4 (2.6)**			
SACCF1	59°00.28'S							
S26	54°02.881'S	*Bulk*	348.2 (44.8)	16.5 (0.3)	119.8 (9.6)	0.002 (0.0002)	0.0009 (2x10^{-5})	0.004 (1x10^{-4})
		Pico	29.6 (44.8)	2.5 (0.8)	20.8 (12.9)	0.0002	0.0007	0.001
		Nano	318.7 (1.9)	13.9 (0.8)	99.1 (8.6)	0.003	0.001	0.007
		Micro	0.0 (0.0)	0.0 (0.0)	0.0 (0.0)	0	0	0
S20								
	57°16.961'S	*Bulk*	460.3 (0.9)	25.8 (2.9)	22.3 (1.0)	0.003 (4 x10^{-5})	0.0007 (2x10^{-5})	0.001 (2x10^{-5})
		Pico	46.2 (4.8)	0 (2.9)	0.0 (3.2)	0	0	0.002
		Nano	414.3 (4.7)	16.4 (0.4)	23.7 (3)	0.002	0.001	0.001
		Micro	0 .0 (0.1)	0.0 (0.0)	0.0 (0.0)	0	0	0
S18								
	59°33.601'S	*Bulk*	1094.4 (38.0)	32.4 (0.9)	175.8 (6.0)	0.004 (±7 x10^{-5})	0.0009 (1x10-^{5})	0.005 (0.0001)
		Pico	0.0 (105.5)	4.8 (1.1)	6.2 (7.4)	0	0.001	0.0002
		Nano	1107.7 (98.4)	20.8 (0.8)	141.6 (4.4)	0.006	0.0008	0.002
		Micro	99.7 (13.4)	6.7 (0.6)	28.1 (0.8)	0.004	0.002	0.002
S17								
	59°58.420'S	*Bulk*	188.3 (11.1)	23.3 (0.8)	24 (2.2)	0.002 (±3 x10^{-5})	0.002 (2x10^{-5})	0.002 (9x10^{-5})
		Pico	0.0 (12.3)	0.1 (9.5)	2.6 (2.4)	0	3x10^{-5}	0.0006
		Nano	154.9 (5.3)	17.2 (9.4)	16.6 (0.8)	0.004	0.003	0.002
		Micro	33.5 (1.0)	6.0 (0.7)	4.9 (0.1)	0.001	0.002	0.001
S16								
	61°16.027'S	*Bulk*	740.9 (29.2)	53.1 (0.4)	56.7 (1.3)	0.004 (±2 x10^{-5})	0.002 (4x10^{-6})	0.002 (4x10^{-7})
		Pico	0.0 (42.6)	0.0 (6.4)	0.0 (1.4)	0	0	0
		Nano	752.6 (31.1)	59.5 (6.4)	60 (0.6)	0.007	0.003	0.003
		Micro	96.0 (1.2)	6.6 (0.4)	7.3 (0.2)	0.003	0.002	0.002
S15								
	67°02.462'S	*Bulk*	704.9 (188.4)	54.5 (nd)	29.5 (3.9)	0.003 (0.0009)	0.002 (0.001)	0.001 (9x10^{-5})
		Pico	83.5 (202.5)	0.0 (1.9)	0.0 (5.4)	0.0006	0.003	0
		Nano	554.3 (74.1)	55.6 (1.9)	28.8 (3.7)	0.005	0.002	0.002
		Micro	67.0 (5.0)	4.8 (0.2)	2.9 (0.2)	0.002	0.001	0.0006
PAZ mean								
		Bulk	**1692.6 (43.4)**	**162.2 (9.1)**	**85.6 (1)**			
SACCF2	67°99.06'S							
S19	59°28.431'S							
		Bulk	1628.2 (60.7)	100 (4.2)	19.2 (0.6)	0.002 (0.002)	0.003 (5x10^{-5})	0.0005 (4x10^{-5})
		Pico	0.0 (204.1)	2.7 (4.7)	2.0 (3.4)	0	0.0007	0.0002
		Nano	1515.3 (194.8)	81.5 (2.1)	13.1 (3.4)	0.01	0.003	0.0006
		Micro	180.8 (3.2)	15.8 (1.5)	4.2 (0.2)	0.005	0.003	0.0008
S14								
	70°17.060'S	*Bulk*	1757 (1271.2)	224.4 (55.0)	152.0 (nd)	0.001 (3 x10^{-5})	0.006 (0.0002)	0.004 (0.002)
		Pico	0.0 (1271.6)	0.0 (55.0)	0.0 (60.5)	0.008	0	0.002
		Nano	1669.3	223.4 (55.0)	150.4 (60.5)	0.008	0.006	0.003
		Micro	(1271.6)	1.0 (0.1)	1.6 (0.5)	0.005	0.0003	0.0003
			88.0 (32.0)					
SG Zone mean	~ 54-59.4˚S	***Bulk***	**1165.6 (6.9)**	**43.8 (1.8)**	**61.3 (1.8)**			

Table 3b: Surface daily rates of NPP and N uptake [nM d^{-1}] and specific rates of C and N uptake [hr^{-1}] for the late-summer transect. The mean zone values are reported with one standard deviation (± 1 S.D.) and size-fractionated values are reported with standard error, calculated according to standard statistical practices.

	Latitude	Size-class (µm)	f-ratio$_{urea}$	f-ratio	Absolute C export (nM d^{-1})	% size-class contribution to [PON] (%)	% size-class contribution to NPP (%)
STZ mean		***Bulk***	**0.50**	**0.50**	**548.9 ± 300.4**		
		Pico	**0.09**	**0.09**		**22.0**	**41.4**
		Nano	**0.47**	**0.47**		**68.4**	**57.6**
		Micro	**0.53**	**0.53**		**9.6**	**1.1**
STF	41°41.15'S						
S1	34°13.6'S	*Bulk*	0.72	0.72	529.5		
		Pico	0.00	0.00		17/0	0.0
		Nano	0.34	0.34		70.7	96.3.3
		Micro	0.67	0.67		12.3	3.7
S2	35°06.134'S	*Bulk*	0.36	0.36	250.5		
		Pico	0.22	0.22		36.2	40.6
		Nano	0.47	0.47		52.9	59.3
		Micro	0.45	0.45		10.9	0.2
S3	38°56.464'S	*Bulk*	0.48	0.48	452.2		
		Pico	0.00	0.00		7.5	96.1
		Nano	0.54	0.54		84.0	3.7
		Micro	0.61	0.61		8.6	0.2
S4	39°58.562'S	*Bulk*	0.45	0.45	963.5		
		Pico	0.16	0.16		27.3	28.8
		Nano	0.54	0.54		66.0	71.0
		Micro	0.41	0.41		6.7	0.2
SAZ mean		***Bulk***	**0.11**	**0.57**	**193.5 ± 47.8**		
		Pico	**0.19**	**0.19**		**8.8**	**5.8**
		Nano	**0.28**	**0.61**		**52.3**	**76.8**
		Micro	**0.54**	**0.60**		**38.8**	**17.4**
SAF	50°09.39'S						
S5	46°17.175'S	*Bulk*	0.06	0.55	171.7		
		Pico	0.00	0.00		0.8	0.0
		Nano	0.11	0.64		60.6	82.7
		Micro	0.40	0.54		38.5	17.3
S6	46°46.152'S	*Bulk*	0.08	0.65	160.5		
		Pico	0.00	0.00		5.4	0.0
		Nano	0.18	0.63		49.1	80.4
		Micro	0.60	0.60		45.5	19.6
S7	49°02.003'S	*Bulk*	0.17	0.52	248.3		
		Pico	0.56	0.56		20.3	17.5
		Nano	0.56	0.56		47.3	67.3
		Micro	0.63	0.63		32.5	15.2
PFZ mean		***Bulk***	**0.44**	**0.44**	**312.5 ± 0.0**		
		Pico	**0.00**	**0.00**		**14.6**	**0.0**
		Nano	**0.44**	**0.44**		**74.4**	**98.0**
		Micro	**0.81**	**0.81**		**10.9**	**2.0**
PF	51°72.87'S						
S8	52°29.857'S	*Bulk*	0.44	0.44	312.5		
		Pico	0.00	0.00		14.6	0.0
		Nano	0.44	0.44		74.4	98.0
		Micro	0.81	0.81		10.9	2.0

OAZ mean		***Bulk***	**0.90**	**0.90**	**243.8 ± 0.0**	**19.3**	**0.0**
		Pico	**0.92**	**0.92**		**64.5**	**84.5**
		Nano	**0.90**	**0.90**		**13.8**	**15.5**
		Micro	**0.90**	**0.90**			
SACCF	54°48.09'S						
S9	53°44.284'S	*Bulk*	0.90	0.90	243.8	19.3	0.0
		Pico	0.92	0.92		64.5	84.5
		Nano	0.90	0.90		13.8	15.5
		Micro	0.90	0.90			
PAZ mean		***Bulk***	**0.77**	**0.77**	**513.3 ± 213.0**	**23.3**	**4.5**
		Pico	**0.43**	**0.43**		**65.8**	**86.0**
		Nano	**0.77**	**0.77**		**10.1**	**9.5**
		Micro	**0.78**	**0.78**			
S10	56°53.195'S	*Bulk*	0.87	0.87	767.3	27.2	16.1
		Pico	0.00	0.00		58.8	73.8
		Nano	0.91	0.91		11.0	10.0
		Micro	0.88	0.88			
S11	61°05.928'S	*Bulk*	0.72	0.72	672.1	16.9	1.7
		Pico	0.74	0.74		72.9	89.0
		Nano	0.71	0.71		10.2	9.3
		Micro	0.80	0.80			
S12	61°58.890'S	*Bulk*	0.78	0.78	276.4	29.9	0.0
		Pico	0.97	0.97		60.4	91.8
		Nano	0.72	0.72		9.7	8.2
		Micro	0.79	0.79			
S13	64°29.838'S	*Bulk*	0.74	0.74	337.5	19.4	0.0
		Pico	0.00	0.00		71.0	89.6
		Nano	0.72	0.72		9.6	10.4
		Micro	0.63	0.63			

Table 4a: Late-summer values for the f-ratio, f-ratio$_{urea}$, absolute carbon export (± 1 S.D.) and percentage size-class contribution to NPP and surface biomass concentration (PON).

	Latitude	Size-class (µm)	f-ratio$_{urea}$	f-ratio	Absolute C export (nM d^{-1})	% size-class contribution to [PON] (%)	% size-class contribution to NPP (%)
		Bulk	**0.02**	**0.31**			
STZ		***Pico***	**0.05**	**0.30**	**4.4 ± 4.4**	**36.2**	**36.2**
mean		***Nano***	**0.02**	**0.33**		**58.6**	**62.4**
		Micro	**0.10**	**0.10**		**5**.2	**1.4**
STF	41°33.71'S						
		Bulk	0.01	0.25			
S31	37°14.119'S	*Pico*	0.00	0.12	1.2	23.3	48.7
		Nano	0.01	0.28		71.1	48.6
		Micro	0.20	0.20		5.6	2.7
		Bulk	0.02	0.36			
S30	38°28.859'S	*Pico*	0.10	0.48	7.5	49.1	23.8
		Nano	0.04	0.39		46.2	76.2
		Micro	0.00	0.00		4.7	0.0
		Bulk	**0.07**	**0.47**			
SAZ		***Pico***	**0.19**	**0.22**	**21.8 ± 4.0**	**50.3**	**25.0**
mean		***Nano***	**0.30**	**0.50**		**49.7**	**75.0**
		Micro	**0.00**	**0.00**		**0.0**	**0.0**
SAF	51°44.93'S						
		Bulk	0.07	0.50			
S29	45°52.110'S	*Pico*	0.05	0.11	19.0	57.0	21.2
		Nano	0.48	0.48		43.0	78.8
		Micro	0.00	0.00		0.0	0.0
		Bulk	0.06	0.50			
S28	47°11.759'S	*Pico*	0.33	0.33	24.7	43.5	28.8
		Nano	0.12	0.52		56.5	71.2
		Micro	0.00	0.00		0.0	0.0
		Bulk	**0.04**	**0.45**			
PFZ		***Pico***	**0.15**	**0.21**	**37.9 ± 20.0**	**21.9**	**4.7**
mean		***Nano***	**0.04**	**0.46**		**79.5**	**95.3**
		Micro	**0.00**	**0.00**		**0.2**	**0.0**
PF1	54°00.96'S						
PF2	54°05.53'S						
		Bulk	0.03	0.53			
S27	53°59.275'S	*Pico*	0.04	0.37	26.2	28.6	14.0
		Nano	0.04	0.49		71.4	86.0
		Micro	0.00	0.00		0.0	0.0
		Bulk	0.04	0.52			
S25	54°03.170'S	*Pico*	0.00	0.00	24.6	33.4	13.9
		Nano	0.05	0.54		86.5	86.1
		Micro	0.00	0.00		0.0	0.0
		Bulk	0.03	0.28			
S24	54°05.350'S	*Pico*	0.00	0.00	19.4	6.1	0.0
		Nano	0.03	0.25		83.2	100.0
		Micro	0.00	0.00		0.0	0.0
		Bulk	0.03	0.46			
S23	54°05.379'S	*Pico*	0.00	0.00	65.9	21.0	0.0
		Nano	0.02	0.48		79.0	100.0
		Micro	0.00	0.00		0.0	0.0
		Bulk	0.07	0.47			
S22	54°09.363'S	*Pico*	0.00	0.00	60.6	13.4	0.0
		Nano	0.06	0.64		86.6	100.0
		Micro	0.00	0.00		0.0	0.0
		Bulk	0.06	0.45			
S21	56°28.321'S	*Pico*	0.89	0.89	31.1	28.8	0.0
		Nano	0.04	0.38		70.0	100.0
		Micro	0.00	0.00		1.2	0.0
OAZ		***Bulk***	**0.16**	**0.40**	**65.0 ± 27.5**		
mean		***Pico***	**0.21**	**0.21**		**17.2**	**5.1**

		Nano	**0.21**	**0.43**		**70.6**	**87.1**
		Micro	**0.38**	**0.38**		**11.9**	**7.8**
SACCF1	59°00.28'S						
		Bulk	0.19	0.19			
S26	54°02.881'S	*Pico*	0.35	0.35	66.5	41.7	8.5
		Nano	0.12	0.12		58.3	91.5
		Micro	0.00	0.00		0.0	0.0
		Bulk	0.04	0.42			
S20	57°16.961'S	*Pico*	0.00	0.00	19.8	1.8	10.0
		Nano	0.07	0.48		95.1	90.0
		Micro	0.00	0.00		3.1	0.0
		Bulk	0.04	0.16			
S18	59°33.601'S	*Pico*	0.87	0.87	46.1	16.3	0.0
		Nano	0.02	0.30		71.9	91.7
		Micro	0.44	0.44		11.8	8.3
		Bulk	0.47	0.47			
S17	59°58.420'S	*Pico*	0.06	0.06	89.4	22.8	0.0
		Nano	0.63	0.63		51.8	82.2
		Micro	0.62	0.62		25.3	17.8
		Bulk	0.12	0.49			
S16	61°16.027'S	*Pico*	0.00	0.00	88.3	8.8	0.0
		Nano	0.19	0.44		74.9	88.7
		Micro	0.53	0.53		16.3	11.3
		Bulk	0.11	0.66			
S15	67°02.462'S	*Pico*	0.00	0.00	79.9	12.0	11.8
		Nano	0.22	0.60		71.6	78.7
		Micro	0.66	0.66		14.8	9.5
		Bulk	**0.13**	**0.72**			
PAZ		***Pico***	**0.39**	**0.39**	**220.9 ±**	**20.5**	**0.0**
mean		***Nano***	**0.38**	**0.77**	**146.4**	**65.3**	**92.2**
		Micro	**0.63**	**0.63**		**14.3**	**7.8**
SACCF2	67°99.06'S						
		Bulk	0.07	0.85			
S19	59°28.431'S	*Pico*	0.77	0.77	117.3	20.5	0.0
		Nano	0.06	0.84		65.3	89.3
		Micro	0.82	0.82		14.3	10.7
		Bulk	0.18	0.58			
S14	70°17.060'S	*Pico*	0.00	0.00	324.4	0.0	0.0
		Nano	0.70	0.70		0.0	95.0
		Micro	0.45	0.45		0.0	5.0

Table 4b: Late-summer values for the f-ratio, f-ratio$_{urea}$, absolute carbon export (± 1 S.D.) and percentage size-class contribution to NPP and surface biomass concentration (PON).

5. DISCUSSION

5.1. Summertime progression in NPP and carbon export potential across the Atlantic Southern Ocean

5.1.1. Regional comparison of rates of NPP and biomass accumulation in the context of earlier measurements and broad community compositions

Primary production across the Southern Ocean is highly variable over spatial and temporal timescales, with the Atlantic sector generally supporting some of the highest observed rates of NPP (Sullivan et al., 1993; Sigman & Hain, 2012), likely due to enhanced Fe supply from upstream landmasses and the multiple islands within the sector (Henley et al., 2020 and references therein).

The quantification of a frontal zone's fertility can be directly assessed based on measurements of total community (i.e., bulk) and size-fractionated rates of NPP, with the expectation that NPP and ultimately C sequestration is strongly controlled by the regional and seasonal variability in phytoplankton community composition and the role of nutrient recycling within the surface ecosystem (Eppley & Peterson, 1979; Henley et al., 2020). Phytoplankton size-class dominance and, hence, relative contribution to NPP is particularly important in determining the potential for C export in a region because of the implications of size for nutrient acquisition, susceptibility to grazing pressures and capacity for sinking (Froneman et al., 2004; Sigman & Hain, 2012; Quéguiner, 2013). Larger-celled species (i.e., microphytoplankton) are typically associated with greater C export potential compared to that of smaller-celled species (i.e., picophytoplankton), attributed to their ability to rapidly sink through the water column and tendency to evade microphagous predation (Legendre & Le Fevre, 1989; Tremblay et al., 2001).

The STF separates the polar and subtropical waters, marking the STZ as distinct from the regions south of the front (Orsi et al., 1994), where the signal of biogeochemical disparity is evident (Sarmiento et al. 2004). Rates of NPP were fairly high in early-summer (Fig. 11a) with the uptake of NO_3^- and NH_4^+ being similar (Fig. 12a and 13a) and pico- and nanophytoplankton dominating the assemblage over the entire season (Table 4a and 4b). Shallow MLDs are characteristic of the region in summer (Sallée et al. 2010), such that light availability is generally not a limiting factor for NPP. Instead, NPP is controlled by the availability of macronutrients, particularly surface [NO_3^-], which is perpetually low across the STZ (Fig. 3) (Sigman & Hain, 2012; Joubert et al., 2011; Viljoen et al., 2019; Weir et al. 2020). While surface [NO_3^-] was similar in early- and late-summer, the rates of NPP were more than four-fold lower in late-summer (Fig. 11b). This can be explained by an elevated supply of NO_3^- in early-summer, before intense thermal stratification set in, that was rapidly consumed by phytoplankton (such that elevated surface [NO_3^-] was never measured), followed by more stratified, NO_3^-deplete conditions in late summer.

The dominance of smaller-celled species has been hypothesised as a response to warmer SSTs and low macronutrient concentrations (Takahashi, 1982), with Si-limitation in particular driving the failure of diatom succession in the STZ (Weir et al., 2020 and references therein). The available size-fractionated data provide no evidence for a seasonal shift in the phytoplankton community composition, with the relative contributions of all size classes to biomass, NPP and N uptake remaining similar over the study period (Fig. 8-9 and 11-13). However, despite a ~80% decline in productivity between early- and late summer, the [PON] hardly varied, which implies that phytoplankton growth rates were much higher at the beginning of summer (as evinced by the specific C fixation rates; Table 3). At the same time, surface

Chl-a concentrations declined modestly from early- to late-summer across the STZ, indicating an increase in the proportion of heterotrophic organisms (i.e., containing no photosynthetic pigments) and detritus in late-summer. A seasonal increase in the proportion of detritus is borne out by the biomass C:N ratios in the STZ that increase from 7.7 ± 2.1 in early-summer to a value significantly higher than the Redfield ratio in late-summer (12.6 ± 2.1; Fig. 9), consistent with an elevated contribution of C-rich detrital material (Dugdale & Wilkerson, 1986; Legendre & Gosselin, 1996; Bronk et al., 2002).

One implication of the STZ observations detailed above is that surface nutrient recycling was likely high, particularly in late-summer, with the consequence for C export being negative (Eppley & Peterson, 1979; Tremblay et al., 2001; Sigman & Hain, 2012). In early-summer, C export potential (i.e., inferred from the NO_3^- uptake rates) across the STZ was in fact the highest, albeit highly variable, compared to all other regions (average of 548.9 ± 300.4 nM C d^{-1} for the STZ versus 315.8 ± 140.4 nM C d^{-1} for all other zones; Table 4a). This is likely the result of STZ phytoplankton occupying a high-light, Fe-replete environment in early-summer that had recently been supplied with NO_3^- (and PO_4^{3-}). Conversely, in late-summer, the STZ exhibits the lowest C export compared to all other frontal zones (average of 4.4 ± 4.4 nM C d^{-1} for the STZ versus a range from 21.8 ± 4.0 to 220.9 ± 146.4 nM C d^{-1} for all other zones; Table 4b), evidencing the shift to a regenerated N-fuelled phytoplankton community where, consequently, the strength of the biological pump is greatly reduced (Dugdale & Goering 1967; Eppley & Peterson, 1979; Le Fevre et al., 1998).

During the early-summer period, the SAZ was the region supporting the highest rates of NPP (Fig. 11a), coincident with the greatest accumulation of biomass (i.e., PON) (Fig 8a and 10a). Here, the contribution to total surface [PON] and NPP by microphytoplankton was high compared to all other regions (average of 38.8% of total [PON] and 17.4% of total NPP; Table 4a), with nanoplankton contributing most of the remaining PON. The shared dominance of nano- and microphytoplankton across the SAZ, coupled with elevated rates of NPP, leads to the expectation that export production should be high (Eppley & Peterson, 1979; Tremblay et al., 2001; Sigman & Hain, 2012). This appears not to be the case, however, with considerably lower C export potential estimated for the early-summer SAZ compared to the other zones (average of 193.5 ± 47.8 nM C day^{-1} for the SAZ versus 356.6 ± 140.1 nM C day^{-1} for all other zones south of the STF; Table 4a). This is possibly a consequence of elevated grazing pressures imposed on the phytoplankton community following the spring bloom (Sigman & Hain, 2012), which would have occurred earlier in the SAZ than the PFZ and AZ (Arteaga et al., 2020), enhancing the degree of nutrient recycling and bolstering the microbial loop in the surface layer (*see further details in Section 2.1.2*) (Lourey et al., 2003; Henley et al., 2020). Additionally, by the time of the early-summer sampling, SAZ phytoplankton may have already been experiencing Fe-limitation (Tagliabue et al. 2012; Mtshali et al. 2019), which is required for NO_3^- consumption (Morel and Price, 2003). Indeed, phytoplankton that use NO_3^- as their primary N source have a higher Fe requirement than those that depend on recycled N (e.g., ammonium; NH_4^+) (Price et al., 1994). In late-summer, C export potential estimated for the SAZ was low (average of 21.8 ± 4.0 nM C day^{-1}), concurrent with the SAZ experiencing the highest surface [NH_4^+] (Table 1b), substantiating the notion that the SAZ was characterized by a high degree of surface nutrient recycling throughout the sampling period (*see further details in Section 2.1*). Additionally, the uptake of urea (i.e., an additional regenerated N source; *see further details in section 2.1.1.*) accounted for ~54% of SAZ NPP in early-summer, while the contribution across all other zones was negligible (Table 4a). Furthermore, the SAZ is a region of perennial Si-limitation (Sarmiento et al., 2004), inhibiting the growth of large diatoms, a phytoplankton species highly efficient at C export (Weber & Deutsch, 2010; Quéguiner, 2013).

The SAZ has been observed as a region of high seasonality in NPP due to the seasonal supply of nutrients and variable irradiance (Sarmiento et al., 2004; Sigman & Hain, 2012; Arteaga et al., 2020; Henley et al., 2020 and references therein). In spring and early-summer, the repletion of micro- and macronutrients by nutrient-rich waters advected from high latitudes and mixed up from the thermocline, coupled with favourable light conditions as a result of the seasonally shoaling ML provide optimal conditions for phytoplankton growth (Lucas et al., 2007), enabling the SAZ to support a high degree of productivity before the onset of Fe-limitation in the later summer months (Laubscher et al., 1993; Sarmiento et al. 2004; Sigman & Hain, 2012; Deppeler & Davidson, 2017). This is consistent with the decrease in NPP from early- to late-summer (Fig. 11), as well as with the surface Chl-a, where elevated Chl-a was observed in early-summer and decreased substantially in late-summer (Fig. 10). The observations presented here implicating the SAZ as the most productive region during early-summer are consistent with those of Laubscher et al. (1993) from the Atlantic sector of the Southern Ocean, where similar to the present study, a shift to a phytoplankton assemblage dominated by smaller-celled species was observed with the seasonal progression.

The relevance of such high rates of NPP across the SAZ pertains to the region being able to support a plethora of higher trophic communities (Obernosterer et al., 2008; Deppeler & Davidson, 2017), which rely heavily on this elevated productivity, consequentially being affected by the high seasonality in NPP. Furthermore, the region is host to the Subantarctic Islands (De Broyer & Danis, 2011), a broad oceanic region home to diverse communities of seals, seabirds, and other marine mammals that indeed are dependent (albeit indirectly) on these elevated rates of NPP (Perissinotto et al., 1992; Deppeler & Davidson, 2017; Holmes et al., 2019). Large phytoplankton blooms are common in the vicinity of such oceanic landmasses (Doty & Oguri, 1956; Salter et al., 2007), whereby concurrent mechanisms of island runoff (i.e., inputting nutrients into surrounding surface waters) and bathymetric-induced upwelling result in the alleviation of Fe- (and Si-) limitation, positively affecting surface rates of NPP and C export potential (Doty & Oguri, 1956; Salter et al., 2007; Obernosterer et al., 2008; Forrer, 2020). This phenomenon is known as the Island Mass Effect (IME), where physical and chemical alterations to the shallow waters surrounding islands yields elevated rates of NPP and enhanced biological activity (Doty & Oguri, 1956; Salter et al., 2007). The alleviation of Si-limitation in particular drives the increased abundances of diatoms in the waters surrounding and downstream of the Subantarctic Islands, with positive implications for C export potential (Cullen, 1991; Smetacek et al., 2004; de Baar et al., 2005; Poulton et al., 2007; Boyd et al., 2000; Forrer 2020).

The PFZ is a highly variable region with respect to NPP and C export on an annual basis (Laubscher et al., 1993; Tremblay et al., 2001). The PFZ showed the least variability in NPP over the sampling period, with observed rates of NPP being moderate in early-summer and elevated in late-summer (Table 3a and 3b; Fig. 11). Concurrent with this was an increase in surface biomass accumulation (Fig. 8) as well as an increase in Chl-a over the season (Fig. 10), particularly at the PF boundary in late-summer where Chl-a was substantially elevated. The PF is widely recognised as a "hotspot" for diatom-dominated bloom development in response to latitudinally increasing Si-availability and localised upwelling along the frontal boundary (Kanda & Fukuchi, 1979; Allanson et al., 1981; De Baar et al., 1995; Froneman et al., 2001; Landry et al., 2002; Boyd, 2002; Sarmiento et al. 2004), resulting in elevated rates of NPP and the expectation that C export potential will be high (Laubscher et al., 1993; Sigman & Hain, 2012).

Deep MLDs are common in the PFZ (Boyd, 2002; Lucas et al., 2007; Joubert et al., 2011), and coupled with low Fe-availability (<0.2 nmol l^{-1}; Chever et al., 2010), result in Fe and light co-limitation across the region, with the effect becoming increasingly enhanced with the summertime progression (i.e., MLDs deepen as the season progresses, however, usually to a depth insufficient to entrain Fe into the

surface waters, resulting in Fe becoming increasingly deplete) (Lucas et al., 2007; Cochlan, 2008; Joubert et al., 2011; Holmes et al., 2019). Such conditions favour the growth of smaller diatom species (Brzezinski et al., 2003; Leynart et al., 2004; Lucas et al., 2007; Chever et al., 2010), consistent here with the observed negligible contribution to NPP by pico- and microphytoplankton over the sampling period, while nanophytoplankton dominated both surface [PON] (Fig. 8) and NPP (Fig. 11; Table 4a and 4b). The dominance of smaller-celled species may be due to enhanced grazing in the region, or to the suppression of the development of larger-celled species in response to the highly competitive smaller-celled species (in particular with respect to competition for Fe; Salter et al., 2007; Weber & Deutsch, 2012; Deppeler & Davidson, 2017), reflected in the moderate and low contributions to C export in early- and late-summer PFZ, respectively (average of 312.5 ± nd nM C d^{-1} and 37.9 ± 20.0 nM C d^{-1} for early- and late-summer; Table 4a and 4b).

The highest rate of NPP over the entire study period was observed at S23 in the PFZ during late-summer (2433.9 ± 59.7 nM C d^{-1}; Fig. 11b; Table 3b), a station in close proximity to the PF where elevated rates of NPP are common (Jacques & Minas, 1981; Lutjeharms et al., 1985), and falling within the region downstream of SG Island (located at 54˚15'S and 36˚45'W), where the IME likely had substantial influence on primary productivity (Doty & Oguri, 1956; Korb & Whitehouse, 2004; Schlitzer & Borrione, 2013; Robinson et al., 2016; Forrer, 2020). Elevated surface concentrations of NH_4^+ (0.9 ± 0.5 µM), NO_3^- (23.1 ± 2.7 µM), $Si(OH)_4$ (30.4 ± 9.4 µM) and PO_4^{3-} (2.1 ± 0.1 µM) were apparent, likely derived from an enhanced vertical supply by bathymetric-induced upwelling and/or island runoff, with the implication that some amount of Fe was also likely supplied (Doty & Oguri, 1956; Robinson et al., 2016). This notion is supported by substantially elevated rates of NPP across the broader SG zone (~54-58˚S and 20-40˚W, with a rate of NPP average of 1165.6 ± 6.9 nM C d^{-1}) concurrent with a fairly low estimation of C export (average of 56.8 ± 34.4 nM C d^{-1}), comparable to the late-summer PFZ and OAZ (Table 4b). Although the IME may drive the high rates of NPP, the estimate of C export relative to NPP implies that the phytoplankton community was strongly fuelled by regenerated production, and that surface nutrient recycling was intense.

The OAZ was the region of lowest NPP in early-summer, with a roughly two-fold increase apparent with the seasonal progression (Fig. 11; Table 3a and 3b). Here, nanophytoplankton made the greatest contribution to NPP and biomass accumulation over the season, while the contribution by microphytoplankton was observed to decrease with time (Table 4a and 4b). This, coupled with the increase in biomass over the season (Fig. 8) and increased Si-availability (Fig. 3) implicates the OAZ as a region likely dominated by diatom species (Tréguer, 2014), with the associated C export expected to be high (Sarmiento et al. 2004; Queguiner, 2013; Tréguer et al., 2018). The moderate and low estimates of export production computed for the region in early- and late-summer, respectively, do not reflect this, however (average of 243.8 ± nd nM C d^{-1} and 65 ± 27.5 nM C d^{-1} for early- and late-summer, respectively). Characteristic of an open Southern Ocean region, the OAZ is characterized by deep MLDs, which were likely responsible for the low rates of NPP (i.e., due to enhanced light-limitation) (Boyd, 2002; Joubert et al., 2011). At the same time, Fe-availability would have been low at the surface (Chever et al., 2010), driving the preferential uptake of NH_4^+ over NO_3^- as the season progressed (Table 3b; Fig. 13b) (Martin & Fitzwater, 1988; Sunda, 1989; Lourey et al. 2003). The coupled effect of light- and Fe-limitation was indicated by a phytoplankton community dominated by smaller cells, resulting in a high degree of surface nutrient recycling with the seasonal progression and hence a decreased potential for C export (Sunda & Huntsman, 1997; Deppeler & Davidson, 2017) (Table 4b).

Moderate rates of NPP were observed across the early-summer PAZ (Fig. 11a), concurrent with high surface biomass accumulation (Fig. 8), high rates of NO_3^- uptake (Fig. 12a; Table 3a) and a high

estimation of C export (average of 513.3 ± 213.0 nM C d^{-1}; Table 4a). Falling within the Seasonal Ice Zone (SIZ), the seasonal reduction in sea ice cover is considered an important mechanism of surface stratification (i.e., yields shallower MLDs that result in the alleviation of light-limitation; Sakshaug & Holm-Hansen, 1984; Smith & Nelson, 1985; El-Sayed, 1988) and source of Fe to the surface layer ecosystem, particularly towards the end of the growing season (Armstrong, 1999; Boyd, 2002; Lin et al., 2011), resulting in elevated rates of NPP and the uptake of NO_3^-, and hence enhanced potential for C export (Martin & Fitzwater, 1988; Laubscher et al., 1993; Henley et al., 2020). The PAZ supported the highest rates of NPP during late-summer (Fig. 11b; Table 3b), coincident with previous studies reporting elevated rates of NPP south of 65˚S, near the ice-edge (Lancelot et al., 2000; Froneman et al., 2001; Mdutyana et al., 2020; Henley et al., 2020). The southward propagation of high NPP over the growing season (i.e., from the SAZ being most productive in early-summer to the PAZ in late-summer) is consistent with the timing of the seasonal phytoplankton bloom, which is expected to occur later at higher latitudes (Arteaga et al. 2020). The PAZ was also the region of greatest biomass accumulation in late-summer (Fig. 8b), and microphytoplankton made the greatest relative contribution to biomass and NPP compared to all other zones (average of 14.3% of total [PON] and 7.8% of total NPP; Table 4b). This result, coupled with the considerable estimate of C export potential (average of 220.9 ± 146.4 nM C d^{-1}) and the high ambient $Si(OH)_4$ concentrations likely indicates a phytoplankton community dominated by diatoms throughout the summer season (Quéguiner, 2013; Tréguer et al., 2018). Thus, the elevated uptake of NO_3^- over the season is attributed to the apparent dominance of diatoms, a group of phytoplankton with the capacity to consume (and store) large amounts of NO_3^- (Wheeler et al., 1983; Litchman et al., 2006; Fawcett & Ward, 2011).

Diatoms also have the ability to evade predation due to their size and growth rates that generally exceed zooplankton grazing rates (Landry et al., 2002; Poulton et al., 2007). Diatom-dominated assemblages south of the PF, particularly near the ice edge (Lancelot et al., 2000), are major drivers of the biological carbon pump (Tréguer et al., 1995; Buesseler et al., 2005), meaning that export production in this region should be elevated (Sigman & Hain, 2012; ; Tréguer et al., 2018; Henley et al., 2020). In a study conducted in winter across the Indian sector of the Southern Ocean, the relative importance of diatom-dominated assemblages for C export was made remarkably evident, where diatoms constituted 5-67% of the measured biomass across the AZ (Weir et al., 2020). This implies the prevalence of diatom-dominance in the Southern Ocean on an annual basis, highlighting their essential role in Southern Ocean export production. Hence, the likely dominance of diatoms in the PAZ of the present study suggests the enhanced efficiency of the biological pump functionality in this region (Tréguer et al., 1995; Tréguer et al., 2018; Weir et al., 2020).

5.2. Preferential uptake of nitrate versus ammonium in the context of export production

5.2.1. Evidence for enhanced surface recycling of N with the seasonal progression

5.2.1.a. Urea as a missing N source

While subsurface NO_3^- and recycled NH_4^+ are commonly recognized as the dominant N species utilized for primary production in the sunlit euphotic layer, other sources of N (e.g., forms of dissolved organic N (DON), N deriving from N_2 fixation and/or atmospheric deposition, NO_3^- recycled in the surface layer) are conjointly utilized to varying degrees based on the conditions of the surrounding environment and nutrient availability (Mulholland & Lomas 2008 and references therein; Glibert et al. 2016). Within the new production paradigm framework, whereby the uptake of NO_3^- and NH_4^+, are equated to new and regenerated production, respectively (*see further details in Section 2.3.*), not accounting for

"missing" sources of N may lead to an underestimation of NPP (unless C fixation is simultaneously measured) while export production may be over- or underestimated, depending on the provenance of the "missing" N (Bronk et al., 1994; Bronk et al., 2002; Yool et al. 2007; Peng et al., 2018).

In order to determine whether the contribution of an unaccounted for N source to NPP is substantial, rates of NPP are plotted against total N uptake rates that are converted to C values by normalizing to the Redfield ratio (i.e., $\rho N_x \times 6.63$) (Redfield et al., 1934, 1958) (Fig. 16). At stations where the relationship between NPP and $\rho N_x \times 6.63$ falls within an acceptable range of the 1:1 slope, NPP is solely sustained by NO_3^- and NH_4^+. This is the case across all early-summer stations, except those in the SAZ (Fig. 16a). On the contrary, at stations where NPP exceeds $\rho N_x \times 6.63$ (i.e., falling above the 1:1 slope), the implication is that some portion of the phytoplankton production was supported by an N form that was not measured in the present study (i.e., a "missing" N source). In late-summer, all stations fall above the 1:1 line, with the exception of two stations in the OAZ (S17, S26) and possibly one in the PAZ (S19 (Fig. 16b).

In addition to the vertical supply of NO_3^- to the surface via deep winter mixing and surface advection (Sarmiento et al. 2004), the main sources of N to the euphotic layer include N_2-fixation and atmospheric N deposition (Dugdale & Goering, 1967; Jickells & Moore, 2015). The limited existing estimates suggest that the Southern Ocean receives little in the way of net atmospheric N deposition because it is so far from continental sources of atmospheric N (Jickells et al., 2017; Altieri et al. 2021). Given the unfavourable conditions for summertime N_2-fixation in the Southern Ocean (low temperatures, low Fe-availability and/or high [NO_3^-]; Staal et al., 2003; Paerl et al., 1994; Holl & Montoya, 2005), the most plausible source of this "missing" N is regenerated DON (i.e., urea; Bronk et al., 2002; Peng et al., 2018; Mdutyana et al., 2020), likely deriving from bacterial degradation and/or other heterotrophic metabolisms (Azam, 1998; Bronk et al. 2007; *see further details in Section 2.1.2.*). Supporting this conclusion is previous work conducted across the Atlantic Southern Ocean during late-summer that estimated a contribution of urea to regenerated production on the order of 59% (Joubert et al., 2011).

Generally, urea exists in low concentrations in open ocean regions (<0.3 μM; Croot et al. 2020), although some of the highest concentrations have been recorded for the polar regions where sea ice dynamics come into play (Conover et al., 1999; Bronk et al., 2002). The measured surface [urea] was highly variable across the transect in both early- and late-summer, although when averaged across the frontal regions, no significant seasonal difference was apparent, except for in the late-summer PFZ where surface [urea] was substantially elevated (0.3 ± 0.2 μM versus 0.1 ± 0.1 M in early-summer; Fig. 3). Numerous PFZ stations sampled in the late-summer were in relatively close proximity to SG Island, a known terrestrial refuge for many seabirds and seals (Deppeler & Davidson, 2017 and references therein). An elevated supply of urea, which need not be reflected in the ambient [urea] if it is rapidly consumed by phytoplankton, to shallow waters downstream of the landmass may be due to increased inputs of biotically derived waste, including those from zooplankton (e.g., krill) (Jones et al., 1998; Conover & Gustavson, 1999; Kopczynska et al., 2001).

Although surface [urea] was consistently low (≤ 0.1 ± 0.1 μM; Table 1a and 1b) across the SAZ (Fig. 3), based on the elevated rates of NPP (Fig. 11a) and biomass accumulation (Fig. 8a) in early-summer, it is likely that urea was rapidly recycled within surface, such that surface concentrations never accumulated. Elevated inferred rates of urea uptake in the early-summer SAZ (Table 4a – *see f-ratio versus f-ratio$_{urea}$*), likely favouring the increasing dominance of pico- and nanophytoplankton with the seasonal progression (Peng et al., 2018) (Table 4a and 4b), are consistent with the SAZ as a region of high surface nutrient recycling following the initial stage of the phytoplankton bloom, which is

hypothesized to already have occurred (*see section 1.1*). Nearing the end of the summertime, when surface [Fe] is deplete and in response, the phytoplankton community is shifted towards the dominance of smaller-cell species (Table 4b) (Sunda & Huntsman, 1997; Smetacek et al., 2004; Poulton et al., 2007), the surface system likely becomes increasingly regenerative. This is reflected by the significant increase in inferred rates of urea uptake in late-summer across all frontal zones (Table 4b – *see f-ratio versus f-ratio*$_{urea}$) (Joubert et al., 2011). The shift towards a regenerative system appears slightly delayed across the AZ, where the dependence on urea is lower compared to the zones further north. This may be a result of the sustained summertime bloom apparent in the AZ in late-summer (Fig. 10), as well as the contribution from biological activity associated with sea ice, possibly explaining the slightly higher urea dependence apparent in the PAZ compared to that in the OAZ (Table 4b – *see f-ratio versus f-ratio*$_{urea}$).

The implication of some fraction of NPP being supported by an additional source of recycled N is that, if left unaccounted for, will yield an underestimate of the rate of regenerated production and consequently, the f-ratio and C export potential will be overestimated (*see further details in Section 2.3*; Peng et al. 2018; Mdutyana et al. 2020). In the case of the present study, the inclusion of urea in estimates of the degree to which surface ecosystem NPP is primarily fuelled by new versus regenerated N causes a significant rise in regenerated production and associated decline in export production, particularly in late-summer.

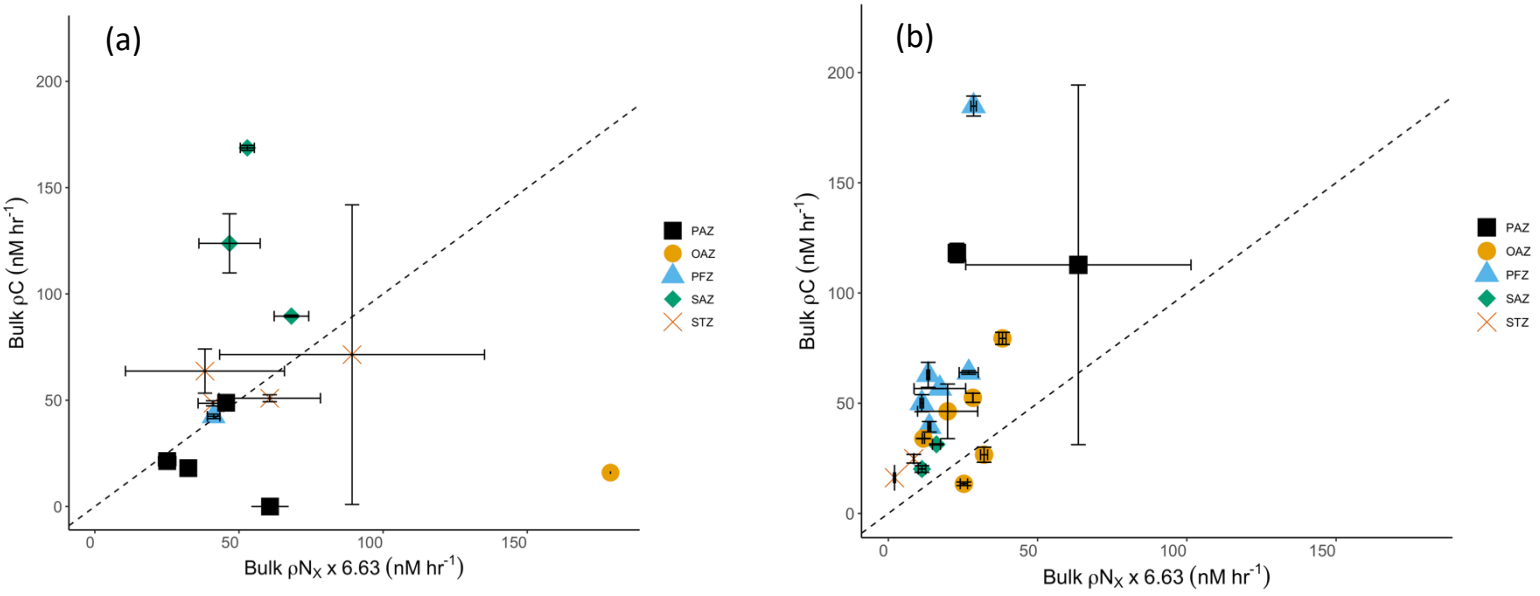

Figure 16: Uptake rates of C (ρC) versus total N ($\rho N_X = \rho NO_3^- + \rho NH_4^+$) normalized to the C:N ratio of 106:16 [nM hr^{-1}] (Redfield et al., 1934 & 1958) for the bulk community (0.3-200 µm) for the 16a) early-summer and 16b) late-summer transects. Error bars indicating ± 1 S.D. are plotted where available. The dashed black slope represents the 1:1 line, the expected absolute uptake rate ratio of C:N for balanced phytoplankton growth under the assumption that the only forms of N utilized by phytoplankton include NO_3^- and NH_4^+.

5.2.1.b. Consideration of the combined plankton community functioning

Generally, surface uptake of N in early-summer is characterised by ρNO_3^- exceeding ρNH_4^+ by up to nine-fold, with the only exception being the PFZ (Fig. 12a; Fig. 13a; Table 3a). Conversely, in late-summer, ρNH_4^+ exceeds that of ρNO_3^- by roughly 2-fold across all frontal regions, with the exception of the PAZ where the opposite relationship is evident (Fig. 12b; Fig. 13b; Table 3b). The possible drivers behind this apparent switch from predominantly NO_3^--fuelled production in early-summer to NH_4^+-fuelled production in late-summer are discussed in depth in *Section 2.2.* Here, the focus is on the evidence for a seasonal switch to a system supported primarily by surface recycling of N and the possible pathways of surface nutrient remineralization.

From the concurrent measurements of NPP and N uptake, the decoupling of NPP and the adjusted ρN_x, where more N is consumed than is accounted for by the corresponding rates of NPP (i.e., falling below the 1:1 slope; Fig. 16), could be indicating two possible processes: 1) NH_4^+ assimilation by heterotrophic bacteria (Kirchman et al., 1991; Bronk et al., 1998; Mdutyana et al. 2020), and 2) luxury N uptake by phytoplankton (Demanche et al., 1979; Burger et al. 2020).

The production of NH_4^+ from organic matter by heterotrophic bacteria is a major pathway of surface nutrient regeneration, and while highly variable (Azam et al., 1993), on average ~50% of surface NPP is transferred via bacteria into the microbial loop (Azam, 1998). While heterotrophic bacteria predominantly consume DON, they can also directly assimilate NH_4^+ (Kirchman et al., 1991). Since this happens without them fixing C, it results in a decoupling of the C:N uptake ratio (Kirchman et al., 1991; Bronk et al., 1998; Mdutyana et al. 2020) (Fig. 16). Bacterial NH_4^+ consumption has been observed during the summertime phytoplankton bloom (Boyton et al., 1982; Conley & Malone, 1992) and inferred for all zones of the Atlantic Southern Ocean in winter (Mdutyana et al. 2020); the expectation if this process were significant during the present study is high abundances of picoplankton, which includes bacteria, coupled with lower-than-Redfield biomass C:N ratios (Kirchman et al., 1991; Bronk et al., 1998). The only frontal zone where this is plausible is the early-summer OAZ (Fig. 16a; Fig. 3a) where the contribution from the smallest size-class was substantial (~20%; Table 4a) and the C:N ratio was the lowest across all early-summer stations (Fig. 9a). However, significant bacterial NH_4^+ assimilation is unlikely due to the competitive advantage phytoplankton have over heterotrophic bacteria in high light environments (Azam et al., 1993 and references therein). Indeed, in a study comparing NH_4^+ assimilation in the Southern Ocean in winter versus summer, significant rates of bacterial NH_4^+ uptake were observed only in the winter mixed layer (Mdutyana et al. 2020). In addition, the surface $[NH_4^+]$ was very low in early-summer (Fig. 3a; Table 1a), with the implication that phytoplankton are extremely efficient at consuming NH_4^+ as soon as it becomes available.

The luxury uptake of NO_3^-, a process whereby excess NO_3^- is consumed by phytoplankton and stored intracellularly to be assimilated later in the season when nutrient depletion is enhanced (Demanche et al., 1979), or in the case of the Southern Ocean when Fe- and/or light availability is increased, is a practice commonly observed in diatoms (Corredor, 1979; Longhurst & Harrison, 1989; Bode et al., 1997). The decoupling of the C:N uptake ratio, together with a low biomass C:N ratio, particularly in the micro- and nanophytoplankton size-classes, could be indicative of luxury NO_3^- uptake (Legendre & Gosselin, 1996; Bronk, 1998; Glover et al., 2007; Burger et al., 2020). In the early-summer OAZ, the ratio of C:N uptake is strongly decoupled (Fig. 16a) and the C:N biomass ratio is the lowest across all zones for the entire season (Fig. 9a). In addition, micro- and nanophytoplankton make a high relative contribution to surface biomass (Table 4a), concurrent with the highest recorded ρNO_3^- for the season (Table 3a). The coincidence of these results likely indicates that the early-summer OAZ supported a

phytoplankton community dominated by diatoms, a group widely recognised as NO_3^- uptake specialists (Wheeler et al., 1983; Fawcett & Ward 2011), that consumed NO_3^- without fixing a stoichiometric quantity of C. If this is the case, the implication is that the f-ratio (*see further details in Section 2.3*) and hence export production would have been overestimated for the early-summer OAZ, unless the stored NO_3^- is used to fuel NPP within a relatively short period of it being taken up (Table 4a).

High biomass C:N ratios compared to that of typical marine biomass (i.e., C:N = 6.63:1; Redfield et al., 1958), where the corresponding relationship between NPP and the adjusted ρN_x is tightly coupled, is indicative of detrital biomass accumulation (Dugdale & Wilkerson, 1986; Legendre & Gosselin, 1996). Detritus is a C-rich, non-photosynthetic organic material, as heterotrophic bacteria utilise detritus as an N source elevating its C content (Bronk et al., 2002). In this regard, detritus is an important source of recycled N, with the implication that where detritus accumulates the microbial loop is perpetuated (Azam, 1983; Azam, 1998; Deppeler & Davidson, 2017). Biomass C:N ratios are elevated across the early-summer STZ, SAZ and PAZ, with picophytoplankton being the size-class most frequently exceeding the Redfield ratio in the STZ and SAZ and microphytoplankton in the PAZ (Redfield et al., 1934 & 1958) (Fig. 9a). The evidence for enhanced surface recycling across the STZ and SAZ is supported by the corresponding peaks in Chl-a (Fig. 10a), particularly in the SAZ, where estimates of export production are low (Table 4a). This suggests that surface N recycling via heterotrophic remineralization of POM is enhanced in response to the proliferating summertime phytoplankton bloom.

The onset of the summer bloom in the PAZ (Fig. 10a) is largely initiated by sea ice melt at the beginning of the season, where inputs of Fe and increased water column stability favour elevated phytoplankton growth (Sakshaug & Holm-Hansen, 1984; Smith & Nelson, 1985; El-Sayed, 1988; Conover et al., 1999), with the effect becoming increasingly enhanced with the seasonal progression, resulting in the 'active' bloom phase being sustained for a longer period of time into the season (i.e., as the Fe supplied via deep winter mixing is exhausted) (Fig. 9-11). Alternatively, the high C:N ratios apparent for the early-summer PAZ (Fig. 9a) may indicate the remnant signal of aggregated detritus accumulation of the previous growing season ice-edge bloom. If this is the case, as the summertime bloom develops and the uptake ratio of C:N is driven back down to ~106:16 (Redfield et al., 1958) and the surface biomass C:N ratio will also decrease.

In late-summer, the biomass C:N ratio exceeds that of Redfield at all stations north of ~60˚S, with picophytoplankton showing the most substantial deviation (Fig. 9b). This finding is consistent with the notion that the functioning of the microbial loop is enhanced as the summer season progresses (Martiny et al., 2013), suggesting a surface ecosystem where regenerated production becomes increasingly dominant over new production (Lourey et al. 2003). Additionally, in the STZ and SAZ, both ρNO_3^- and ρNH_4^+ are very low (compared to both the early-summer and all the other zones in late-summer), consistent with a phytoplankton assemblage under physiological stress (*see further details in Section 2.2*) (Bronk et al., 1998; 2002).

Phytodetritus plays an important role in vertical C export via the grazing food chain (Schnack, 1985), whereby large zooplankton graze on phytoplankton blooms, producing large faecal pellets that rapidly sink out of the surface layer before being remineralized, thus having positive implications for export production (Le Fevre et al., 1998). A large proportion of the downward biogenic C flux across the Southern Ocean is comprised of large diatoms from un-grazed blooms and faecal material produced via zooplankton grazing (Le Fevre et al., 1998), with microphages (e.g., krill, salps and copepods) being the major planktonic grazers (Fortier et al., 1994) and their contribution to export production being

substantial (Schnack, 1985; Le Fevre et al., 1998). Large swarms of krill are commonly observed to forage on phytoplankton blooms in open ocean frontal zones, particularly near summertime retreating sea ice (Le Fevre et al., 1998). Despite evidence for the onset of enhanced surface N recycling across the early-summer SAZ (and PAZ), it is reasonable to assume substantial zooplankton grazing on the bloom, likely resulting in the downward C flux exceeding that of the apparent estimations of export production (via loss from the surface in the form of sinking zooplankton faecal material) (Table 4a). Additionally, the high biomass C:N ratio of microphytoplankton in the PAZ (Fig. 3a), where large diatoms are common (Sarmiento et al., 2004; Weir et al., 2020 and references therein), implies the elevated potential for C export from the surface (Le Fevre et al., 1998), provided the C-rich material constitutes part of the sinking flux.

In sum, the evidence for the enhanced degree of surface N recycling is supported by the shift in community composition to smaller-celled species over the season, particularly the increased abundance of picophytoplankton. Additionally, that their biomass C:N ratios exceed that of Redfield is consistent with the notion of increased late-summer microbial loop-related nutrient regeneration. This result, coincident with elevated ρNH_4^+ and low f-ratios (*see further detail in section 2.3*), evidences the apparent switch in surface N source dependence over the season, with implications for the capacity of the upper ocean ecosystem to sequester atmospheric CO_2.

5.2.2. Potential drivers of N source preference

The general trends in ρNO_3^- corresponded to those observed in previous studies conducted across the Atlantic Southern Ocean (Mdutyana et al., 2020; Joubert et al., 2011; Philibert et al., 2015). Rates across all zones during early-summer are variable, while ρNO_3^- increases with increasing latitude during late-summer (Fig. 12) (Philibert et al. 2015). Similarly, ρNH_4^+ was consistent with rates reported for early-summer, with the maximum rate measured in the SAZ (Mudtyana et al., 2020), as well as for late-summer, where a clear trend of increasing ρNH_4^+ with increasing latitude was observed (Fig. 13) (Joubert et al., 2011).

The apparent shift in the dominant N-source utilized by phytoplankton for NPP between the early- and late-summer sampling is such that NO_3^- was preferentially assimilated during early-summer across all frontal regions, particularly across the OAZ and PAZ, and with the exception of the PFZ, where early-summer ρNH_4^+ exceeded that of ρNO_3^- (Fig. 12a and 13a; Table 3a). In late-summer, ρNO_3^- was substantially reduced across all zones and an increased preference for NH_4^+ was apparent; at most stations, ρNH_4^+ was double ρNO_3^- (Fig. 12b and 13b; Table 3b). The exception to this was observed in the PAZ, where both ρNO_3^- and ρNH_4^+ increased with the seasonal progression (Fig. 12-13; Table 7a and 7b).

The complex interactions determining the preference for the uptake of NO_3^- over NH_4^+, and vice versa, have been shown to be highly variable (Dortch, 1990). The availability of the two N species in the surface layer of the Atlantic Southern Ocean is vastly different, with perennially high surface $[NO_3^-]$ having no effect on ρNO_3^- (Syrett, 1956; Tréguer & Jacques, 1992; Sarmiento et al. 2004; Mdutyana et al. 2020), while ρNH_4^+ appears to be highly concentration-dependent because NH_4^+ is typically present at such low concentrations in the mixed layer (Cochlan, 2008; Mdutyana et al. 2020). In the present study, the relationship between ρNH_4^+ and surface $[NH_4^+]$ is most apparent in late-summer, with an increase in ρNH_4^+ corresponding to an increase in surface $[NH_4^+]$ at most stations (Fig. 13b).

Conversely, ρNO_3^- and surface $[NO_3^-]$ do not well correspond, particularly in late-summer where ambient surface $[NO_3^-]$ remains high and ρNO_3^- is reduced (Fig. 12).

As a result of NO_3^- assimilation requiring more energy compared to that of NH_4^+, ρNO_3^- is highly dependent on light-availability (Olson, 1980; Sambrotto & Mace, 2000; Cochlan, 2008; Mdutyana et al., 2020). In accordance with this is an accentuated preference for ρNH_4^+ under low light conditions, with NH_4^+ requiring significantly less energy to assimilate (Dortch, 1990). Light is likely the driver of the N source preference observed in the PFZ in early-summer, where perennially deep MLDs enhance light limitation (Boyd, 2002; Lucas et al., 2007; Joubert et al., 2011), driving elevated ρNH_4^+ over ρNO_3^-. The reduced ρNO_3^- across all zones (excluding the PAZ) during late-summer is unlikely a response to light availability alone, however, since the observed increase in MLDs across the transect (an increase from ~40 to 60 m between December and March; Pellichero et al., 2016) is insufficient to result in such enhanced limitation (Boyd, 2002; Laubscher et al., 1993)

In addition to the alleviation of light limitation resulting from the shoaling of the mixed layer at the beginning of summer, the surface layer is resupplied with macro- and micronutrients (i.e., Fe) from depth (Lucas et al., 2007; Cochlan, 2008; Joubert et al., 2011; Holmes et al., 2019). Fe is widely recognized as an important limiting factor to phytoplankton growth in the Southern Ocean (Sunda, 1989; Martin, 1990), with the Fe requirement for the reduction of NO_3^- being high (Sunda, 1989; Morel and Price 2003), such that ρNO_3^- is decreased under conditions of low Fe-availability (Martin & Fitzwater, 1988; Joubert et al., 2011; Price et al. 1994). Without having directly measured [Fe] at the time of this study, it is only possible to speculate that enhanced Fe-availability in early-summer was at least partly responsible for the increased ρNO_3^-, while Fe-depletion in late-summer enhanced ρNH_4^+ relative to ρNO_3^- (Fig. 12 and 13). In a study conducted across the SAZ in the Atlantic Southern Ocean, phytoplankton growth showed heavy reliance on Fe supplied from depth during early-summer, whereas in late-summer the reliance was shifted to Fe regenerated within the ML (Tagliabue et al. 2014; Mtshali et al., 2019). This work underscores the role of enhanced surface remineralization processes in the late-summer resupply of recycled N and Fe (Mtshali et al., 2019), at least north of the AZ. Similarly, it is hypothesised that the elevated ρNO_3^- across the PAZ in both early- and late-summer is due to frequent resupply of Fe from meltwater coupled with high insolation and shallow MLDs (Sakshaug & Holm-Hansen, 1984; Martin & Fitzwater, 1988; Laubscher et al., 1993; Tagliabue et al., 2012; Henley et al., 2020).

The comparable rates of NO_3^- and NH_4^+ uptake north of the PF in early-summer is seemingly indicative of a surface ecosystem following the spring bloom, where grazing pressures are heightened and remineralization is enhanced, yet Fe and light availability are still sufficient to sustain ρNO_3^- (Joubert et al., 2011; Tagliabue, 2012; Henley et al., 2020; Mdutyana et al., 2020). This effect is augmented by the dominance of smaller-celled phytoplankton species (nanophytoplankton) (Table 4a; Froneman et al., 2001). The elevated ρNH_4^+ north of the PF during early-summer may therefore occur because of an increase in surface $[NH_4^+]$ resulting from an enhancement of the microbial loop (Fig. 13a; Table 1a and 3a) (Lourey et al., 2003; Cochlan, 2008; Fawcett et al., 2011; Goeyens et al., 1995). Similarly, the increased ρNH_4^+ and corresponding decrease in ρNO_3^- across all zones (except the PAZ) in late-summer may be attributed to the increased dominance of smaller-celled species as Fe becomes deplete, shifting from a nano- and microphytoplankton to nano- and picophytoplankton dominated assemblage (Table 4a and 4b) to accompany the enhancement of surface remineralization processes with the seasonal progression.

Finally, significantly elevated ρNO_3^- across the early-summer OAZ (Fig. 12a), corresponding to low rates of NPP (Fig. 11a) and ρNH_4^+ (Fig. 13a), as well as considerable contributions from nano- and microphytoplankton, is consistent with diatom dominance of the phytoplankton assemblage (Table 3a and 4a). Diatoms are specialists in taking up NO_3^- (Litchman et al., 2006; Fawcett & Ward, 2011) and have the capacity to store high concentrations of N internally (Wheeler et al., 1983). Given the Si-rich waters of the region and the likelihood that Fe-limitation is alleviated with the onset of summer, the dominance of diatoms across the OAZ that contribute substantially to ρNO_3^- is plausible (Goeyens et al., 1995). Since diatoms are a major vector for the downward C flux (Tréguer et al., 2018), their high abundance in the OAZ has positive implications for regional C export (Le Fevre et al., 1998; Sigman & Hain, 2012).

In sum, the variability in preferential uptake of NO_3^- over NH_4^+ between early- and late-summer is attributed to the complex interactions among light, Fe and macronutrient availability, along with associated changes in phytoplankton community composition (i.e., size-class distribution), and the extent to which these environmental conditions favour remineralization in the surface layer. Broadly, the primary control on ρNO_3^- over ρNH_4^+ in early-summer appears to be the alleviation of light and Fe limitation resulting from the enhanced stratification that occurs at the start of the summer season. The apparent control on ρNH_4^+ over ρNO_3^- in late-summer is attributed to the seasonal depletion of Fe coupled with the enhanced functioning of the microbial loop in response to elevated early-summer productivity, which acts to increase surface $[NH_4^+]$ and therefore ρNH_4^+.

5.2.2.a. Intra-seasonal and spatial variability in nutrient ratios in the context of community composition and carbon export potential

The high degree of variability observed in surface nutrient concentration and assimilation ratios is governed by regional differences in the phytoplankton community assemblage, where a complex biological feedback exists between the nutrient requirements and acquisition capabilities of phytoplankton species and the local limiting factors on productivity (Brzezinski et al., 2003; Weber & Deutsch, 2010, 2012).

The incomplete consumption of surface nutrients characteristic of HNLC waters (i.e., south of the STF) is apparent throughout the summer season across the transect, contrasted by rapidly declining concentrations north of the STF, typical of subtropical waters (Fig. 3). While NO_3^- is only limiting north of the STF (and throughout most of the global oceans thereafter) (Gruber 2008), $Si(OH)_4$ becomes limiting at concentrations <5 μM for large, heavily-silicified diatoms and ≤1 μM for smaller, lightly silicified species (Boyd et al., 1999; Hutchins et al., 2001). The onset of Si-limitation in the SAZ (where surface $[Si(OH)_4]$ <5 μM) thus drives an important change in community composition, with implications for the potential for carbon export in the region (Cullen, 1991; Weber & Deutsch, 2012). The markedly low Si* across the SAZ (and PAZ) is indicative of this, with values declining further as the season progresses, implying enhanced Si-limitation (Fig. 4) (Sarmiento et al., 2004). An apparent shift in community composition across the SAZ is evidenced by the decreasing contribution of microphytoplankton and increasing contribution of picophytoplankton to surface NPP with the seasonal progression, with a substantial corresponding decrease in export production estimates (Table 4a and 4b).

Brzezinski (1985) demonstrated in culture experiments that under nutrient-replete conditions, diatoms consumed Si:NO_3^- in a ratio of ~0.90 (i.e., 15:16). In a later study conducted across the Pacific Southern Ocean between the PF and the ice edge during early-summer, the net uptake of Si:NO_3^- by a diatom bloom was significantly higher (3.7 ± 0.4; Brzezinksi et al., 2003). Averaging over the PFZ, OAZ and PAZ, the early-summer Si:NO_3^- consumption ratio was 4.3 ± 1.4 (Fig. 6a; Fig. 14a), while in late-summer it decreased to 2.8 ± 0.9 (Fig. 6b; Fig. 14b). The observation of a Si:NO_3^- consumption ratio >1:1 is consistent with studies a conducted across the Atlantic (Tréguer & Pondaven, 2000; Weir et al. 2020) and Pacific sectors of the Southern Ocean (Smith et al., 2015) showing that the Si:NO_3^- consumption ratios is as high as 5:1. The apparent decrease in Si:NO_3^- consumption ratio with the seasonal progression may evidence a shift from a phytoplankton assemblage dominated by larger diatoms with a high Si requirement to smaller, lightly-silicified diatoms and various non-silicifying phytoplankton species (Fig. 6; Fig. 14) (Sarmiento et al. 2004). This interpretation is complicated, however, by the fact that the control of Fe-availability on Si:NO_3^- consumption by diatoms is such that under conditions of low [Fe], the ratio increases significantly (Takeda, 1998; Weber & Deutsch, 2012). This means that in late-summer when Fe is depleted, a given community of diatoms should consume Si and NO_3^- in a higher ratio than they would under the higher-[Fe] conditions of the early-summer. In the late-summer PAZ (and possibly the southern OAZ), however, where NPP is higher than in early-summer, the associated decline in Si:NO_3^- consumption ratio may indicate the increasing dominance of larger diatoms with the seasonal progression, consistent with the higher relative contribution of microphytoplankton to NPP and ρNO_3^- in late- versus early summer (Fig. 11 and 12; Table 4a and 4b).

The decreased surface consumption of Si:NO_3^- in the region of the SACCF1 (and PF1, where surface Si:NO_3^- consumption is highly variable) in late-summer may indicate the role of frontal upwelling in the localised, small-scale resupply of Fe later in the season, creating favourable conditions for elevated NPP (Fig. 11b) and increased diatom abundances in the regions adjacent to these frontal boundaries (Fig. 6b). The occurrence of mesoscale hydrographic features, including localised frontal upwelling, results in the vertical injection of nutrients to the surface (Strass et al., 2002) as well as causing the MLD to shoal, increasing the stability of the upper water column and thus enhancing the light environment (Boyd, 2002). The effects of such events in the open Southern Ocean are particularly influential in late-summer, when Fe is deplete and NPP is primarily fuelled by regenerated production, where such regions of localised upwelling emerge as C export "hotspots" (Hutchins et al., 1998; Boyd, 2002).

The net ratio of NO_3^- to PO_4^{3-} uptake is also affected by Fe availability, regional changes in phytoplankton species composition, higher trophic level functioning, and the capacity of organisms for intracellular nutrient storage (Weber & Deutsch, 2010). The NO_3^-:PO_4^{3-} consumption ratio has been observed to range widely, from 5-33.5, and a mean global value of 16:1 (although typically slightly lower in the Southern Ocean; Redfield et al., 1958; Weber & Deutsch, 2012 and references therein). In the present study, averages of 14 ± 1.4 and 28.5 ± 11.7 were obtained for early- and late-summer across the transect, respectively (Fig. 7). Surface NO_3^-:PO_4^{3-} consumption ratios have been reported to increase from ~12:1 in the AZ to ~20:1 in the SAZ (Weber & Deutsch, 2010), with low uptake ratios in the AZ associated with diatom dominated blooms (De Baar et al., 1997), while high ratios of NO_3^-:PO_4^{3-} consumption are associated with smaller non-diatom phytoplankton species (e.g., *Phaeocystis*; Arrigo et al. 2002; Martiny et al., 2013). The apparent increase in surface consumption of NO_3^-:PO_4^{3-} with the seasonal progression substantiates the notion that in late-summer, the phytoplankton community shifts from a larger-celled assemblage, where diatom abundances are high, to a smaller-celled community, with potentially substantial effects on export production.

In the SAZ, the surface NO_3^-:PO_4^{3-} consumption ratio decreases over the season (Fig. 15), which may indicate a shift in the phytoplankton assemblage towards dinoflagellates since these phytoplankton commonly consume ~40% more PO_4^{3-} that diatoms (Twining et al., 2004). Alternatively, the low surface NO_3^-:PO_4^{3-} consumption ratio across the late-summer SAZ (where NO_3^-:PO_4^{3-} uptake occurs in a ratio between 16:1 and <11:1) may be indicative of enhanced surface recycling of NO_3^- relative to PO_4^{3-} (Weber & Deutsch, 2012), which would increase the ambient NO_3^- concentration in excess of that of PO_4^{3-}, causing an apparent decline in the NO_3^-:PO_4^{3-} consumption ratio. However, direct measurements of nitrification (i.e., NO_3^- production) in the SAZ mixed layer in summer indicate that this process is negligible (Mdutyana et al. 2020). More likely, therefore, is a shift towards dinoflagellates with a non-Redfieldian N:P requirement. Such a shift has implications for C export potential given that dinoflagellates are less likely to sink than ballasted phytoplankton such as diatoms (or coccolithophores, which can be abundant in the SAZ; Trull et al. 2001; de Sallas et al. 2011).

Suggested first by Gran (1931) and later reviewed by Martin and Fitzwater (1988), the Antarctic Iron Limitation Hypothesis suggests that the extensive variability in N:P observed across the Antarctic Ocean is caused by Fe-stress (De Baar et al., 1997), with less PO_4^{3-} consumed relative to N under conditions of Fe-limitation (Brzezinski et al., 2003; Weber & Deutsch, 2010). In early-summer, the ratio of surface DIN to PO_4^{3-} concentrations showed little deviation from the Redfield ratio south of the STF (~16:1), whereas in late-summer, surface DIN:PO_4^{3-} decreased to 11.9 ± 0.4 (Fig. 5), implying decreased uptake of PO_4^{3-} relative to DIN. Similarly in early-summer, the surface NO_3^-:PO_4^{3-} consumption ratio ranged from 11:1 to 20:1, with the exception of part of the PAZ (likely to high abundances of diatoms, that have an lower-than-Redfield N:P requirement, <10:1 in some cases; Bertilsson et al., 2003) (Fig. 15a). Conversely, the late-summer surface NO_3^-:PO_4^{3-} ratio falls above the 16:1 in all zones except the SAZ, in most cases exceeding 20:1 (Fig. 15b). The clear shift towards decreased consumption of PO_4^{3-} with the seasonal progression is consistent with the enhanced growth of smaller-celled phytoplankton species, as well as the likelihood of Fe-limitation incident on the (non-diatom) community (Brzezinski et al., 2003; Weber & Deutsch, 2012).

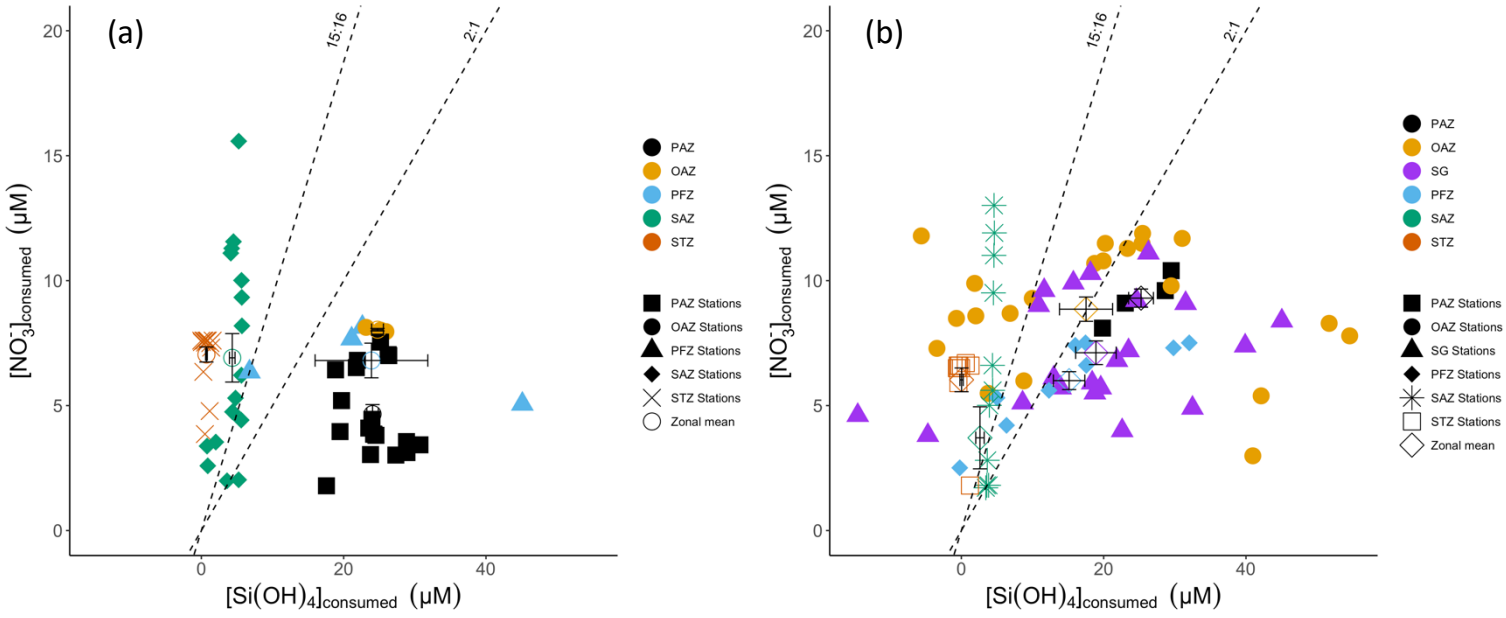

Figure 14: Surface concentrations [µM] of $Si(OH)_4$ versus NO_3^- consumed in surface waters relative to the concentration available following wintertime nutrient recharge for a) the early-summer and b) the late-summer transects. The average surface $Si(OH)_4$ and NO_3^- consumptions for each zone is represented by the open circle symbols (a) and open diamond symbols (b), with error bars indicating ± 1 S.D. The Redfield ratio for $Si(OH)_4$:NO_3^- of 15:16 for iron-replete diatoms (Redfield et al., 1934 & 1958; Brzezinski et al., 2003) and a ratio of 2:1 commonly observed in Southern Ocean regions of high diatom abundance (Weber & Deutsch, 2012) are denoted by the dashed black slopes.

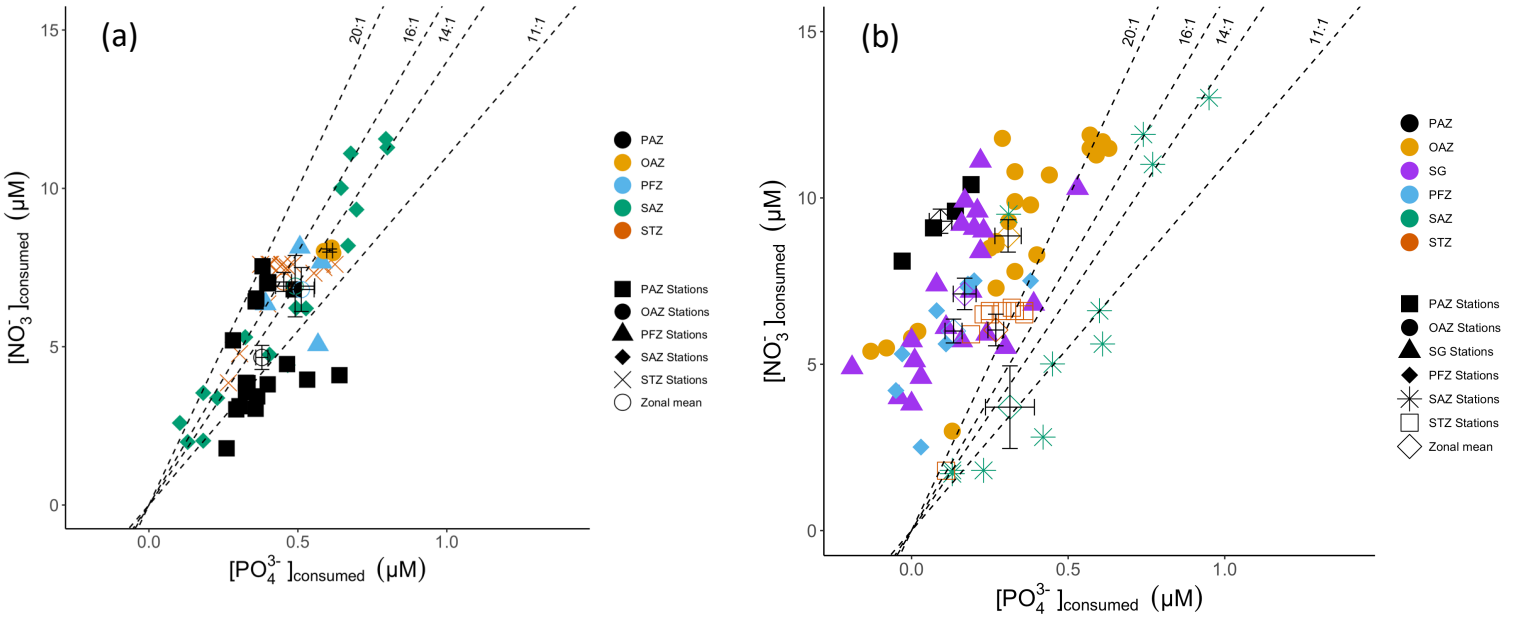

Figure 14: Surface concentrations [µM] of $Si(OH)_4$ versus NO_3^- consumed in surface waters relative to the concentration available following wintertime nutrient recharge for a) the early-summer and b) the late-summer transects. The average surface $Si(OH)_4$ and NO_3^- consumptions for each zone is represented by the open circle symbols (a) and open diamond symbols (b), with error bars indicating ± 1 S.D. The Redfield ratio for $Si(OH)_4$:NO_3^- of 15:16 for iron-replete diatoms (Redfield et al., 1934 & 1958; Brzezinski et al., 2003) and a ratio of 2:1 commonly observed in Southern Ocean regions of high diatom abundance (Weber & Deutsch, 2012) are denoted by the dashed black slopes.

5.2.3. f-ratio estimates and implications for export production

The f-ratio estimates calculated for the early- and late-summer are indicative of the relative utilization of new versus regenerated N sources to sustain surface NPP across a single growing season.

In early-summer, the f-ratios calculated for the AZ (i.e., OAZ and PAZ) were relatively high (average of 0.84 ± 0.09; C export average of 378.6 ± 190.6 nM C d^{-1}), while the SAZ and PFZ f-ratios were low (average of 0.28 ± 0.23; C export average of 253.0 ± 84.2 nM C d^{-1}) and the STZ f-ratio was moderate (0.50 ± 0.16; C export average of 548.9 ± 300.4 nM C d^{-1}) (Table 4a; Fig. 17a). Taken as an indication of the proportion of NPP available for export from the surface (Dugdale & Goering, 1967; Eppley & Peterson, 1979), these f-ratios suggest that in early-summer, the AZ was characterised predominantly by new production, with ~84% of total NPP potentially exportable, while the SAZ and PFZ were largely

characterised by regenerated production, with only ~28% total NPP equitable to export production. These early-summer f-ratio estimates are consistent with those reported for November-January across the Atlantic, Pacific and Indian sectors of the Southern Ocean (Sambrotto & Mace, 2000; Savoye et al., 2004; Joubert et al., 2011), with the f-ratio estimate for the early-summer SAZ comparable to that previously reported for the wintertime Atlantic sector (Philibert et al., 2015; Mdutyana et al., 2020) as well as to one late-summer study conducted along the GoodHope line (Philibert et al., 2015).

The f-ratios calculated for late-summer were significantly lower, particularly north of the PF (i.e., STZ, SAZ and PFZ; range of 0.02-0.07, average of 0.04 ± 0.03; C export average of 21.4 ± 16.8 nM C d^{-1}), with a substantial seasonal decline across the AZ as well (average of 0.15 ± 0.02; C export average of 142.9 ± 110.2 nM C d^{-1}) (Table 4b; Fig. 17b). The implication is that in late-summer, >90% of total NPP was recycled in surface waters, thereby not contributing to C export. The f-ratio estimates for late-summer are similar to those reported for February-April across the Indian sector (Thomalla et al., 2011); however, they are lower than previous reports for the late-summer Atlantic sector (Joubert et al., 2011), being more comparable to estimates reported for the wintertime Atlantic Southern Ocean (Philibert et al., 2015; Mdutyana et al., 2020).

To highlight the importance of accounting for all sources of recycled N in the f-ratio calculation, two equations were used, one excluding the estimated specific uptake rate of urea (i.e., uncorrected f-ratio; equation 1.15) and the another including urea (i.e., urea-corrected f-ratio; equation 1.16). The average uncorrected f-ratio across the transect in early-summer was 0.64 ± 0.19 while the urea-corrected f-ratio was 0.54 ± 0.31 (Table 4a). More pronounced is the effect in late-summer, where the average uncorrected f-ratio was 0.47 ± 0.15 and the urea-corrected f-ratio was 0.08 ± 0.06 (Table 4b). Based on the corrected f-ratios, it is apparent that the urea (and/or a similar form of recycled DON) fuelled ~10% of early-summer NPP, while in late-summer, urea supported ~39% of the NPP (Table 4a and 4b). It should be noted that the calculation for V_{urea} assumes that where concurrent measurements of NPP and ρN_x (adjusted value; *see further details in section 2.1.*) are decoupled, all the unaccounted-for N is regenerated. In the event that this is not the case, the f-ratios will have been underestimated. Nonetheless, excluding urea uptake when calculating the f-ratio for the summertime Southern Ocean clearly leads to an overestimation of C export potential.

The discrepancy between the late-summer f-ratio estimates reported here and those of Joubert et al. (2011) (0.42 ± 0.26) could be due to the time of sampling being slightly different, with the present study including data for March 2019 only, while Joubert et al. (2011) included data from February and March 2010. Since the surface ecosystem appears to become increasingly regenerative as the summer season progresses (over a relatively short period of time), the inclusion of an earlier summer month (February) in the dataset of Joubert et al. (2011) may explain the higher f-ratios that they computed. In accordance with this are the substantially higher ρNH_4^+ measured in the present study, with ρNH_4^+ during late-summer that were three- to five-fold greater across the AZ than those reported by Joubert et al. (2011).

Although the f-ratio is useful for demonstrating the potential for C export on a seasonal basis, its meaning should be interpreted with caution. C exported from the surface during summer that is remineralized to CO_2 above the depth of deep winter mixing (~150-250 m across the Atlantic Southern Ocean; Sallée et al., 2010), cannot be considered sequestered as it will be re-exposed to the atmosphere in the months following the cessation of summer (Mdutyana et al., 2020). Despite this shortcoming, using the f-ratios to assess the dominant source of N sustaining surface NPP confirms the hypothesised shift from the predominance of new production to regenerated production within the surface ecosystem. This shift occurs in response to numerous interactions between the phytoplankton assemblage and the

changing environmental conditions imposed on the community between the beginning and end of the growing season.

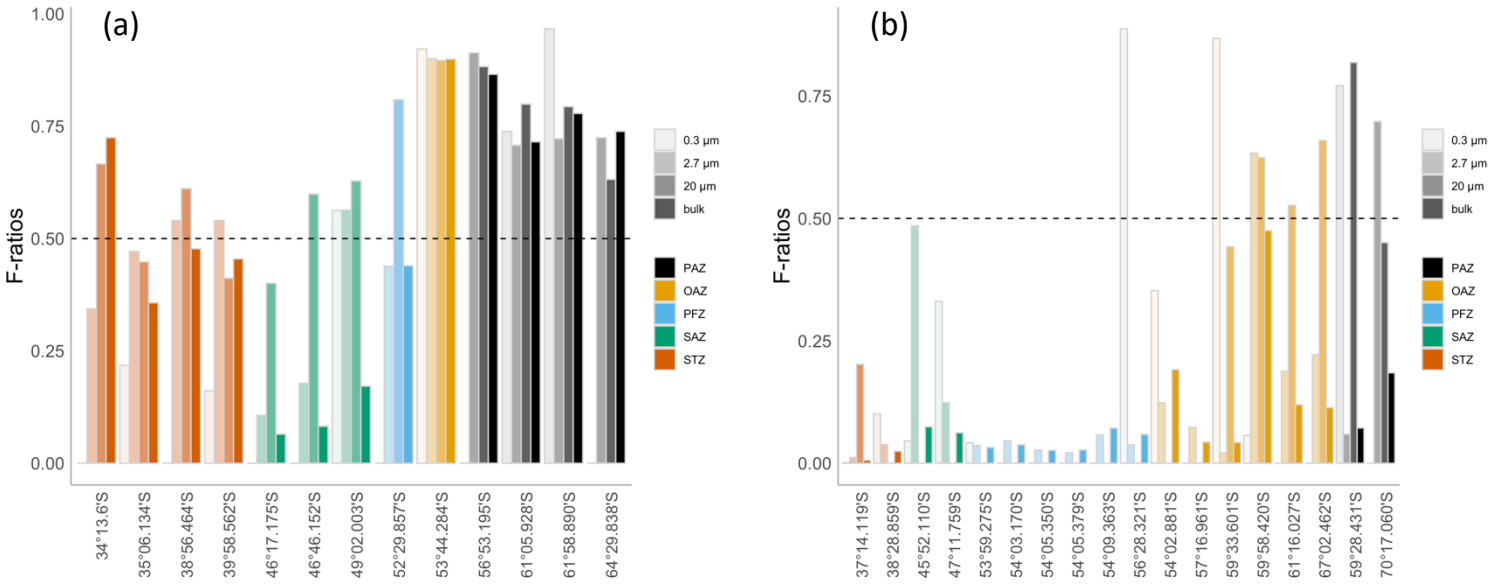

Figure 17: Size-fractionated f-ratios at each station for a) the early-summer and b) the late-summer transects. The colour and shading of the bars are representative of the size-class and frontal zones as defined in Figure 8. f-ratios were calculated from equation 1.16, an amended version of the original equation of Dugdale & Goering (1967) that includes the specific uptake rate of urea. The dashed black horizonal line shows an f-ratio = 0.5, with bars exceeding 0.5 indicating a phytoplankton community fueled predominantly by new production and bars below 0.5 indicating a community fueled mainly by regenerated production.

6. CONCLUSIONS

Rates of NPP and N uptake were measured across the Atlantic Southern Ocean in early- and late-summer, to investigate the variability in surface biological activity between the beginning and end of the growing season. The response of the upper ocean N cycle to changing surface conditions and resource availability over the season was investigated, with N cycle measurements used to estimate C export potential (i.e., via the f-ratio) and thus the seasonal evolution of the strength and efficiency of the biological pump (Dugdale & Goering, 1967; Eppley & Peterson, 1979).

Early-summer was characterised by relatively high rates of NPP north of the PF (i.e., the broader Subantarctic and STZ), with corresponding f-ratio estimates indicating that the phytoplankton community was predominantly reliant on regenerated N sources. The contribution from an additional regenerated N source (i.e., urea) was strongly evident across the SAZ, indicating a substantial degree of surface nutrient regeneration following the peak of the spring phytoplankton bloom; consequently, the SAZ emerged as the region of lowest C export potential during early-summer. A high proportion of larger-celled phytoplankton (i.e., diatoms) were observed in early-summer, likely due to the increased $Si(OH)_4$ availability. That the associated C export was low implicates an important role for large grazers (Le Fèvre et al., 1998). The near-exclusive dominance of nanophytoplankton across the PFZ along with conditions of elevated surface regeneration likely owed to light-limitation, while the near co-dominance of nano- and picophytoplankton across the STZ can be attributed to the co-limitation of $Si(OH)_4$ and NO_3^-.

The Antarctic Zone was characterised by high f-ratio estimates and a strong preference for NO_3^- over NH_4^+ in early-summer. In the OAZ, however, NPP and ρN_x were decoupled, with far more NO_3^- consumed than expected from the rate of C fixation. A possible explanation for this is a phytoplankton community dominated by diatoms engaging in luxury NO_3^- uptake. Diatoms can store NO_3^- intracellularly until conditions become favourable for them to assimilate it (e.g., when Fe and/or light availability increases). Elevated rates of NPP and high C export potential across the PAZ are attributed to diatom dominance, driven by the seasonally retreating sea ice resulting in favourable bloom conditions (e.g., stratified surface waters and increased Fe supply).

In late-summer, significantly lower rates of NPP were measured across the STZ and SAZ, while a substantial increase was apparent southwards of the PF. The decoupling of NPP and ρN_x in this case revealed the essential role of urea (and/or other regenerated DON forms) in the late-summer ρN dynamics across all frontal regions, with the low f-ratios underscoring the importance of regenerated production across the late-summer Atlantic Southern Ocean. As a consequence, the apparent C export was significantly decreased, with the only moderate estimate occurring across the PAZ where sea ice dynamics and resupply of Fe likely facilitated the enhanced uptake of NO_3^- and the prolonged duration of a diatom-dominated bloom. The general shift in phytoplankton community composition to smaller-celled species in late-summer indicates an up-regulation of the microbial loop and elevated surface nutrient regeneration (with zooplankton grazing on biomass produced earlier in the season likely also supplying recycled N). An enhancement of the microbial loop is supported by the accumulation of C-rich biomass at the surface, particularly across the PFZ, SAZ and STZ, which results from the preferential remineralization by heterotrophic bacteria of N over C.

Previous studies in the Southern Ocean have suggested that late-summer and autumn, following the period of elevated phytoplankton growth, should be periods of intense surface layer N recycling (Lourey

et al., 2003; Smart et al., 2015) The seasonally-resolved dataset present here confirms these suggestions, demonstrating that late-summer in the Atlantic Southern Ocean is dominated by a phytoplankton community that is heavily reliant on recycled sources of N. It is proposed here that localised availability of Fe, light and $Si(OH)_4$ drive the shift in the preferential N source supporting NPP to varying degrees depending on the primary limiting factor for growth across the various frontal zones over the summer season. These factors, Fe in particular (where a direct association exists between Fe availability and N source utilized, based on cellular energy requirements for assimilation; Martin & Fitzwater, 1988; Sunda, 1989; Price et al. 1994), act to restructure the phytoplankton community (e.g., smaller cells succeeding larger ones), in turn governing the structure of the dominant food web (i.e., sinking flux versus microbial loop versus grazing food chain; Azam, 1998) and thus significantly impacting C export potential (Lancelot et al., 2000). The dominance of nanophytoplankton throughout the summer across the Atlantic Southern Ocean may be attributed to their competitive advantage over larger species under conditions of low Fe-availability (Sunda & Huntsman, 1995; Hutchins et al., 1995; Armstrong, 1999). The observed dynamics of ρN and associated export production are thus controlled by a series of complex feedbacks between Fe, light, $Si(OH)_4$ and phytoplankton community composition.

In sum, the data presented here confirm that the Southern Ocean experiences a switch from a surface ecosystem sustained by new production in early-summer to one fuelled predominantly by regenerated production in late-summer. This phenomenon is particularly evident across the AZ, as previous work suggested it should be (Lourey et al. 2003). One implication of these findings is that biology contribute significantly to making the region a sink for atmospheric CO_2 in early-summer through a strong biological pump. In late-summer, by contrast, the biological pump appears to weaken, resulting in the broad region of the Atlantic Southern Ocean where the biological contribution to atmospheric CO_2 removal is minor (Broecker, 1982; Sarmiento & Toggweiler, 1984; Sigman & Boyle, 2000).

There is a paucity of data characterising the dynamics of N cycling in the surface Southern Ocean, and fewer still that distinguish between the beginning and end of a single growing season (Laubscher et al., 1993; Lourey et al., 2003). Future work is therefore required to substantiate these results, possibly including a dataset wherein depth integrated ρN is measured to establish a higher resolution perspective of euphotic layer N cycling over a single summer season, with the role of heterotrophic activity expected to be enhanced with depth in the water column (Deppeler & Davidson, 2017). Furthermore, a better understanding of the major phytoplankton players (i.e., at a species level) is required if we are to assess group-specific contributions to C export in the Southern Ocean; indeed, only one such dataset is currently available, for the Subantarctic Indian Ocean (Forrer, 2020). With an improved understanding of the variability in group-specific contributions to C export, as well as the varied responses to resource supply and availability, it should be possible to better predict how the Southern Ocean's biological pump is likely to change with the imminent change in global climate.

7. REFERENCES

Allanson, B. R., Hart, R. C., & Lutjeharms, J. R. E. (1981). Observations on the nutrients, chlorophyll and primary production of the Southern Ocean south of Africa. *Vol 4*.

Altabet, M. A., & Francois, R. (2001). Nitrogen isotope biogeochemistry of the Antarctic Polar Frontal Zone at 170 W. *Deep Sea Research Part II: Topical Studies in Oceanography* 48.19-20: 4247- 4273.

Altieri, K.E., Fawcett, S.E., Hastings, M.G. (2021) Reactive nitrogen cycling in the atmosphere and ocean. Annual Review of Earth and Planetary Science 49.

Armstrong, R. A. (1999). An optimization-based model of iron—light—ammonium colimitation of nitrate uptake and phytoplankton growth. *Limnology and Oceanography*, *44*(6), 1436-1446.

Arteaga, L. A., Boss, E., Behrenfeld, M. J., Westberry, T. K., & Sarmiento, J. L. (2020). Seasonal modulation of phytoplankton biomass in the Southern Ocean. *Nature communications*, *11*(1), 1-10.

Azam, F., Fenchel, T., Field, J. G., Gray, J. S., Meyer-Reil, L. A., & Thingstad, F. (1983). The ecological role of water-column microbes in the sea. *Marine ecology progress series*, 257-263.

Azam, F. (1998). Microbial control of oceanic carbon flux: the plot thickens. *Science*, *280*(5364), 694-696.

Azam, F., Smith, D. C., Steward, G. F., & Hagström, Å. (1994). Bacteria-organic matter coupling and its significance for oceanic carbon cycling. *Microbial ecology*, *28*(2), 167-179.

Bertilsson, S., & Jones Jr, J. B. (2003). Supply of dissolved organic matter to aquatic ecosystems: autochthonous sources. In *Aquatic Ecosystems* (pp. 3-24). Academic Press.

Bode, A., Botas, J.A., Fernández, E., 1997. Nitrate storage by phytoplankton in a coastal upwelling environment. Mar. Biol. 129, 399–406.

Borrione, I., & Schlitzer, R. (2013). Distribution and recurrence of phytoplankton blooms around South Georgia, Southern Ocean. *Biogeosciences*, *10*(1), 217-231.

Boyd, P. W., & Newton, P. P. (1999). Does planktonic community structure determine downward particulate organic carbon flux in different oceanic provinces?. *Deep Sea Research Part I: Oceanographic Research Papers*, *46*(1), 63-91.

Boyd, P. W., Watson, A. J., Law, C. S., Abraham, E. R., Trull, T., Murdoch, R., ... & Charette, M. (2000). A mesoscale phytoplankton bloom in the polar Southern Ocean stimulated by iron fertilization. *Nature*, *407*(6805), 695-702.

Boyd, P. W. (2002). Environmental factors controlling phytoplankton processes in the Southern Ocean1. *Journal of Phycology*, *38*(5), 844-861.

Bracher, A. U., Kroon, B. M. A., & Lucas, M. I. (1999). Primary production, physiological state and composition of phytoplankton in the Atlantic Sector of the Southern Ocean. *Marine Ecology Progress Series*, *190*, 1-16.

Bronk, D. A., Glibert, P. M., & Ward, B. B. (1994). Nitrogen uptake, dissolved organic nitrogen release, and new production. *Science*, *265*(5180), 1843-1846.

Bronk, D. A., Glibert, P. M., Malone, T. C., Banahan, S., & Sahlsten, E. (1998). Inorganic and organic nitrogen cycling in Chesapeake Bay: autotrophic versus heterotrophic processes and relationships to carbon flux. *Aquatic microbial ecology*, *15*(2), 177-189.
Bronk, D. A. (2002). Dynamics of DON. *Biogeochemistry of marine dissolved organic matter*, *384*, p153-247.

Brzezinski, M. A. (1985), The Si:C:N ratio of marine diatoms: Interspecific variability and the effect of some environmental variables, *Journal of Phycology, 21*, 347–357.

Brzezinski, M. A., Dickson, M. L., Nelson, D. M., & Sambrotto, R. (2003). Ratios of Si, C and N uptake by microplankton in the Southern Ocean. *Deep Sea Research Part II: Topical Studies in Oceanography*, *50*(3-4), 619-633.

Buesseler, K. O., Andrews, J. E., Pike, S. M., Charette, M. A., Goldson, L. E., Brzezinski, M. A., & Lance, V. P. (2005). Particle export during the southern ocean iron experiment (SOFeX). *Limnology and Oceanography*, *50*(1), 311-327.

Burger, J. M., Moloney, C. L., Walker, D. R., Parrott, R. G., & Fawcett, S. E. (2020). Drivers of short- term variability in phytoplankton production in an embayment of the southern Benguela upwelling system. *Journal of Marine Systems*, 103341.

Chapman, C. C., Lea, M. A., Meyer, A., Sallée, J. B., & Hindell, M. (2020). Defining Southern Ocean fronts and their influence on biological and physical processes in a changing climate. *Nature Climate Change*, 1-11.

Cullen, J. J. (1991). Hypotheses to explain high-nutrient conditions in the open sea. *Limnology and Oceanography*, *36*(8), 1578-1599.

Mulholland, M. R., & Lomas, M. W. (2008). Nitrogen uptake and assimilation. *Nitrogen in the marine environment*, 303-384.

Chever, F., Bucciarelli, E., Sarthou, G., Speich, S., Arhan, M., Penven, P., & Tagliabue, A. (2010). Physical speciation of iron in the Atlantic sector of the Southern Ocean along a transect from the subtropical domain to the Weddell Sea Gyre. *Journal of Geophysical Research: Oceans*, *115*(C10).

Clowes, A. J. (1938). *Phosphate and silicate in the Southern Ocean*. University Press.

Cochlan, W. P. (2008). Nitrogen uptake in the Southern Ocean. *Nitrogen in the Marine Environment, edited by: Capone, DG, Bronk, DA, Mulholland, MR, and Carpenter, EJ, 2nd Edition, Academic Press, Elsevier*, 569-596.

Conley, D. J., & Malone, T. C. (1992). Annual cycle of dissolved silicate in Chesapeake Bay: implications for the production and fate of phytoplankton biomass. *Marine ecology progress series. Oldendorf*, *81*(2), 121-128.

Conover, R. J., & Gustavson, K. R. (1999). Sources of urea in arctic seas: zooplankton metabolism. *Marine Ecology Progress Series*, *179*, 41-54.

Cornwall, C. (2021). *NOAA Solar Calculator*. NOAA Earth System Research Lab. 22/05/2020. https://www.esrl.noaa.gov/gmd/grad/solcalc/

Corredor, J.E., 1979. Phytoplankton response to low level nutrient enrichment through upwelling in the Columbian Caribbean Basin. Deep-Sea Res. 26, 731–741.

Croot, P. L., Wieczorek, A., & Heller, M. I. (2020, February). Towards a global understanding of the role of urea in the ocean nitrogen cycle. In *Ocean Sciences Meeting 2020*. AGU.

De Baar, H. J. W., Van Leeuwe, M. A., Scharek, R., Goeyens, L., Bakker, K. M. J., & Fritsche, P. (1997). Nutrient anomalies in Fragilariopsis kerguelensis blooms, iron deficiency and the nitrate/phosphate ratio (AC Redfield) of the Antarctic Ocean. *Deep Sea Research Part II: Topical Studies in Oceanography*, *44*(1-2), 229-260.
DeManche, J. M., Curl, H. C., Lundy, D. W., & Donaghay, P. L. (1979). The rapid response of the marine diatom Skeletonema costatum to changes in external and internal nutrient concentration. *Marine Biology*, *53*(4), 323-333.

Deppeler, S. L., & Davidson, A. T. (2017). Southern Ocean phytoplankton in a changing climate. *Frontiers in Marine Science*, *4*, 40.

Deutsch, C., & Weber, T. (2012). Nutrient ratios as a tracer and driver of ocean biogeochemistry. *Annual Review of Marine Science*, *4*, 113-141.

Doty, M. S., & Oguri, M. (1956). The island mass effect. *ICES Journal of Marine Science*, *22*(1), 33- 37.

Dortch, Q. (1990). The interaction between ammonium and nitrate uptake in phytoplankton. *Marine ecology progress series. Oldendorf*, *61*(1), 183-201.

Dugdale, R. C., & Goering, J. J. (1967). Uptake of new and regenerated forms of nitrogen in primary productivity 1. *Limnology and oceanography*, *12*(2), 196-206.

Dugdale, R. C., & Wilkerson, F. P. (1986). The use of 15N to measure nitrogen uptake in eutrophic oceans; experimental considerations 1, 2. *Limnology and Oceanography*, *31*(4), 673-689.

El-Sayed, S. Z. (1988). Productivity of the Southern Ocean: a closer look. *Comparative Biochemistry and Physiology Part B: Comparative Biochemistry*, *90*(3), 489-498.

Eppley, R. W., & Peterson, B. J. (1979). Particulate organic matter flux and planktonic new production in the deep ocean. *Nature*, *282*(5740), 677-680.

Fawcett, S. E., & Ward, B. B. (2011). Phytoplankton succession and nitrogen utilization during the development of an upwelling bloom. *Marine Ecology Progress Series*, *428*, 13-31.

Froneman, P. W., McQuaid, C. D., & Perissinotto, R. (1995). Biogeographic structure of the microphytoplankton assemblages of the south Atlantic and Southern Ocean during austral summer. *Journal of plankton research*, *17*(9), 1791-1802.

Froneman, P. W., Laubscher, R. K., & McQuaid, C. D. (2001). Size-fractionated primary production in the south Atlantic and Atlantic sectors of the Southern Ocean. *Journal of plankton research*, *23*(6), 611-622.

Froneman, P. W., Pakhomov, E. A., & Balarin, M. G. (2004). Size-fractionated phytoplankton biomass, production and biogenic carbon flux in the eastern Atlantic sector of the Southern Ocean in late austral summer 1997–1998. *Deep Sea Research Part II: Topical Studies in Oceanography*, *51*(22-24), 2715-2729.

Gandhi, N., Ramesh, R., Laskar, A. H., Sheshshayee, M. S., Shetye, S., Anilkumar, N., ... & Mohan, R. (2012). Zonal variability in primary production and nitrogen uptake rates in the southwestern Indian Ocean and the Southern Ocean. *Deep Sea Research Part I: Oceanographic Research Papers*, *67*, 32-43.

Goeyens, L., Tréguer, P., Baumann, M. E. M., Baeyens, W., & Dehairs, F. (1995). The leading role of ammonium in the nitrogen uptake regime of Southern Ocean marginal ice zones. *Journal of marine systems*, *6*(4), 345-361.

Gordon, A. L., Molinelli, E., & Baker, T. (1978). Large-scale relative dynamic topography of the Southern Ocean. *Journal of Geophysical Research: Oceans*, *83*(C6), 3023-3032.

Fortier, L., Le Fèvre, J., & Legendre, L. (1994). Export of biogenic carbon to fish and to the deep ocean: the role of large planktonic microphages. *Journal of Plankton Research*, *16*(7), 809-839.

Forrer, H., Knapp, A. N., Bornman, T. G., Thomas, R., Waterworth, S. C., Dorrington, R., & Fawcett, S. (2020, February). Toward an Improved Understanding of the Subantarctic Biological Pump: Phytoplankton Group-specific Contributions to and Potential Drivers of Carbon Export in the Indian Sector of the Subantarctic Ocean. In *Ocean Sciences Meeting 2020*. AGU.

Glover, H.E., Garside, C., Trees, C.C., 2007. Physiological responses of Sargasso Sea pi- coplankton to nanomolar nitrate perturbations. J. Plankton Res. 29 (3), 263–274.

Gruber, N. (2008). The marine nitrogen cycle: overview and challenges. *Nitrogen in the marine environment*, *2*, 1-50.

Henley, S. F., Cavan, E. L., Fawcett, S. E., Kerr, R., Monteiro, T., Sherrell, R. M., ... & Smith, S. (2020). Changing biogeochemistry of the Southern Ocean and its ecosystem implications. *Frontiers in Marine Science*, *7*, 581.

Holl, Carolyn M., and Joseph P. Montoya. 2005. “Interactions between Nitrate Uptake and Nitrogen Fixation in Continuous Cultures of the Marine Diazotroph Trichodesmium (Cyanobacteria).” Journal of Phycology 41 (6): 1178–83. https://doi.org/10.1111/j.1529-8817.2005.00146.x.

Holliday, N. P., & Read, J. F. (1998). Surface oceanic fronts between Africa and Antarctica. *Deep Sea Research Part I: Oceanographic Research Papers*, *45*(2-3), 217-238.

Holmes, T. M., Wuttig, K., Chase, Z., van der Merwe, P., Townsend, A. T., Schallenberg, C., ... & Bowie, A. R. (2019). Iron availability influences nutrient drawdown in the Heard and McDonald Islands region, Southern Ocean. *Marine Chemistry*, *211*, 1-14.

Hutchins, D. A., & Bruland, K. W. (1998). Iron-limited diatom growth and Si: N uptake ratios in a coastal upwelling regime. *Nature*, *393*(6685), 561-564.

Hutchins, D. A., Sedwick, P. N., DiTullio, G. R., Boyd, P. W., Queguiner, B., Griffiths, F. B., & Crossley, C. (2001). Control of phytoplankton growth by iron and silicic acid availability in the subantarctic Southern Ocean: Experimental results from the SAZ Project. *Journal of Geophysical Research: Oceans*, *106*(C12), 31559-31572.

Jacques, G., & Minas, M. (1981). Primary production in the Indian sector of the Antarctic Ocean in late summer. *Oceanologica Acta* , *4* (1), 33-41.

Jones, G. B., Curran, M. A., Swan, H. B., Greene, R. M., Griffiths, F. B., & Clementson, L. A. (1998). Influence of different water masses and biological activity on dimethylsulphide and dimethylsulphoniopropionate in the subantarctic zone of the Southern Ocean during ACE 1. *Journal of Geophysical Research: Atmospheres*, *103*(D13), 16691-16701.

Joubert, W. R., Thomalla, S. J., Waldron, H. N., Lucas, M. I., Boye, M., Le Moigne, F. A., ... & Speich, S. (2011). Nitrogen uptake by phytoplankton in the Atlantic sector of the Southern Ocean during late austral summer.

Kirchman, D. L. (1994). The uptake of inorganic nutrients by heterotrophic bacteria. *Microbial Ecology*, *28*(2), 255-271.

Kopczyńska, E. E., Dehairs, F., Elskens, M., & Wright, S. (2001). Phytoplankton and microzooplankton variability between the Subtropical and Polar Fronts south of Australia: Thriving under regenerative and new production in late summer. *Journal of Geophysical Research: Oceans*, *106*(C12), 31597-31609.

Korb, R. E., & Whitehouse, M. (2004). Contrasting primary production regimes around South Georgia, Southern Ocean: large blooms versus high nutrient, low chlorophyll waters. *Deep Sea Research Part I: Oceanographic Research Papers*, *51*(5), 721-738.
Lancelot, C., Hannon, E., Becquevort, S., Veth, C., & De Baar, H. J. (2000). Modeling phytoplankton blooms and carbon export production in the Southern Ocean: dominant controls by light and iron in the Atlantic sector in Austral spring 1992. *Deep Sea Research Part I: Oceanographic Research Papers*, *47*(9), 1621-1662.

Laubscher, R. K., Perissinotto, R., & McQuaid, C. D. (1993). Phytoplankton production and biomass at frontal zones in the Atlantic sector of the Southern Ocean. *Polar biology*, *13*(7), 471-481.

Le Fèvre, J., Legendre, L., & Rivkin, R. B. (1998). Fluxes of biogenic carbon in the Southern Ocean: roles of large microphagous zooplankton. *Journal of Marine Systems*, *17*(1-4), 325-345.

Legendre, L., Gosselin, M., 1996. Estimation of N or C uptake rates by phytoplankton using ^{15}N or ^{13}C: revisiting the usual computation formulae. J. Plankton Res. 19 (2), 263–271.

Legendre, L., Le Fèvre, J., Berger, W. H., Smetacek, V. S., & Wefer, G. (1989). Productivity of the ocean: present and past.

Levitus, S., Conkright, M. E., Reid, J. L., Najjar, R. G., & Mantyla, A. (1993). Distribution of nitrate, phosphate and silicate in the world oceans. *Progress in Oceanography*, *31*(3), 245-273.

Lin, H., Rauschenberg, S., Hexel, C. R., Shaw, T. J., & Twining, B. S. (2011). Free-drifting icebergs as sources of iron to the Weddell Sea. *Deep Sea Research Part II: Topical Studies in Oceanography*, *58*(11-12), 1392-1406.

Litchman, E., Klausmeier, C. A., Miller, J. R., Schofield, O. M., & Falkowski, P. G. (2006). Multi-nutrient, multi-group model of present and future oceanic phytoplankton communities.

Lourey, M. J., Trull, T. W., & Sigman, D. M. (2003). Sensitivity of δ15N of nitrate, surface suspended and deep sinking particulate nitrogen to seasonal nitrate depletion in the Southern Ocean. *Global Biogeochemical Cycles*, *17*(3).

Lucas, M., Seeyave, S., Sanders, R., Moore, C. M., Williamson, R., & Stinchcombe, M. (2007). Nitrogen uptake responses to a naturally Fe-fertilised phytoplankton bloom during the 2004/2005 CROZEX study. *Deep Sea Research Part II: Topical Studies in Oceanography*, *54*(18-20), 2138-2173.

Longhurst, A. R., & Harrison, W. G. (1989). The biological pump: profiles of plankton production and consumption in the upper ocean. *Progress in Oceanography*, *22*(1), 47-123.

Lutjeharms, J. R. E., Walters, N. M., & Allanson, B. R. (1985). Oceanic frontal systems and biological enhancement. In *Antarctic nutrient cycles and food webs* (pp. 11-21). Springer, Berlin, Heidelberg.

Marinov, I., Gnanadesikan, A., Toggweiler, J. R., & Sarmiento, J. L. (2006). The southern ocean biogeochemical divide. *Nature*, *441*(7096), 964-967.

Martin, J. H., & Fitzwater, S. E. (1988). Iron deficiency limits phytoplankton growth in the north-east Pacific subarctic. *Nature*, *331*(6154), 341-343.

Martin, J. H. (1990). Glacial-interglacial CO2 change: The iron hypothesis. *Paleoceanography*, *5*(1), 1- 13.

Martiny, A. C., Vrugt, J. A., Primeau, F. W., & Lomas, M. W. (2013). Regional variation in the particulate organic carbon to nitrogen ratio in the surface ocean. *Global Biogeochemical Cycles*, *27*(3), 723-731.

Mdutyana, M., Thomalla, S. J., Philibert, R., Ward, B. B., & Fawcett, S. E. (2020). The seasonal cycle of nitrogen uptake and nitrification in the Atlantic sector of the Southern Ocean. *Global Biogeochemical Cycles*, *34*(7), e2019GB006363.
Mtshali, T. N., van Horsten, N. R., Thomalla, S. J., Ryan-Keogh, T. J., Nicholson, S. A., Roychoudhury, A. N., ... & Monteiro, P. M. (2019). Seasonal depletion of the dissolved iron reservoirs in the sub-Antarctic zone of the Southern Atlantic Ocean. *Geophysical Research Letters*, *46*(8), 4386-4395.

Neori, A., & Holm-Hansen, O. (1982). Effect of temperature on rate of photosynthesis in Antarctic phytoplankton. *Polar Biology*, *1*(1), 33-38.

Obernosterer, I., Christaki, U., Lefèvre, D., Catala, P., Van Wambeke, F., & Lebaron, P. (2008). Rapid bacterial mineralization of organic carbon produced during a phytoplankton bloom induced by natural iron fertilization in the Southern Ocean. *Deep Sea Research Part II: Topical Studies in Oceanography*, *55*(5-7), 777-789.

Olson, R. J. (1980). Nitrate and ammonium uptake in Antarctic waters 1. *Limnology and Oceanography*, *25*(6), 1064-1074.

Orsi, A. H., Whitworth III, T., & Nowlin Jr, W. D. (1995). On the meridional extent and fronts of the Antarctic Circumpolar Current. *Deep Sea Research Part I: Oceanographic Research Papers*, *42*(5), 641-673.

Paerl, H. W., L. E. Prufert-Bebout, and C. Guo. 1994. "Iron-Stimulated N2 Fixation and Growth in Natural and Cultured Populations of the Planktonic Marine Cyanobacteria Trichodesmium Spp." Applied and Environmental Microbiology 60 (3): 1044–47.

Peng, X., Fawcett, S. E., Van Oostende, N., Wolf, M. J., Marconi, D., Sigman, D. M., & Ward, B. B. (2018). Nitrogen uptake and nitrification in the subarctic North Atlantic Ocean. *Limnology and Oceanography*, *63*(4), 1462-1487.

Pellichero, V., Sallée, J. B., Schmidtko, S., Roquet, F., & Charrassin, J. B. (2017). The ocean mixed layer under Southern Ocean sea-ice: Seasonal cycle and forcing. *Journal of Geophysical Research: Oceans*, *122*(2), 1608-1633.

Perissinotto, R., Laubscher, R. K., & McQuaid, C. D. (1992). Marine productivity enhancement around Bouvet and the South Sandwich Islands (Southern Ocean). *Marine Ecology-Progress Series*, *88*, 41-41.

Philibert, R., H. Waldron, and D. Clark. 2015. "A Geographical and Seasonal Comparison of Nitrogen Uptake by Phytoplankton in the Southern Ocean." Ocean Science 11 (2): 251–67. https://doi.org/10.5194/os-11- 251-2015.

Pomeroy, L. R. (1974). The ocean's food web, a changing paradigm. *Bioscience*, *24*(9), 499-504.

Poulton, A. J., Moore, C. M., Seeyave, S., Lucas, M. I., Fielding, S., & Ward, P. (2007). Phytoplankton community composition around the Crozet Plateau, with emphasis on diatoms and Phaeocystis. *Deep Sea Research Part II: Topical Studies in Oceanography*, *54*(18-20), 2085-2105.

Queguiner, B. (2013). Iron fertilization and the structure of planktonic communities in high nutrient regions of the Southern Ocean. *Deep Sea Research Part II: Topical Studies in Oceanography*, *90*, 43-54.

Robinson, J. O. S. I. E., Popova, E. E., Srokosz, M. A., & Yool, A. (2016). A tale of three islands: Downstream natural iron fertilization in the Southern Ocean. *Journal of Geophysical Research: Oceans*, *121*(5), 3350-3371.

Sakshaug, E., & Holm-Hansen, O. (1984). Factors governing pelagic production in polar oceans. In *Marine phytoplankton and productivity* (pp. 1-18). Springer, Berlin, Heidelberg.

Sakshaug, E., & Slagstad, D. A. G. (1991). Light and productivity of phytoplankton in polar marine ecosystems: a physiological view. *Polar Research*, *10*(1), 69-86.
Salter, I., Lampitt, R. S., Sanders, R., Poulton, A., Kemp, A. E., Boorman, B., ... & Pearce, R. (2007). Estimating carbon, silica and diatom export from a naturally fertilised phytoplankton bloom in the Southern Ocean using PELAGRA: A novel drifting sediment trap. *Deep Sea Research Part II: Topical Studies in Oceanography*, *54*(18-20), 2233-2259.

Sallée, J. B., Speer, K. G., & Rintoul, S. R. (2010). Zonally asymmetric response of the Southern Ocean mixed-layer depth to the Southern Annular Mode. *Nature Geoscience*, *3*(4), 273-279.

Sambrotto, R. N., & Mace, B. J. (2000). Coupling of biological and physical regimes across the Antarctic Polar Front as reflected by nitrogen production and recycling. *Deep Sea Research Part II: Topical Studies in Oceanography*, *47*(15-16), 3339-3367.

Sarmiento, J. L., & Toggweiler, J. R. (1984). A new model for the role of the oceans in determining atmospheric pCO2. *Nature*, *308*(5960), 621-624.

Sarmiento, J. L., Gruber, N., Brzezinski, M. A., & Dunne, J. P. (2004). High-latitude controls of thermocline nutrients and low latitude biological productivity. *Nature*, *427*(6969), 56-60.

Savoye, N., Buesseler, K. O., Cardinal, D., & Dehairs, F. (2004). 234Th deficit and excess in the Southern Ocean during spring 2001: Particle export and remineralization. *Geophysical Research Letters*, *31*(12).

Schlitzer, R. 12/11/2019. *eWOCE – Electronic Atlas of WOCE Data.* Alfred Wegener Institute for Polar and Marine Research, Bremerhaven, Germany. 15/08/2020. https://www.ewoce.org/data/index.html

Sigman, D. M., & Boyle, E. A. (2000). Glacial/interglacial variations in atmospheric carbon dioxide. *Nature*, *407*(6806), 859-869.

Sigman, D. M., & Hain, M. P. (2012). The biological productivity of the ocean. *Nature Education Knowledge*, *3*(6), 1-16.

Smart, S. M., Fawcett, S. E., Thomalla, S. J., Weigand, M. A., Reason, C. J., & Sigman, D. M. (2015). Isotopic evidence for nitrification in the Antarctic winter mixed layer. *Global Biogeochemical Cycles*, *29*(4), 427-445.

Smith, W. O., & Nelson, D. M. (1985). Phytoplankton bloom produced by a receding ice edge in the Ross Sea: spatial coherence with the density field. *Science*, *227*(4683), 163-166.

Staal, Marc, Filip J.R. Meysman, and Lucas J. Stal. 2003. "Temperature Excludes N2-Fixing Heterocystous Cyanobacteria in the Tropical Oceans." Nature 425 (6957): 504–7. https://doi.org/10.1038/nature01999.

Strass, V. H., Garabato, A. C. N., Pollard, R. T., Fischer, H. I., Hense, I., Allen, J. T., ... & Smetacek, V. (2002). Mesoscale frontal dynamics: shaping the environment of primary production in the Antarctic Circumpolar Current. *Deep Sea Research Part II: Topical Studies in Oceanography*, *49*(18), 3735-3769.

Sullivan, C. W., Arrigo, K. R., McClain, C. R., Comiso, J. C., & Firestone, J. (1993). Distributions of phytoplankton blooms in the Southern Ocean. *Science*, *262*(5141), 1832-1837.

Sunda, W. G. (1989). Trace metal interactions with marine phytoplankton. *Biological Oceanography*, *6*(5-6), 411-442.

Sunda, W. G., & Huntsman, S. A. (1997). Interrelated influence of iron, light and cell size on marine phytoplankton growth. *Nature*, *390*(6658), 389-392.

Sverdrup, H. U. (1953). On conditions for the vernal blooming of phytoplankton. *J. Cons. Int. Explor. Mer*, *18*(3), 287-295.

Tagliabue, A., Mtshali, T., Aumont, O., Bowie, A. R., Klunder, M. B., Roychoudhury, A. N., & Swart, S. (2012). A global compilation of dissolved iron measurements: focus on distributions and processes in the Southern Ocean. *Biogeosciences*, *9*(6).

Tagliabue, A., Sallée, J. B., Bowie, A. R., Lévy, M., Swart, S., & Boyd, P. W. (2014). Surface-water iron supplies in the Southern Ocean sustained by deep winter mixing. *Nature Geoscience*, *7*(4), 314-320.

Takahashi, M., Koike, I., Hattori, A., Iseki, K., & Bienfang, P. K. (1982). Phytoplankton species' responses to nutrient changes in experimental enclosures and coastal waters. In *Marine mesocosms* (pp. 333-340). Springer, New York, NY.

Takeda, S. (1998). Influence of iron availability on nutrient consumption ratio of diatoms in oceanic waters. *Nature*, *393*(6687), 774-777.

Talley, L. D. (2013). Closure of the global overturning circulation through the Indian, Pacific, and Southern Oceans: Schematics and transports. *Oceanography*, *26*(1), 80-97.

Thomalla, S. J., Waldron, H. N., Lucas, M. I., Read, J. F., Ansorge, I. J., & Pakhomov, E. (2011). Phytoplankton distribution and nitrogen dynamics in the southwest indian subtropical gyre and Southern Ocean waters. *Ocean science*, *7*(1), 113-127.

Tréguer, P., & Jacques, G. (1992). Review Dynamics of nutrients and phytoplankton, and fluxes of carbon, nitrogen and silicon in the Antarctic Ocean. In *Weddell Sea Ecology* (pp. 149-162). Springer, Berlin, Heidelberg.

Tréguer, P., Nelson, D. M., Van Bennekom, A. J., DeMaster, D. J., Leynaert, A., & Queguiner, B. (1995). The silica balance in the world ocean: a reestimate. *Science*, *268*(5209), 375-379.

Tréguer, P. J. (2014). The Southern Ocean silica cycle. *Comptes Rendus Geoscience*, *346*(11-12), 279- 286.

Tréguer, P., Bowler, C., Moriceau, B., Dutkiewicz, S., Gehlen, M., Aumont, O., ... & Pondaven, P. (2018). Influence of diatom diversity on the ocean biological carbon pump. *Nature Geoscience*, *11*(1), 27-37.

Tréguer, P., & Pondaven, P. (2000). Silica control of carbon dioxide. *Nature*, *406*(6794), 358-359.

Tremblay, J. E., Lucas, M. I., Kattner, G., Pollard, R., Strass, V. H., Bathmann, U., & Bracher, A. (2002). Significance of the Polar Frontal Zone for large-sized diatoms and new production during summer in the Atlantic sector of the Southern Ocean. *Deep Sea Research Part II: Topical Studies in Oceanography*, *49*(18), 3793-3811.

Trull, T. W., Bray, S. G., Manganini, S. J., Honjo, S., & Francois, R. (2001b). Moored sediment trap measurements of carbon export in the Subantarctic and Polar Frontal Zones of the Southern Ocean, south of Australia. *Journal of Geophysical Research: Oceans*, *106*(C12), 31489-31509.

Veth, C., Peeken, I., & Scharek, R. (1997). Physical anatomy of fronts and surface waters in the ACC near the 6° W meridian during austral spring 1992. *Deep Sea Research Part II: Topical Studies in Oceanography*, *44*(1-2), 23-49.

Viljoen, J. J., Weir, I., Fietz, S., Cloete, R., Loock, J., Philibert, R., & Roychoudhury, A. N. (2019). Links between the phytoplankton community composition and trace metal distribution in summer surface waters of the Atlantic Southern Ocean. *Frontiers in Marine Science*, *6*, 295.

Volk, T., & Hoffert, M. I. (1985). Ocean carbon pumps: Analysis of relative strengths and efficiencies in ocean-driven atmospheric CO2 changes. *The carbon cycle and atmospheric CO2: natural variations Archean to present*, *32*, 99-110.

Weber, T. S., & Deutsch, C. (2010). Ocean nutrient ratios governed by plankton biogeography. *Nature*, *467*(7315), 550-554.

Weir, I., Fawcett, S., Smith, S., Walker, D., Bornman, T., & Fietz, S. (2020). Winter biogenic silica and diatom distributions in the Indian sector of the Southern Ocean. *Deep Sea Research Part I: Oceanographic Research Papers*, *166*, 103421.

Wheeler, W. N., & Weidner, M. (1983). Effects of external inorganic nitrogen concentration on metabolism, growth and activities of key carbon and nitrogen assimilatory enzymes of laminaria saccharina (phaeophyceae) in culture 1. *Journal of Phycology*, *19*(1), 92-96.

Yool, A., Martin, A. P., Fernández, C., & Clark, D. R. (2007). The significance of nitrification for oceanic new production. *Nature*, *447*(7147), 999-1002.